Electronic Supplementary Information

Dynamic Covalent Chemistry Constrained Diphenylethenes: Control over Reactivity and Luminescence both in Solution and in the Solid State

Guoshan Jiang, [a, b] Yu Hai, [a, b] Hebo Ye, [a] and Lei You*[a, b, c]

a State Key Laboratory of Structural Chemistry, Fujian Institute of Research on the Structure of Matter, Chinese Academy of Sciences, Fuzhou 350002, China.

b University of Chinese Academy of Sciences, Beijing 100049, China.

c Fujian Science & Technology Innovation Laboratory for Optoelectronic Information of China, Fuzhou, Fujian 350108, China.

TABLE OF CONTENTS

1. General Methods

^{1}H NMR and ^{13}C NMR spectra were recorded on a 400 MHz Bruker Biospin avance III spectrometer. Deuterated reagents for characterization and *in situ* reactions were purchased from Sigma-Aldrich Chemical Co. and Cambridge Isotope Laboratories, Inc. (purity ≥ 99.9%). Mass spectra were recorded on a Bruker IMPACT-II mass spectrometer or Thermo Scientific LCQ Fleet mass spectrometer. X-ray diffraction data were recorded on a MM007-Saturn724 diffractometer. Photochemical experiments were carried out by using a CEL-HXUV300 xenon lamp with 313 nm cutoff filter at a power density of 220 mW/cm^2. Acetonitrile for optical experiments was purchased from Energy Chemical (purity ≥ 99.9%), dried over calcium hydride, and freshly distilled. All other reagents were obtained from commercial sources and were used without further purification, unless indicated otherwise.

Dynamic covalent reactions in solution and solid state. Dynamic Covalent Reactions (DCRs) were performed *in situ* in CD_3CN at room temperature without isolation and purification. To a stirred solution of an aldehyde (~16.7 mM, 1.0 equiv.) in CD_3CN (0.60 mL), was added an amine (1-$BuNH_2$, 1.2 equiv.) and activated 3Å molecular sieves (MS, 4-8 mesh). The mixture was stirred and characterized by ^{1}H NMR and ESI mass spectral analysis. DCRs in solid state were performed by manual grinding in a quartz mortar. To a powder of an aldehyde (~10 mg, 1.0 equiv.) in a quartz mortar, was added an amine (1.2 equiv.). The solid mixture was ground and then characterized by ^{1}H NMR and ESI mass spectral analysis. See specific conditions in figure captions of the main text or supplementary information if necessary.

Fluorescence experiments in solution and solid state. The spectrally pure solvents used for spectral measurement were deaerated by a nitrogen flow. UV-Vis absorption spectra were recorded on a LAMBDA 365 spectrophotometer (PerkinElmer). Fluorescence spectra in solution were recorded on a FLS980 fluorescence spectrometer (Edinburgh Instruments) at a concentration of 10 μM of each compound in a solvent, and the PL spectra were corrected for the wavelength dependence of detector unit. Fluorescence lifetimes were determined on a FLS980 fluorescence

spectrometer (Edinburgh Instruments) by using time-correlated single photon counting method under the excitation of a laser (375 nm) at a concentration of 10 μM in a solvent. **2** was created *in situ* with the reaction of **1** and 1-$BuNH_2$ (1.2 equiv.) in CH_3CN, and then the stock solution of **2** was obtained by diluting the CH_3CN solution with THF. Fluorescence spectra in solid state were recorded on a FLS980 fluorescence spectrometer (Edinburgh Instruments). Fluorescence titration experiments in solution were recorded on a microplate reader (BioTek SYNERGY H4) at a concentration of 10 μM of each compound in a solvent. Components were mixed in a similar way as NMR studies, and the spectra were recorded when the equilibrium was reached. See specific conditions in figure captions of the main text or supporting information if necessary.

Absolute quantum yields (ϕ) were determined on a FLS980 fluorescence spectrometer (Edinburgh Instruments) by using a calibrated integrating sphere setup equipped with a xenon high-pressure lamp.[S1,S2] A degassed solution of each compound (10 μM in a solvent, deaerated by a nitrogen flow) was excited at its maximum wavelength. The quantum yield is calculated as Eq.1.

$$\phi = \frac{N_{emission}}{N_{absorption}} = \frac{\int L_{emission}}{\int E_{solvent} - \int E_{sample}} \quad \text{(Eq.1)}$$

Where $N_{emission}$ is the number of photons emitted from a sample, $N_{absorption}$ is the number of photons absorbed by a sample, L_{sample} is the emission intensity of sample, $E_{solvent}$ and E_{sample} are the intensities of the excitation light not absorbed by the sample and the solvent, respectively.

2. Synthesis and Characterization

Scheme S1. General route for the synthesis of compounds **1**(H), **1**(NMe_2), **1**(OMe), **1**(CF_3), **1**(1-Naph), and **1**(2-Naph).

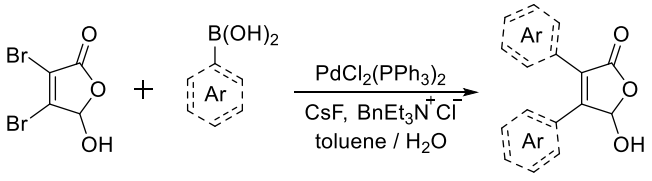

Scheme S2. Synthetic route of compound **1**(Br).[S3, S4]

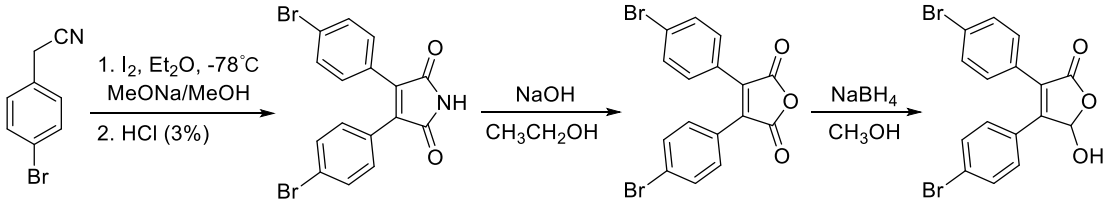

General procedure 1: To a solution of mucobromic acid (1.0 equiv.), arylboronic acid (3.0 equiv.), $PdCl_2(PPh_3)_2$ (0.05 equiv.), and $BnEt_3NCl$ (0.05 equiv.) in toluene cesium fluoride (4.0 equiv.) in water was added. The mixture was then heated at 90 ℃ for 4 h under nitrogen atmosphere. The reaction mixture was quenched with saturated aqueous ammonium chloride solution and extracted with ethyl acetate. The ethyl acetate extract was concentrated under reduced pressure, and the residue was purified by silica gel column chromatography to afford compounds **1**(H), **1**(NMe_2), **1**(OMe), **1**(CF_3), **1**(1-Naph), and **1**(2-Naph), respectively.

Scheme S3. Synthetic route of compounds **3**(H) and **3**(OMe).

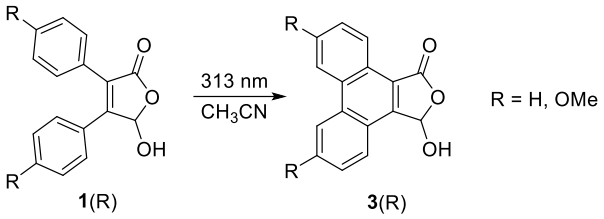

General procedure 2: A solution of **1**(R) in acetonitrile was exposed to 313 nm light at room temperature until the complete consumption of the starting material, and then concentrated under reduced pressure. The residue was purified by silica gel column chromatography to afford compounds **3**(H) and **3**(OMe), respectively.

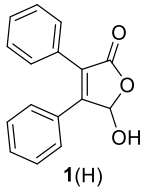

Compound **1**(H) was synthesized from mucobromic acid (200 mg, 0.78 mmol) and phenylboronic acid (284 mg, 2.33 mmol) according to the general procedure 1. The crude product was purified by silica gel column chromatography using petroleum

ether/ethyl acetate (10:1, v/v) as eluent to obtain **1**(H) as a white solid (144 mg, 73%). MP: 147.8-148.6 °C. ^{1}H NMR (CD_3CN): δ 7.46-7.35 (m, 10H), 6.53 (d, *J* = 8.8 Hz, 1H), 5.48 (d, *J* = 8.8 Hz, 1H). ^{13}C NMR ($CDCl_3$): δ 171.2, 155.2, 130.6, 130.2, 129.5, 129.3, 128.9, 128.8, 128.3, 97.2. ESI-HRMS: m/z calculated for $C_{16}H_{12}O_3Na$ [M + Na]$^+$: 275.0684; found: 275.0678.

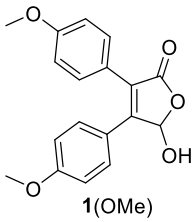

1(OMe)

Compound **1**(OMe) was synthesized from mucobromic acid (200 mg, 0.78 mmol) and (4-methoxyphenyl)boronic acid (354 mg, 2.33 mmol) according to the general procedure 1. The crude product was purified by silica gel column chromatography using petroleum ether/ethyl acetate (4:1, v/v) as eluent to obtain **1**(OMe) as a yellow solid (148 mg, 61%). MP: 61.3-62.6 °C. ^{1}H NMR (CD_3CN): δ 7.43-7.39 (m, 2H), 7.35-7.31 (m, 2H), 7.00-6.96 (m, 2H), 6.93-6.89 (m, 2H), 6.46 (d, *J* = 8.8 Hz, 1H), 5.43 (d, *J* = 8.8 Hz, 1H), 3.83 (s, 3H), 3.82 (s, 3H). ^{13}C NMR ($CDCl_3$): δ 171.6, 161.2, 160.1, 153.4, 130.8, 130.5, 125.7, 122.7, 122.0, 114.2, 97.0, 55.3. ESI-HRMS: m/z calculated for $C_{18}H_{16}O_5Na$ [M + Na]$^+$: 335.0896; found: 335.0889.

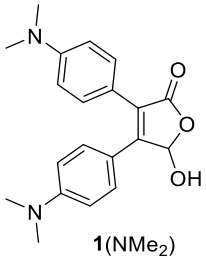

1(NMe_2)

Compound **1**(NMe_2) was synthesized from mucobromic acid (200 mg, 0.78 mmol) and (4-(dimethylamino)phenyl)boronic acid (384 mg, 2.33 mmol) according to the general procedure 1. The crude product was purified by silica gel column chromatography using petroleum ether/ethyl acetate (4:1, v/v) as eluent to obtain **1**(NMe_2) as a yellow solid (113 mg, 43%). MP: 148.1-149.3 °C. ^{1}H NMR (CD_3CN): δ 7.38 (d, *J* = 9.2 Hz, 2H), 7.26 (d, *J* = 8.8 Hz, 2H), 6.77 (d, *J* = 8.8 Hz, 2H), 6.65 (d, *J* = 9.2 Hz, 2H), 6.40 (d, *J* = 8.8 Hz, 1H), 5.28 (d, *J* = 8.8 Hz, 1H), 2.98 (s, 12H). ^{13}C

NMR ($CDCl_3$): δ 171.7, 152.2, 151.3, 150.4, 130.4, 130.1, 123.2, 117.7, 112.2, 111.5, 96.6, 40.4, 40.0. ESI-HRMS: m/z calculated for $C_{20}H_{22}N_2O_3Na$ $[M + Na]^+$: 361.1528; found: 361.1523.

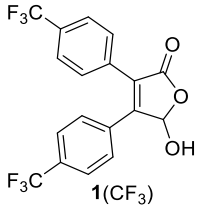

1(CF_3)

Compound **1**(CF_3) was synthesized from mucobromic acid (200 mg, 0.78 mmol) and (4-(trifluoromethyl)phenyl)boronic acid (443 mg, 2.33 mmol) according to the general procedure 1. The crude product was purified by silica gel column chromatography using petroleum ether/ethyl acetate (10:1, v/v) as eluent to obtain **1**(CF_3) as a white solid (191 mg, 63%). MP: 142.6-143.8 ºC. ^{1}H NMR (CD_3CN): δ 7.76-7.69 (m, 4H), 7.60-7.54 (m, 4H), 6.58 (d, *J* = 8.0 Hz, 1H), 5.68 (d, *J* = 8.0 Hz, 1H). ^{13}C NMR ($CDCl_3$): δ 169.8, 154.8, 133.3, 132.3, 131.9, 131.5, 129.9, 129.2, 129.1, 125.9, 122.4, 122.2, 97.0. ESI-HRMS: m/z calculated for $C_{18}H_{10}F_6O_3Na$ $[M + Na]^+$: 411.0432; found: 411.0935.

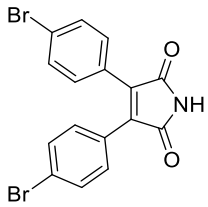

Compound 3,4-bis(4-bromophenyl)-1*H*-pyrrole-2,5-dione was synthesized according to the literature method.[S3]

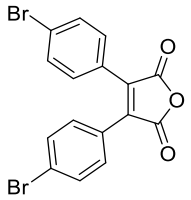

Compound 3,4-bis(4-bromophenyl)furan-2,5-dione was synthesized according to the literature method.[S4]

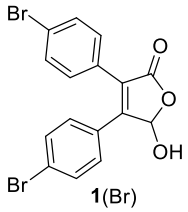

1(Br)

To a solution of 3,4-bis(4-bromophenyl)furan-2,5-dione (200 mg, 0.49 mmol) in methanol (15 mL), was added $NaBH_4$ (18 mg, 0.49 mmol) at 0 ℃. The mixture was stirred for 1 h at room temperature. The reaction was quenched with dilute hydrochloric acid solution (1 M) and extracted with ethyl acetate. The ethyl acetate extract was concentrated under reduced pressure, and the residue was purified by silica gel column chromatography using petroleum ether/ethyl acetate (10:1, v/v) as eluent to obtain compound **1**(Br) as a white solid. (129 mg, 64%). MP: 158.5-159.7 ^{o}C. ^{1}H NMR (CD_3CN): δ 7.63-7.55 (m, 4H), 7.36-7.30 (m, 4H), 6.49 (d, *J* = 8.8 Hz, 1H), 5.59 (d, *J* = 8.8 Hz, 1H). ^{13}C NMR (DMSO-d_6): δ 170.2, 156.3, 132.3, 131.7, 131.1, 130.1, 129.3, 126.9, 124.3, 123.0, 97.8. ESI-HRMS: m/z calculated for $C_{16}H_{10}Br_2O_3Na$ $[M + Na]^+$: 430.8895; found: 430.8879.

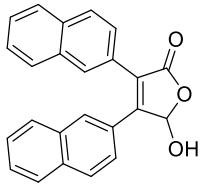

1(2-Naph)

Compound **1**(2-Naph) was synthesized from mucobromic acid (200 mg, 0.78 mmol) and naphthalen-2-ylboronic acid (401 mg, 2.33 mmol) according to the general procedure 1. The crude product was purified by silica gel column chromatography using petroleum ether/ethyl acetate (4:1, v/v) as eluent to obtain **1**(2-Naph) as a pale yellow solid (173 mg, 63%). MP: 212.3-213.2 ^{o}C. ^{1}H NMR (CD_3CN): δ 8.12 (s, 1H), 8.08 (s, 1H), 7.93 (d, *J* = 8.0 Hz, 1H), 7.89-7.83 (m, 4H), 7.78 (d, *J* = 8.0 Hz, 1H), 7.60-7.55 (m, 4H), 7.46-7.39 (m, 2H), 6.78 (s, 1H), 5.74 (s, 1H). ^{13}C NMR (DMSO-d_6): δ 170.4, 156.5, 133.3, 132.8, 132.7, 132.5, 129.0, 128.9, 128.5, 128.3, 128.2, 128.0, 127.7, 127.4, 127.0, 126.9, 126.6, 126.5, 125.5, 97.5. ESI-HRMS: m/z calculated for $C_{24}H_{16}O_3Na$ $[M + Na]^+$: 375.0997; found: 375.0992.

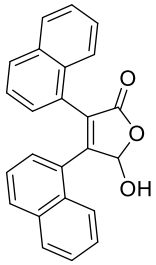

1(1-Naph)

Compound **1**(1-Naph) was synthesized from mucobromic acid (200 mg, 0.78 mmol) and naphthalen-1-ylboronic acid (401 mg, 2.33 mmol) according to the general procedure 1. The crude product was purified by silica gel column chromatography using petroleum ether/ethyl acetate (4:1, v/v) as eluent to obtain **1**(1-Naph) as a white solid (140 mg, 51%). MP: 104.6-105.8 ºC. ^{1}H NMR (CD_3CN): δ 8.11-7.72 (m, 6H), 7.68-7.12 (m, 8H), 6.82-6.66 (br, 1H), 5.72-5.59 (br, 1H). ^{13}C NMR (DMSO-d_6): δ 161.0, 133.4, 133.3, 128.7, 127.0, 126.9, 126.7, 125.9, 125.7, 99.6. ESI-HRMS: m/z calculated for $C_{24}H_{16}O_3Na$ $[M + Na]^+$: 375.0997; found: 375.0992.

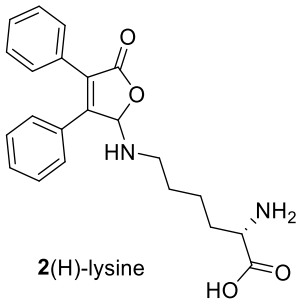

2(H)-lysine

To the powder of **1**(H) (100 mg, 0.40 mmol) in a quartz mortar, was added L-lysine (70 mg, 0.48 mmol). The solid mixture was ground at room temperature until complete consumption of starting materials. The crude product was purified by silica gel column chromatography using dichloromethane/MeOH (2:1, v/v) as eluent to obtain **2**(H)-lysine as a white solid (127 mg, 81%). MP: 150.5-151.8 ºC. ^{1}H NMR (CD_3OD): δ 7.41-7.25 (m, 10H), 6.34 (s, 1H), 3.50-3.47 (dd, J = 6.8, 5.6 Hz, 1H), 2.81 (t, J = 6.8 Hz, 2H), 1.90-1.70 (m, 2H), 1.54-1.47 (m, 2H), 1.44-1.37 (m, 2H). ^{13}C NMR (CD_3OD): δ 173.9, 173.7, 157.8, 157.5, 131.0, 130.7, 130.6, 130.5, 130.3, 129.8, 129.5, 129.4, 95.9, 56.1, 44.8, 40.5, 40.3, 32.1, 31.0, 28.2, 24.3, 23.8, 23.1, 23.0. ESI-HRMS: m/z calculated for $C_{22}H_{23}N_2O_4$ $[M - H]^-$: 379.1658; found: 379.1699.

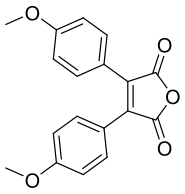

4(OMe)

Compound **4**(OMe) was synthesized according to the literature method.[S5]

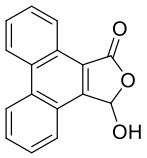

3(H)

Compound **3**(H) was synthesized from **1**(H) (200 mg, 0.79 mmol) according to the general procedure 2. The crude product was purified by silica gel column chromatography using dichloromethane as eluent to obtain **3**(H) as a white solid (107 mg, 54%). MP: 251.6-252.7 ^{o}C. ^{1}H NMR (CD_3CN): δ 9.05 (d, *J* = 8.0 Hz, 1H), 8.94-8.87 (m, 2H), 8.30 (d, *J* = 8.0 Hz, 1H), 7.95 (t, *J* = 8.4 Hz, 1H), 7.90-7.81 (m, 3H), 6.98 (d, *J* = 8.8 Hz, 1H), 5.85 (d, *J* = 8.8 Hz, 1H). ^{13}C NMR (DMSO-d_6): δ 169.5, 148.8, 133.4, 131.5, 130.8, 129.0, 128.9, 128.5, 126.4, 126.0, 125.7, 124.6, 124.4, 124.2, 120.0, 97.3. ESI-HRMS: m/z calculated for $C_{16}H_{11}O_3$ $[M + H]^+$: 251.0708; found: 251.0699.

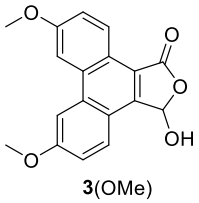

3(OMe)

Compound **3**(OMe) was synthesized from **1**(OMe) (200 mg, 0.64 mmol) according to the general procedure 2. The crude product was purified by silica gel column chromatography using dichloromethane as eluent to obtain **3**(OMe) as a yellow solid (157 mg, 79%). MP: 232.6-233.8 ^{o}C. ^{1}H NMR (CD_3CN): δ 8.89 (d, *J* = 8.8 Hz, 1H), 8.18-8.12 (m, 3H), 7.43 (d, *J* = 8.8 Hz, 2H), 6.86 (s, 1H), 5.71 (s, 1H), 4.09 (s, 3H), 4.06 (s, 3H). ^{13}C NMR (DMSO-d_6): δ 169.8, 161.1, 159.4, 146.3, 134.9, 132.7, 128.0, 125.6, 120.7, 120.4, 118.6, 118.3, 117.4, 106.6, 97.1, 56.4, 56.2. ESI-HRMS: m/z calculated for $C_{18}H_{14}O_5Na$ $[M + Na]^+$: 333.0739; found: 333.0732.

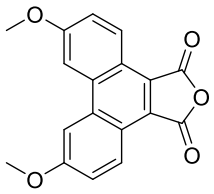

5(OMe)

To a solution of **3**(OMe) (100 mg, 0.32 mmol) in acetonitrile (15 mL), was added MnO_2 (278 mg, 3.2 mmol). The mixture was stirred for 12 h at room temperature. The solids were filtered, and the filtrate was concentrated under reduced pressure. The residue was purified by silica gel column chromatography using petroleum ether/ethyl acetate (10:1, v/v) as eluent to obtain compound **5**(OMe) as a yellow solid (83 mg, 84%). MP: 247.5-248.4 ºC. ^{1}H NMR (CD_2Cl_2): δ 8.78 (d, *J* = 8.0 Hz, 2H), 7.92 (d, *J* = 2.4 Hz, 2H), 7.44 (dd, *J* = 8.0, 2.4 Hz, 2H), 4.10 (s, 6H). ^{13}C NMR (CD_2Cl_2): δ 164.0, 161.3, 135.4, 127.7, 125.7, 119.6, 119.1, 105.4, 55.6. ESI-HRMS: m/z calculated for $C_{18}H_{13}O_5$ $[M + H]^+$: 309.0763; found: 309.0752.

^{1}H NMR and ^{13}C NMR Spectra

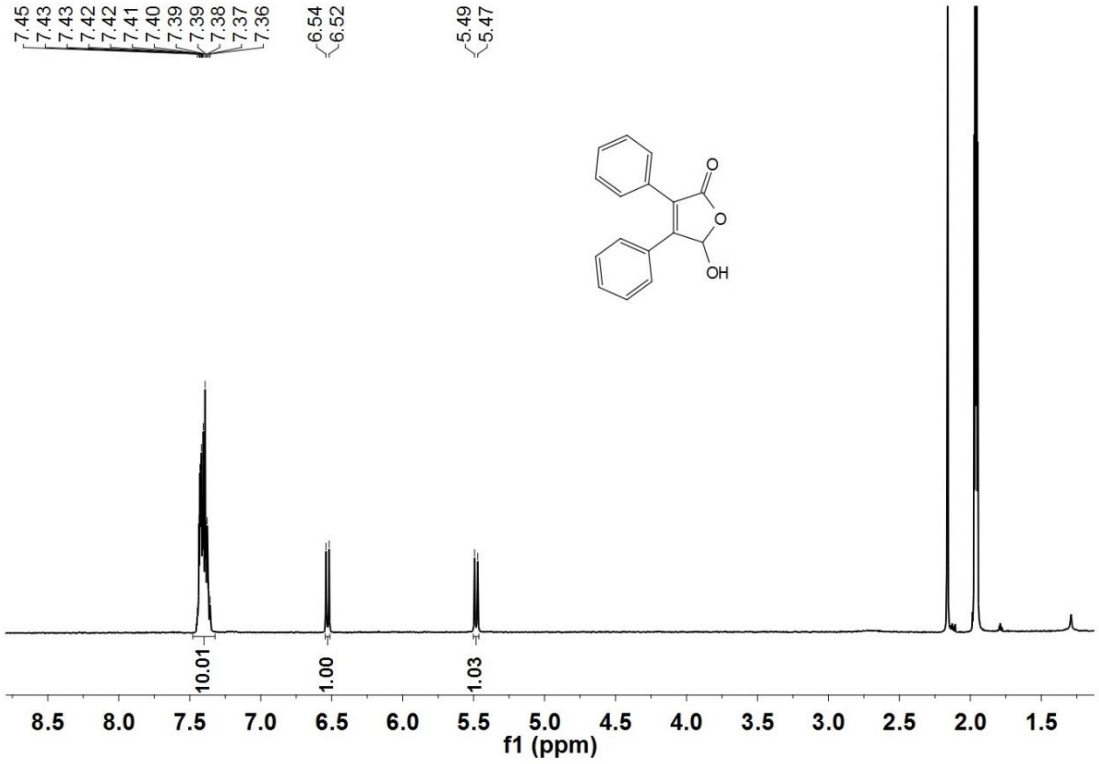

Figure S1. ^{1}H NMR spectrum of **1**(H) in CD_3CN.

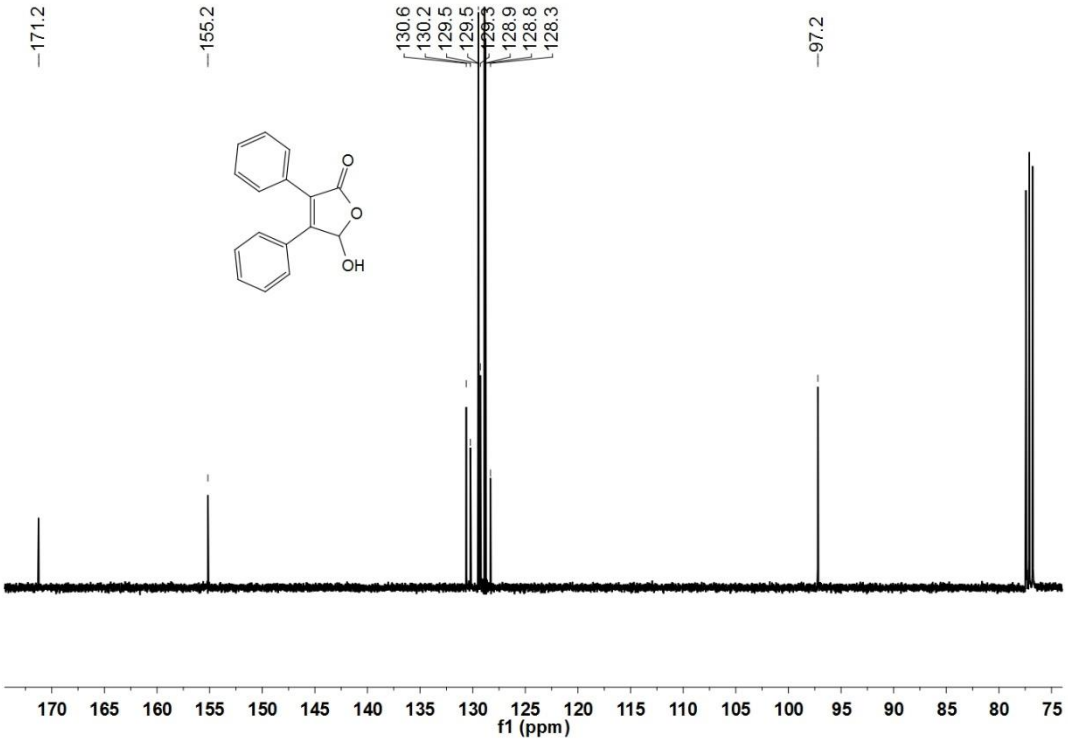

Figure S2. ^{13}C NMR spectrum of **1**(H) in $CDCl_3$.

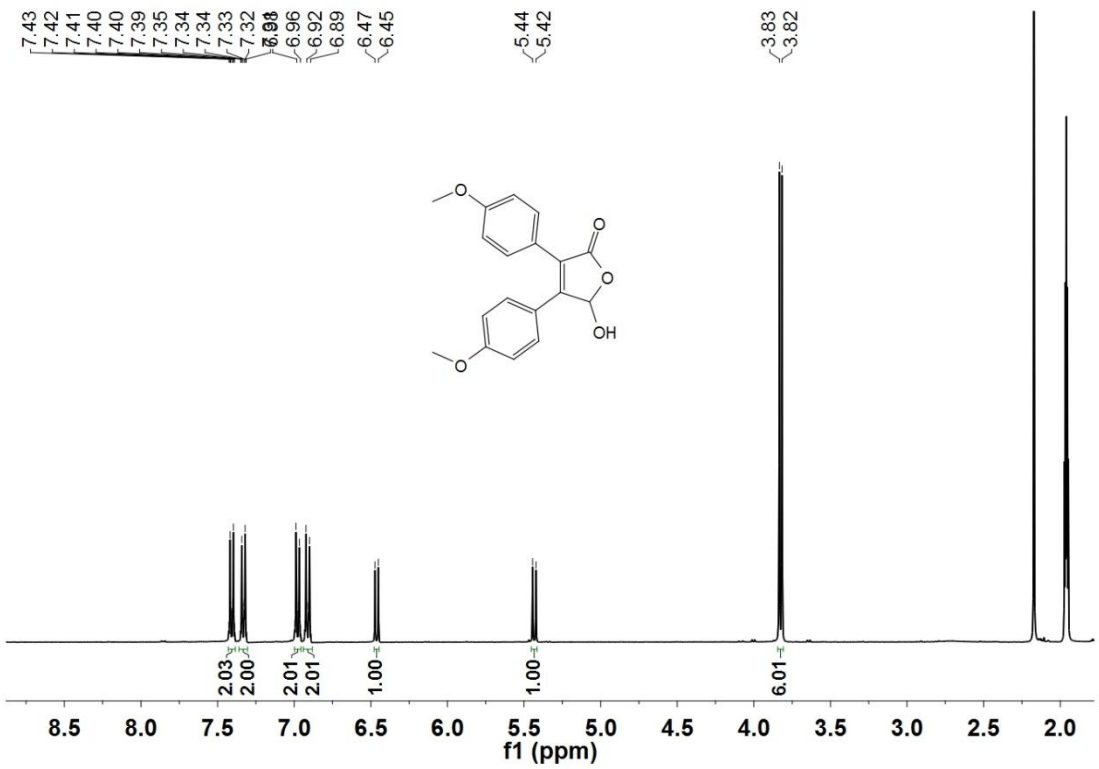

Figure S3. ^{1}H NMR spectrum of **1**(OMe) in CD_3CN.

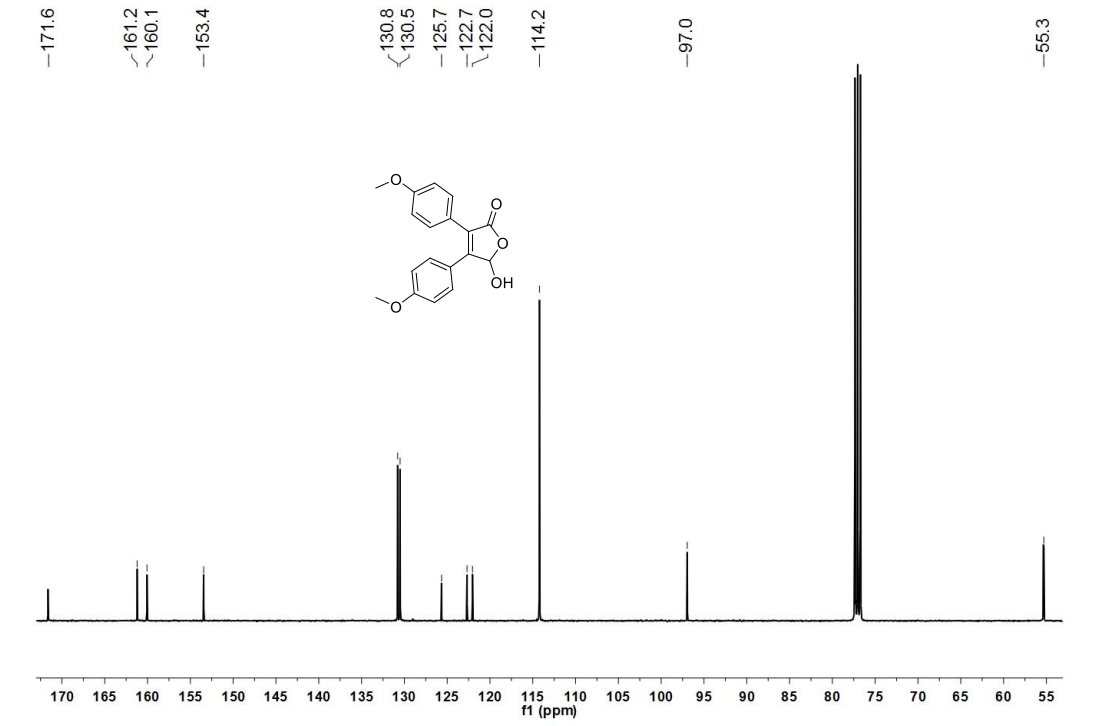

Figure S4. ^{13}C NMR spectrum of **1**(OMe) in $CDCl_3$.

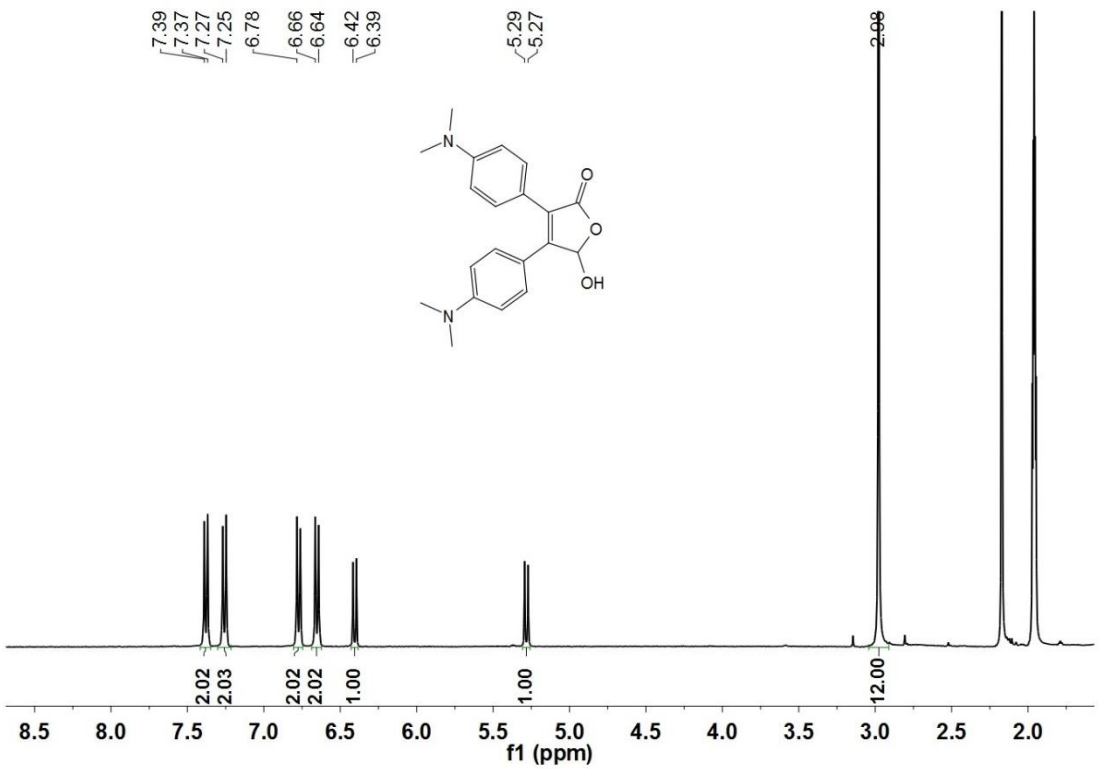

Figure S5. ^{1}H NMR spectrum of **1**(NMe_2) in CD_3CN.

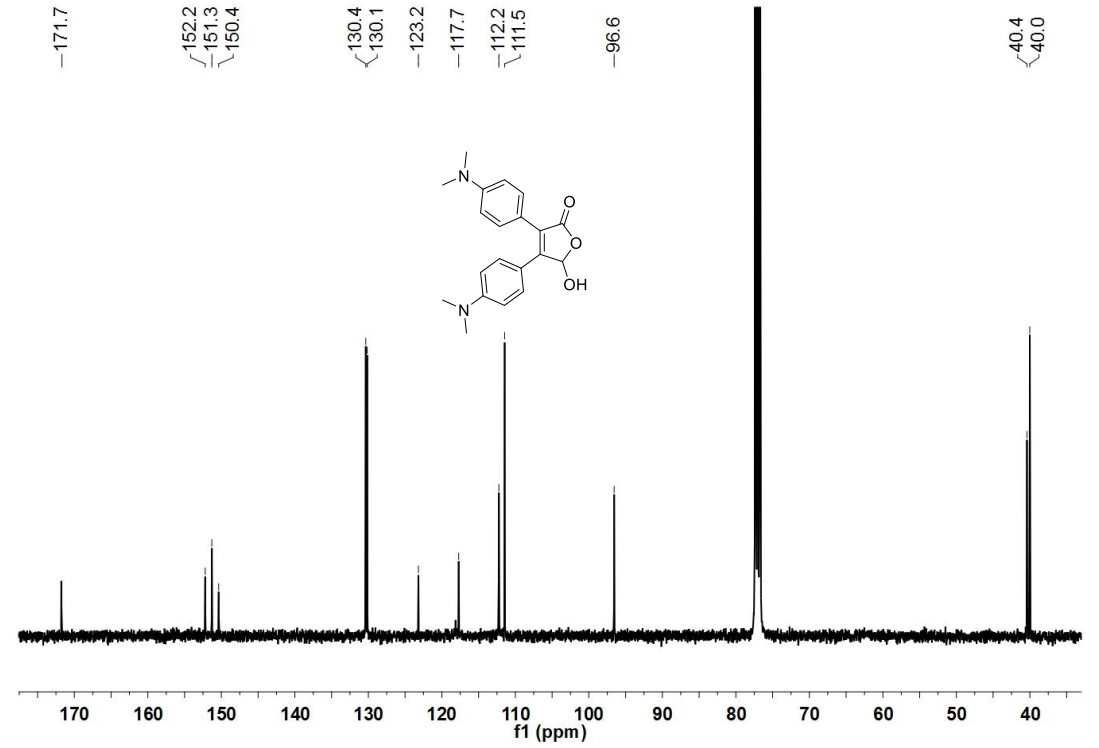

Figure S6. ^{13}C NMR spectrum of **1**(NMe_2) in $CDCl_3$

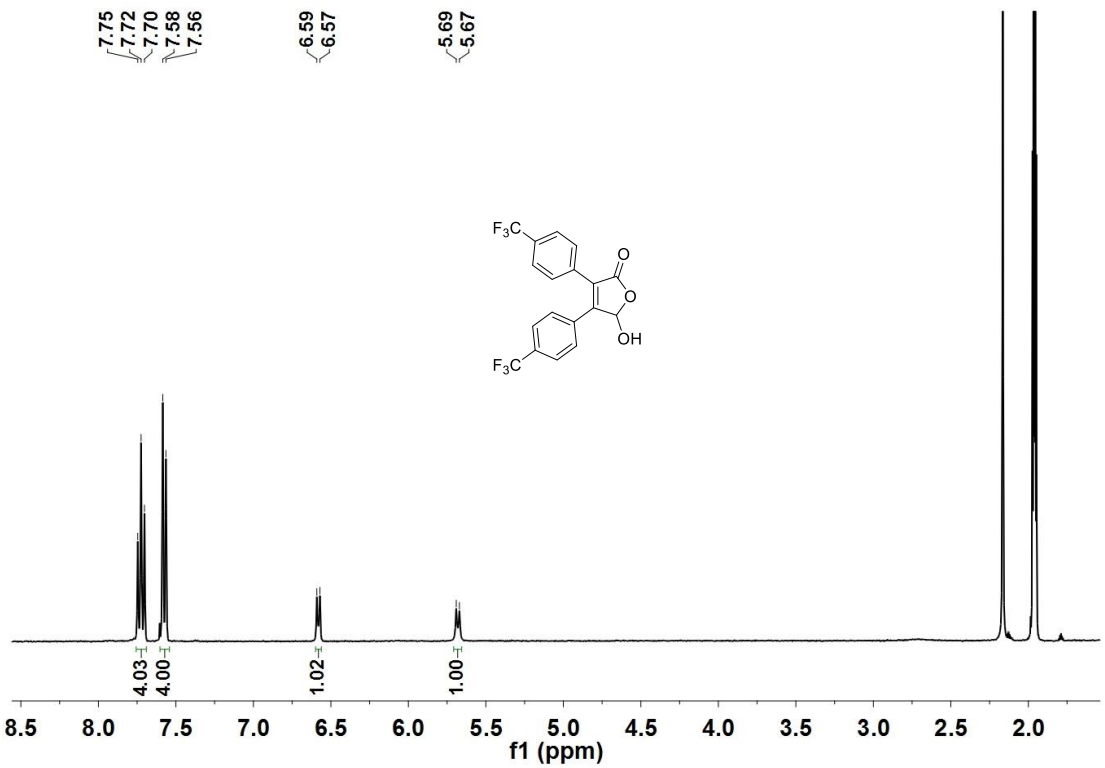

Figure S7. ^{1}H NMR spectrum of **1**(CF_3) in CD_3CN.

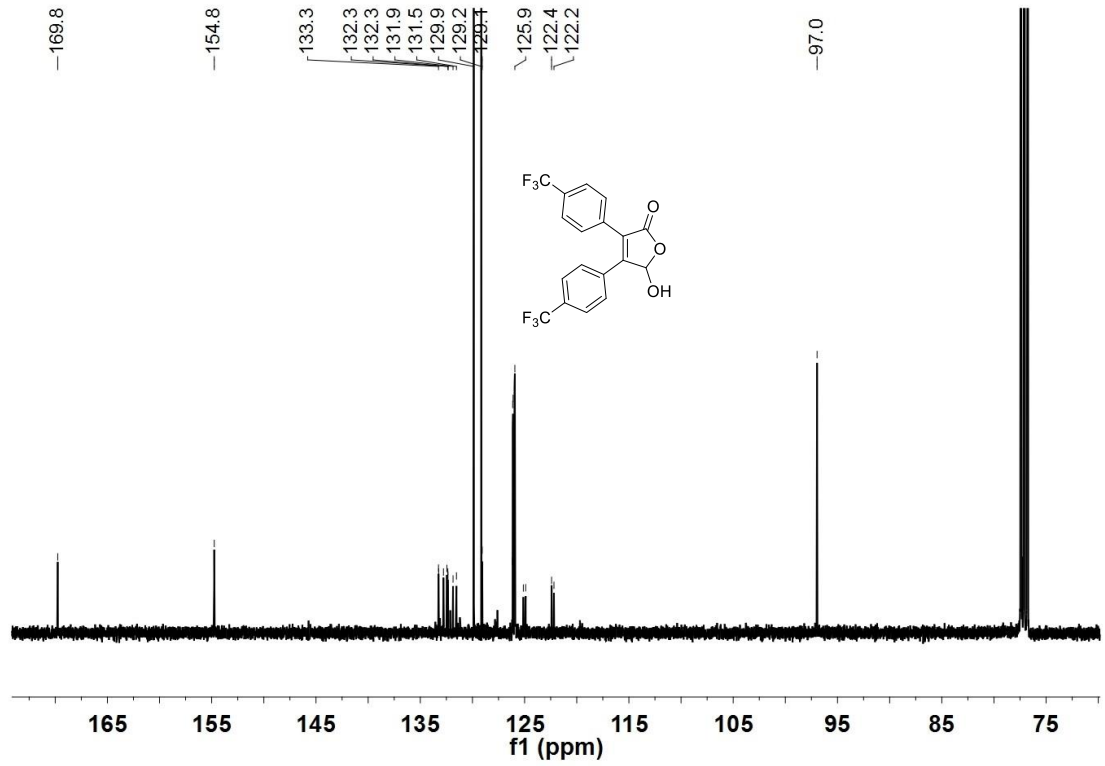

Figure S8. ^{13}C NMR spectrum of **1**(CF_3) in $CDCl_3$.

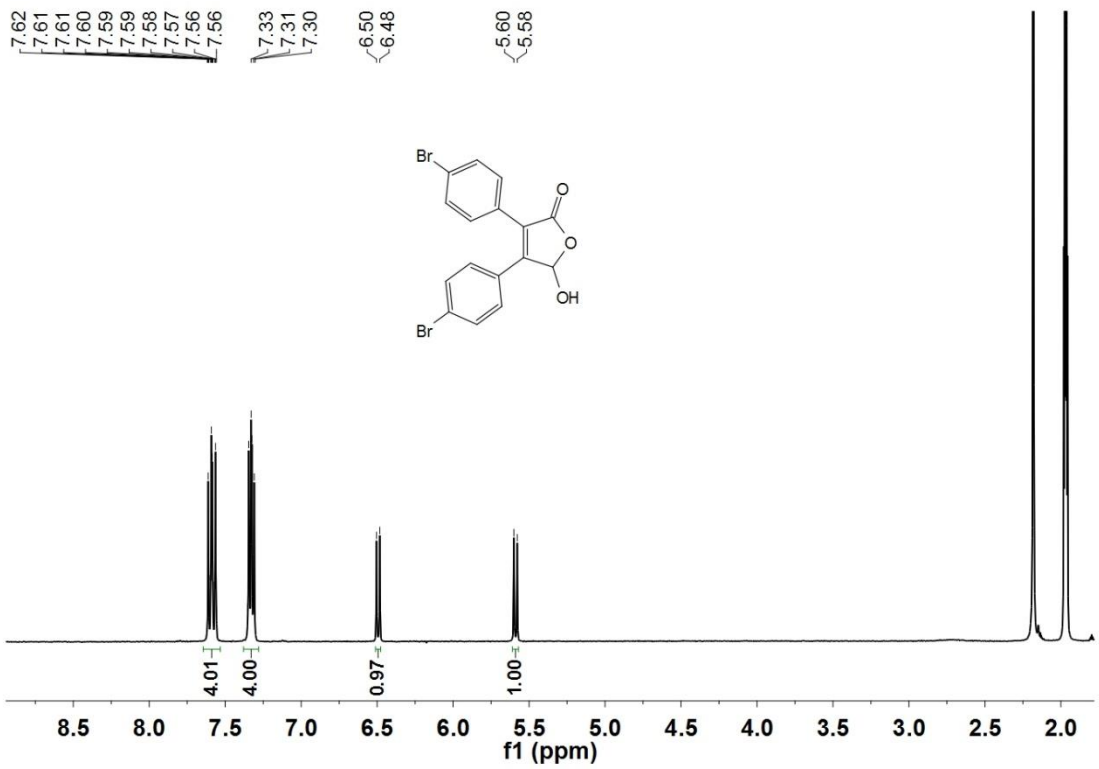

Figure S9. ^{1}H NMR spectrum of **1**(Br) in CD_3CN.

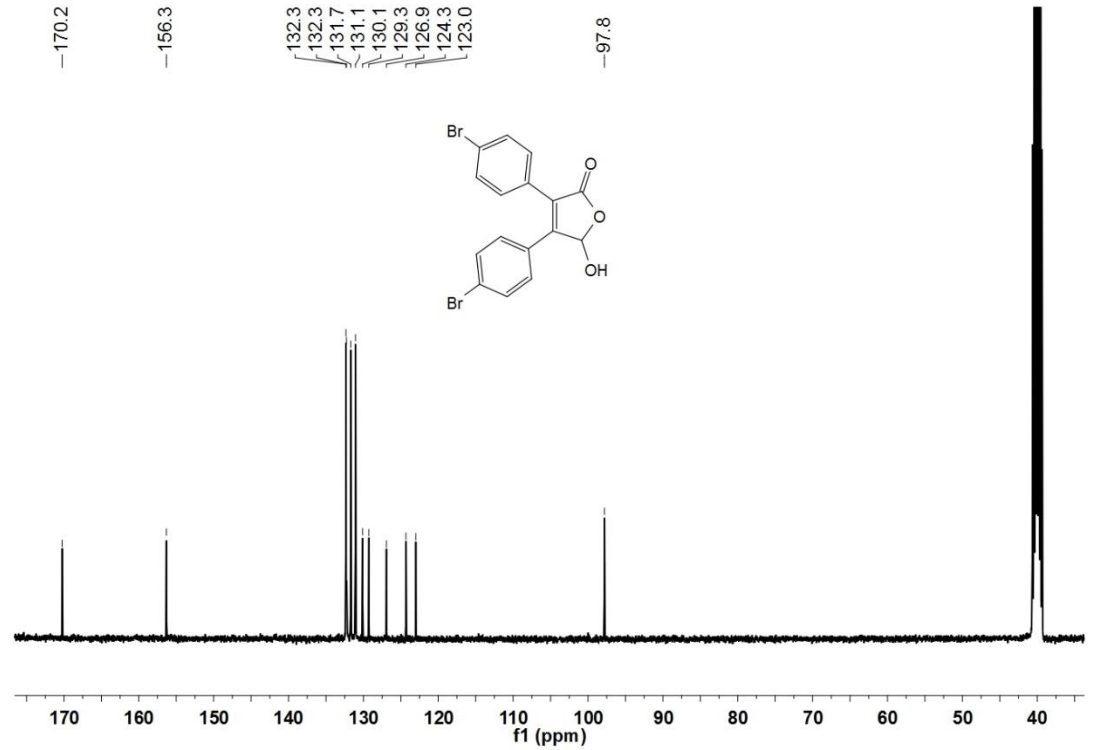

Figure S10. ^{13}C NMR spectrum of **1**(Br) in DMSO-d_6.

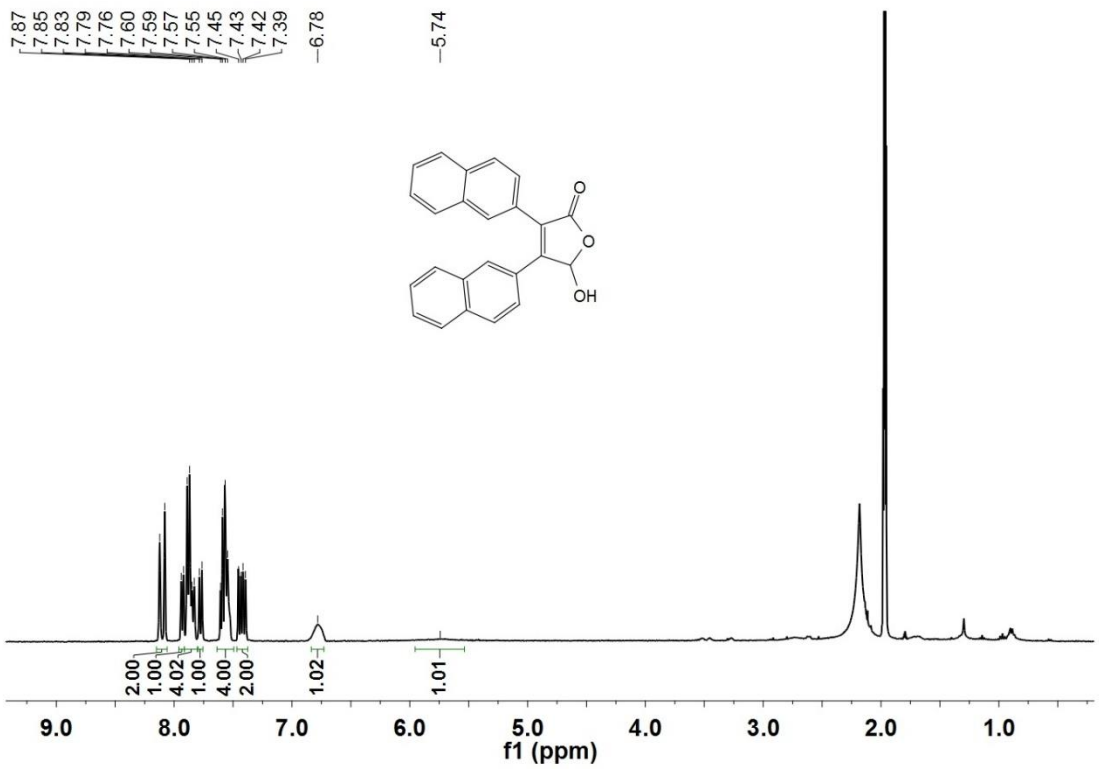

Figure S11. ^{1}H NMR spectrum of **1**(2-Naph) in CD_3CN.

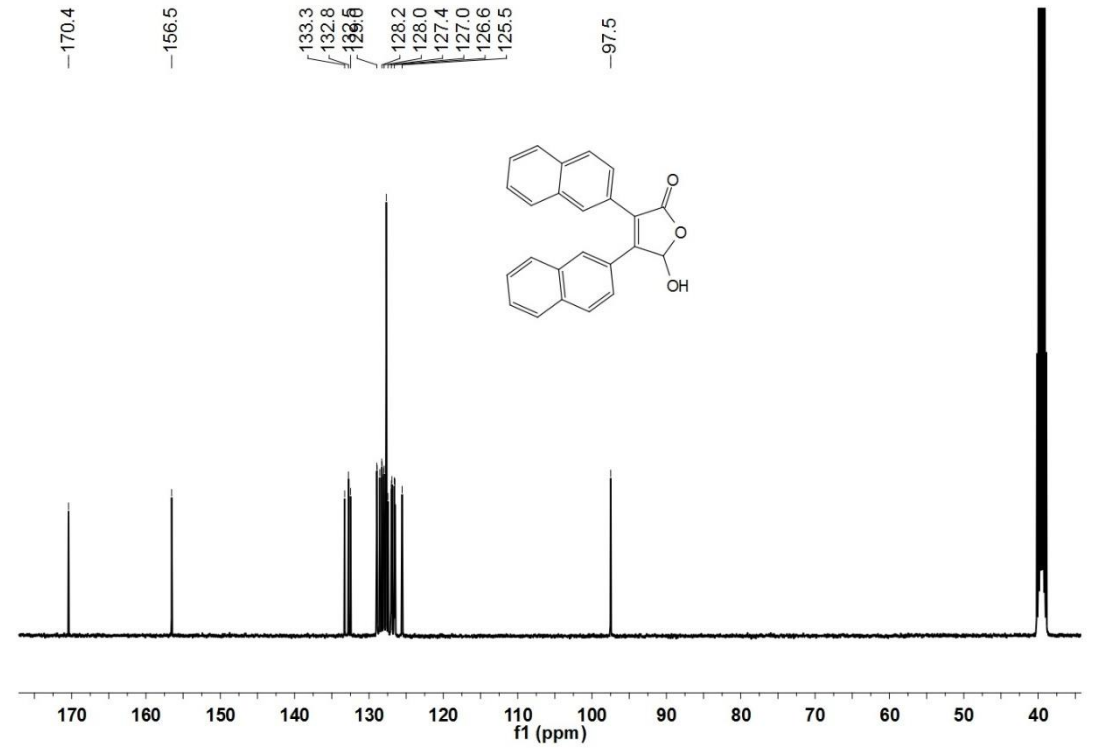

Figure S12. ^{13}C NMR spectrum of **1**(2-Naph) in DMSO-d_6.

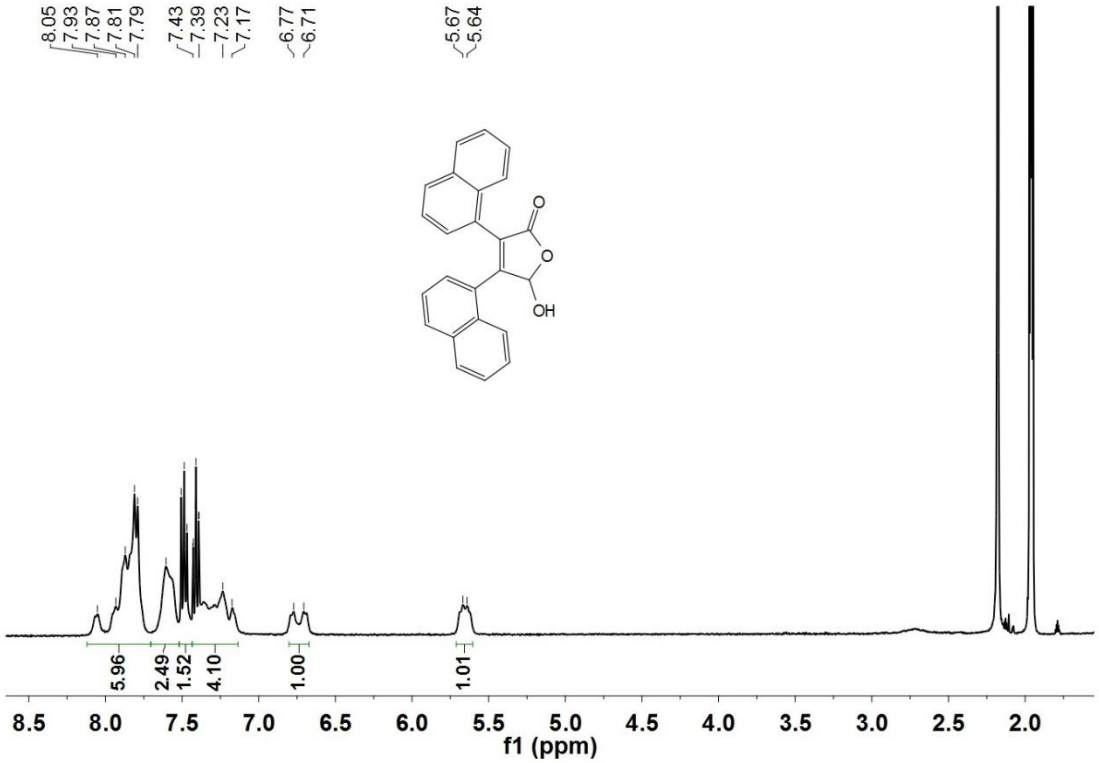

Figure S13. ^{1}H NMR spectrum of **1**(1-Naph) in CD_3CN.The broadening of peaks is likely due to slow rotation about C-C bond arising from steric hindrance of 1-naphthyl.

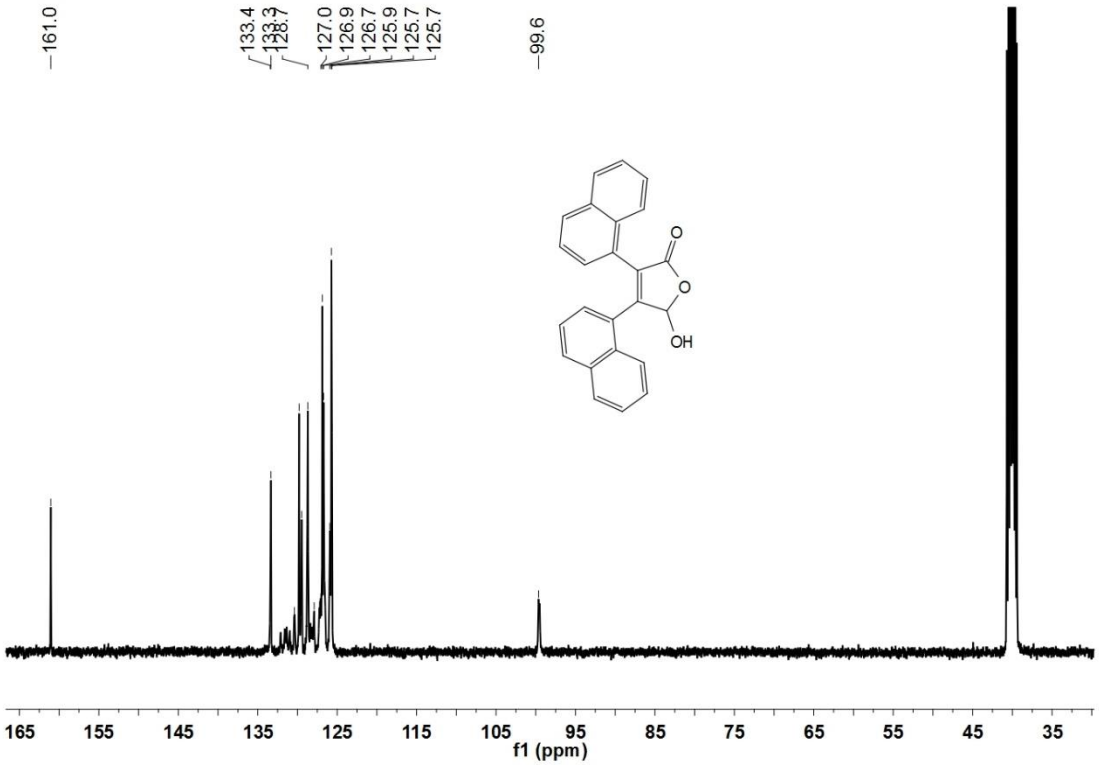

Figure S14. ^{13}C NMR spectrum of **1**(1-Naph) in DMSO-d_6.

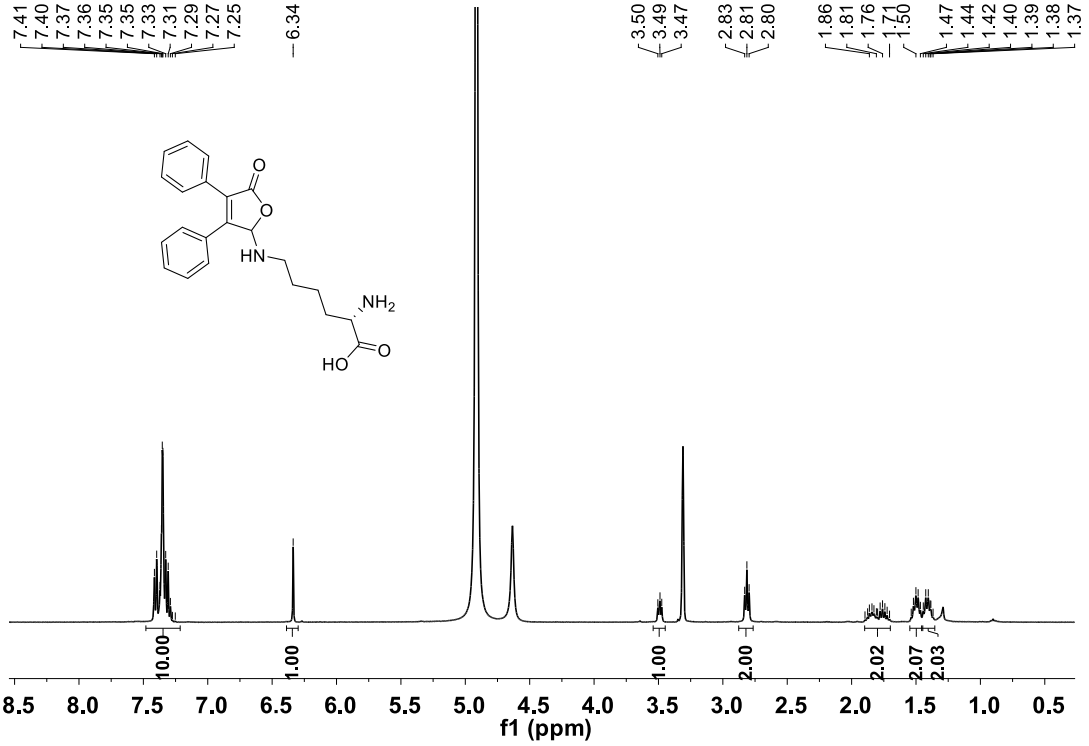

Figure S15. ^{1}H NMR spectrum of **2**(H)-lysine in CD_3OD.

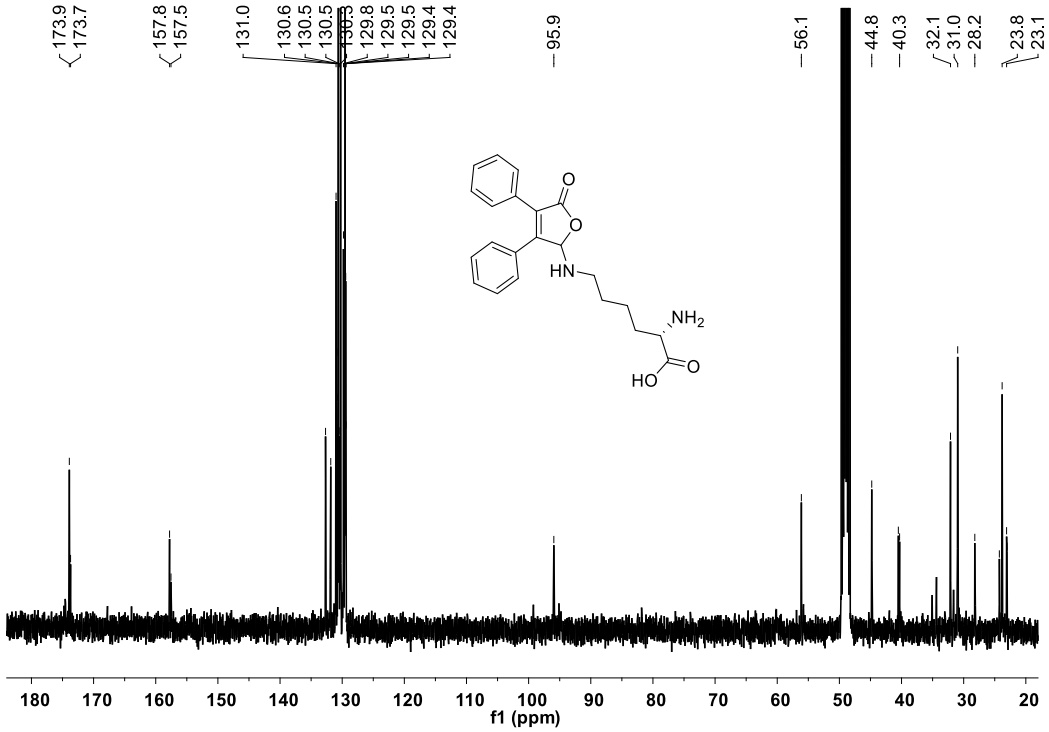

Figure S16. ^{13}C NMR spectrum of **2**(H)-lysine in CD_3OD.

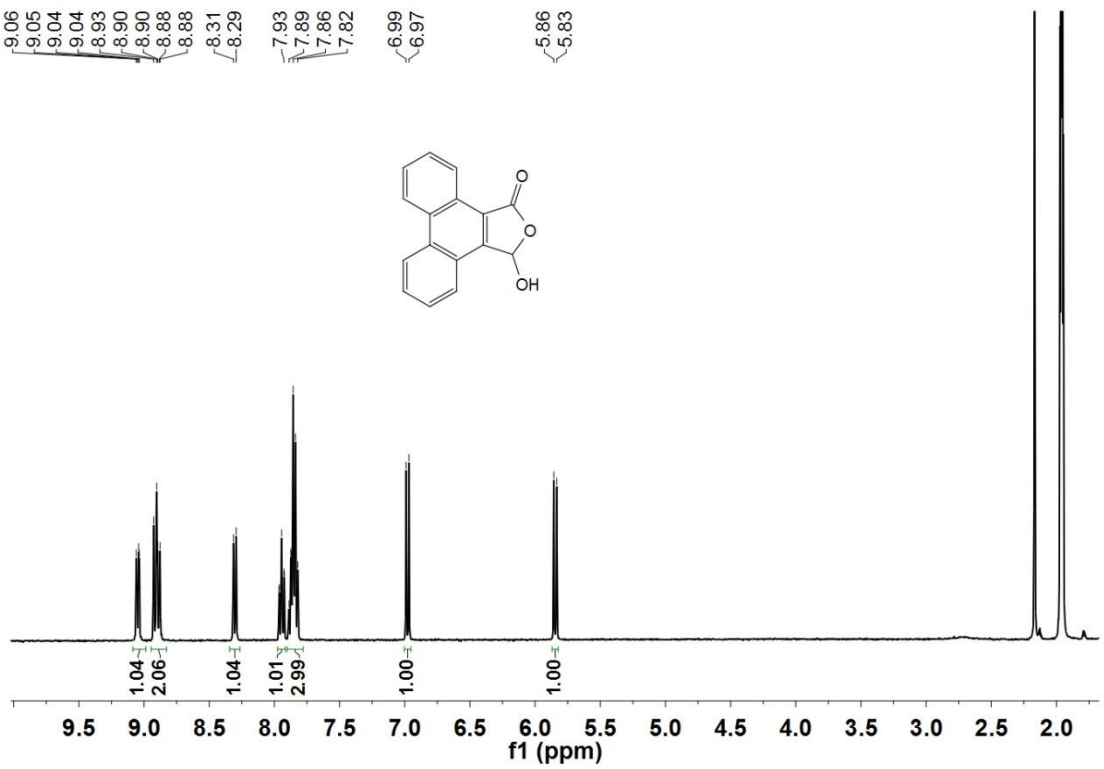

Figure S17. ^{1}H NMR spectrum of **3**(H) in CD_3CN.

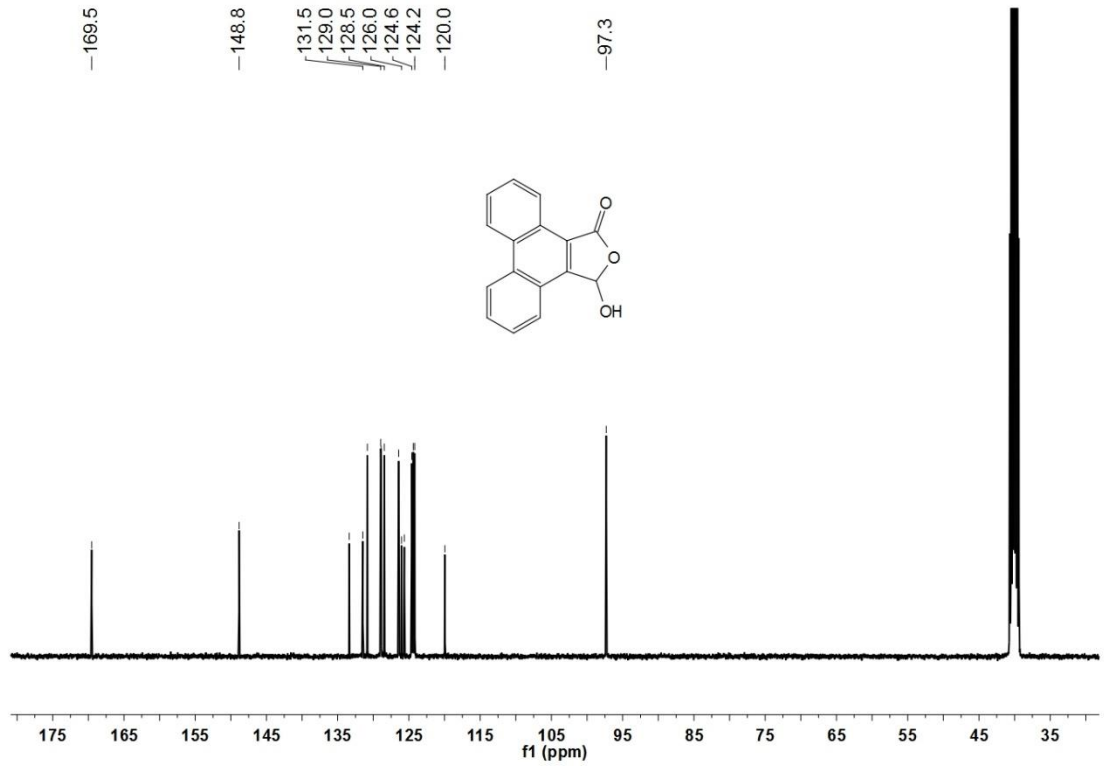

Figure S18. ^{13}C NMR spectrum of **3**(H) in DMSO-d_6.

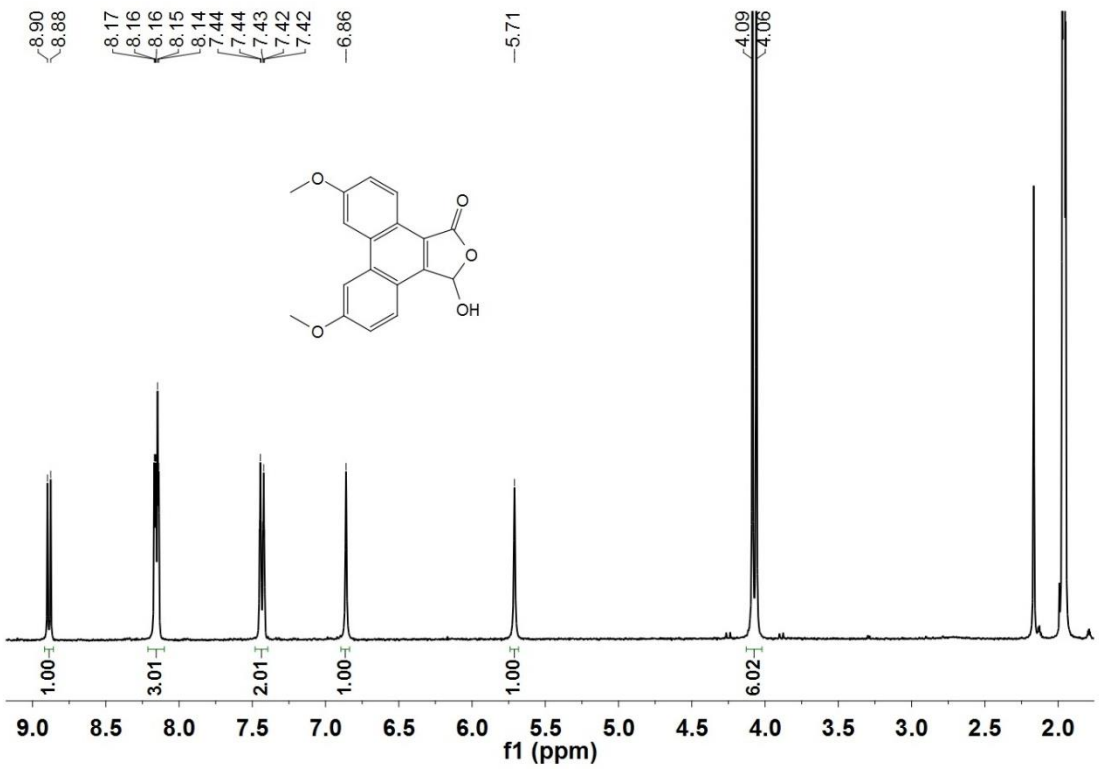

Figure S19. ^{1}H NMR spectrum of **3**(OMe) in CD_3CN.

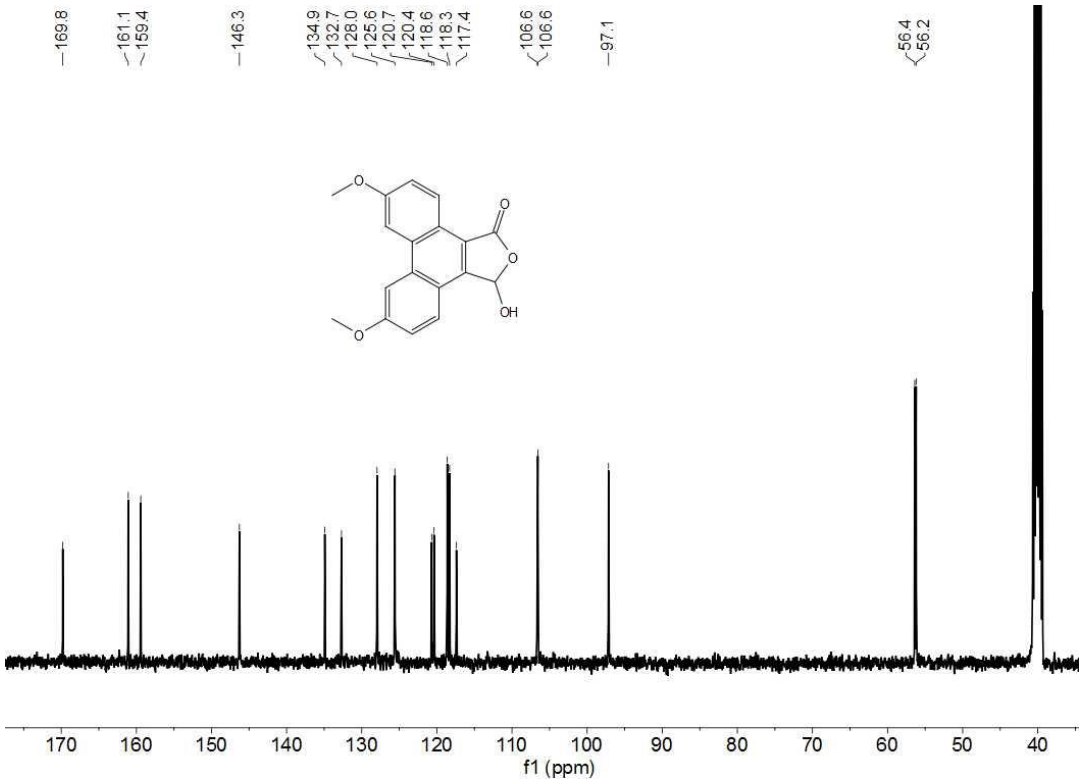

Figure S20. ^{13}C NMR spectrum of **3**(OMe) in DMSO-d_6.

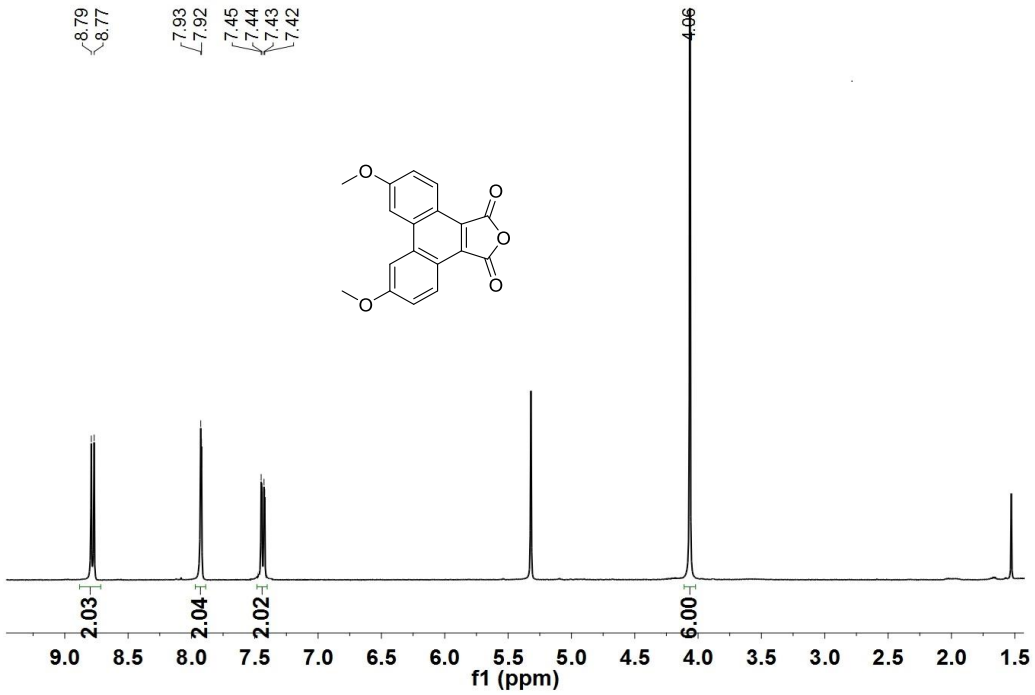

Figure S21. ^{1}H NMR spectrum of **5**(OMe) in CD_2Cl_2.

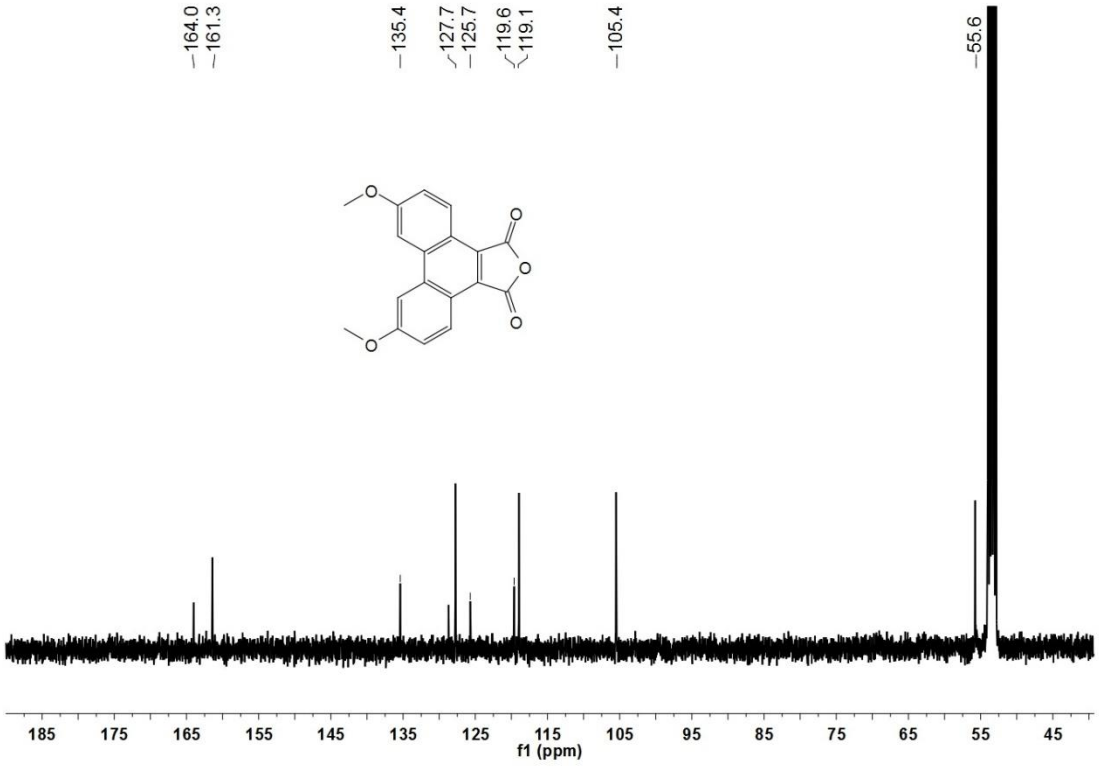

Figure S22. ^{13}C NMR spectrum of **5**(OMe) in CD_2Cl_2.

X-ray Crystallography

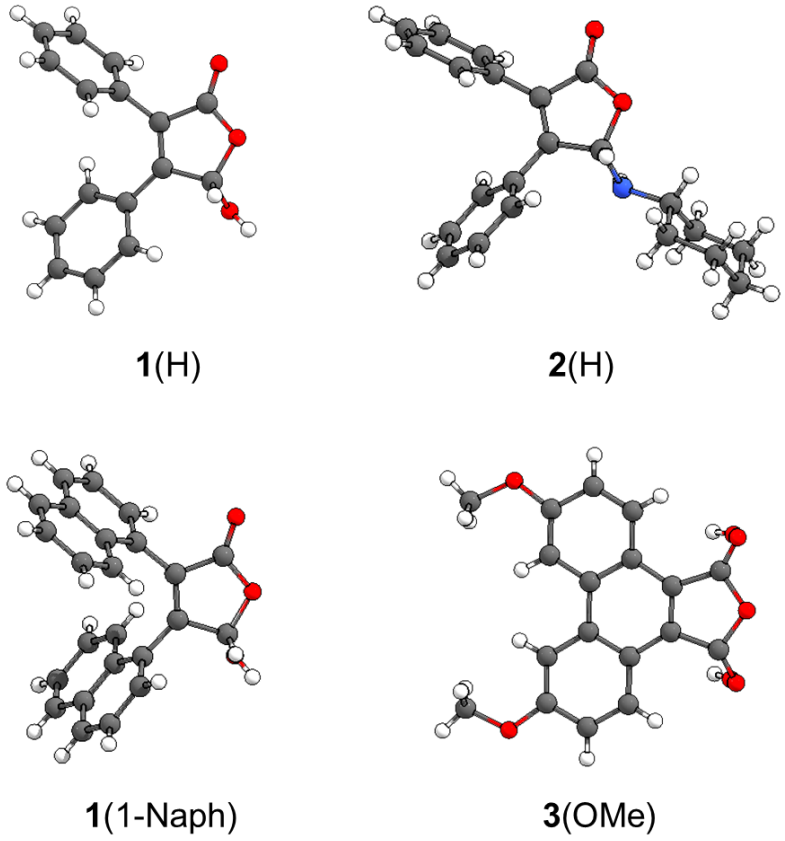

Figure S23. Crystal structures of **1**(H), **2**(H), **1**(1-Naph), and **3**(OMe).

Table S1. Summary of crystallographic data.

Compound	**1**(H)	**2**(H)	**1**(1-Naph)	**3**(OMe)
Formula	$C_{16}H_{12}O_3$	$C_{22}H_{23}NO_2$	$C_{52}H_{39}O_8$	$C_{18}H_{13}O_5$
Formula weight	252.27	333.43	791.88	309.30
T/*K*	193(2)	293(2)	293(2)	293(2)
Crystallization solvent	methanol	methanol	1,4-dioxane	methanol
Color	white	white	white	white
Crystal system	trigonal	monoclinic	monoclinic	monoclinic
Space group	*R*3	$P2_1/n$	$P2_1/n$	$P2_1/c$
a / Å	58.9340(3)	12.1850(4)	7.3767(10)	3.9730(4)
b / Å	58.9340(3)	6.4590(2)	27.2161(5)	20.4290(17)
c / Å	5.7790(4)	23.6610(9)	19.7147(5)	17.7190(15)
α / °	90.000	90.000	90.000	90.000
β / °	90.000	96.458(5)	94.144(2)	94.915(15)
γ / °	120.000	90.000	90.000	90.000
V/ Å^3	17382.40(16)	1850.40(11)	3947.67(14)	1433(2)
Z	54	4	4	4
D_x / g cm^{-3}	1.301	1.197	1.332	1.434
μ / mm^{-1}	0.090	0.076	0.463	0.105
F(000)	7132	712	1664	644
θ range / °	2.073 to 27.493	2.547 to 27.540	2.547 to 27.540	3.603 to 27.458
GOF on F^2	1.037	1.051	1.080	1.043
R_1 [$I > 2\sigma(I)$]	0.1395	0.0495	0.0830	0.1310
wR_2 (all data)	0.2933	0.1362	0.2312	0.2807

3. DCC with Amines

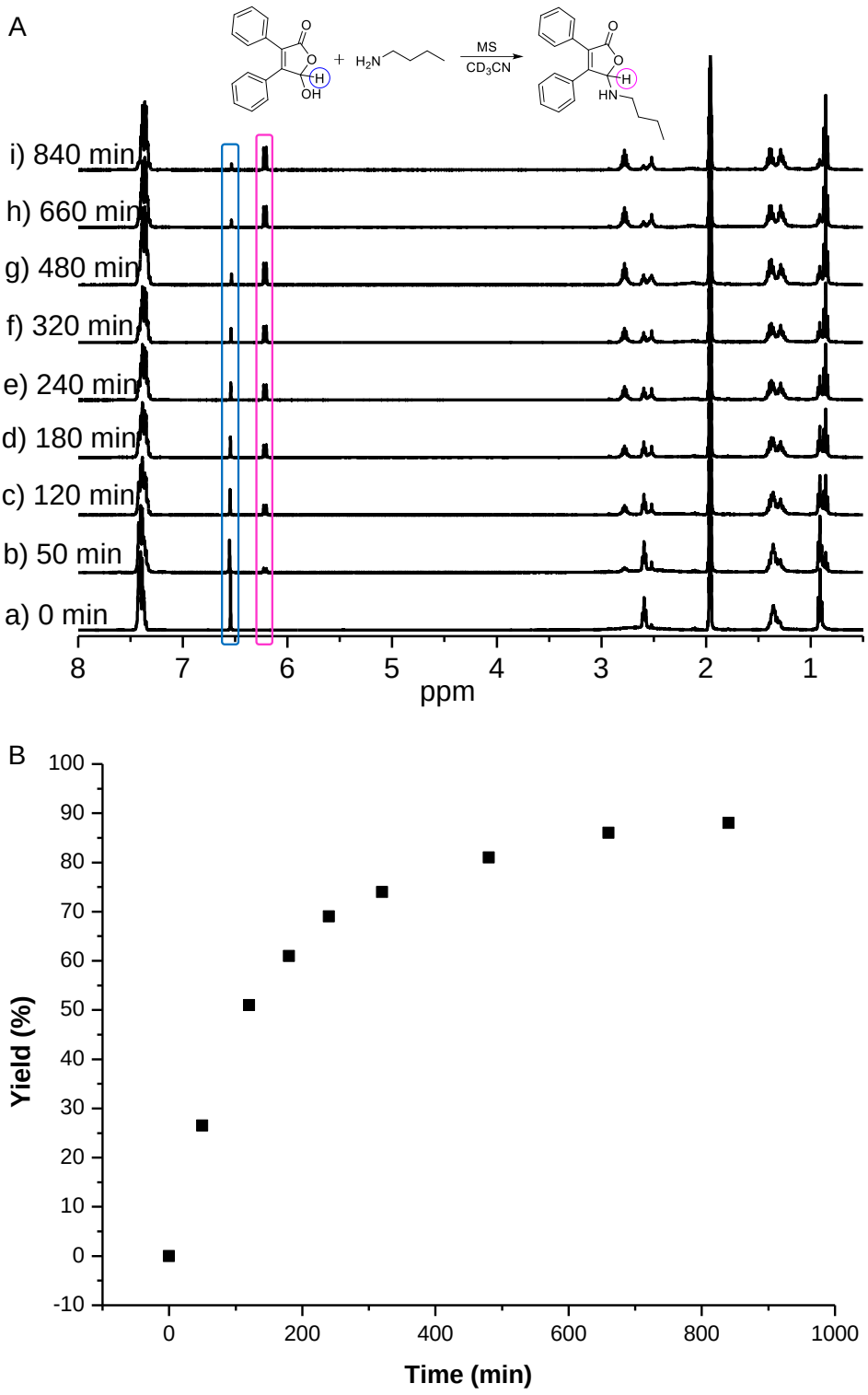

Figure S24. (A) ^{1}H NMR spectra of the reaction of **1**(H) and 1-butylamine (1.2 equiv.) in CD_3CN at varied time. (B) Kinetic curve of the reaction of **1**(H) and 1-butylamine.

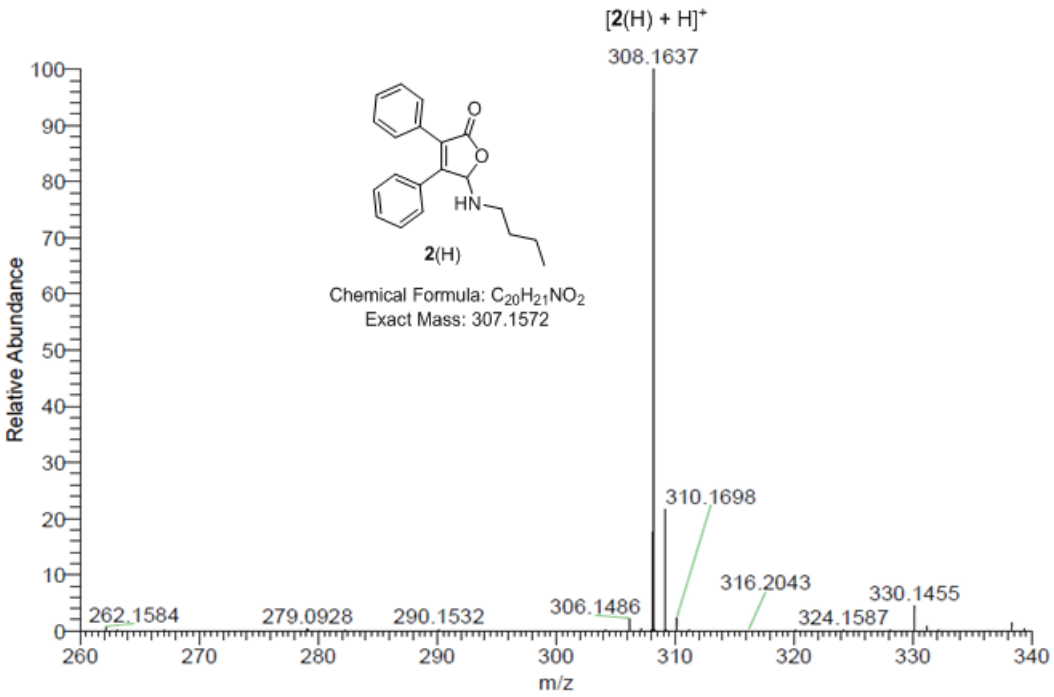

Figure S25. ESI mass spectrum of the reaction of **1**(H) and 1-butylamine in CH_3CN.

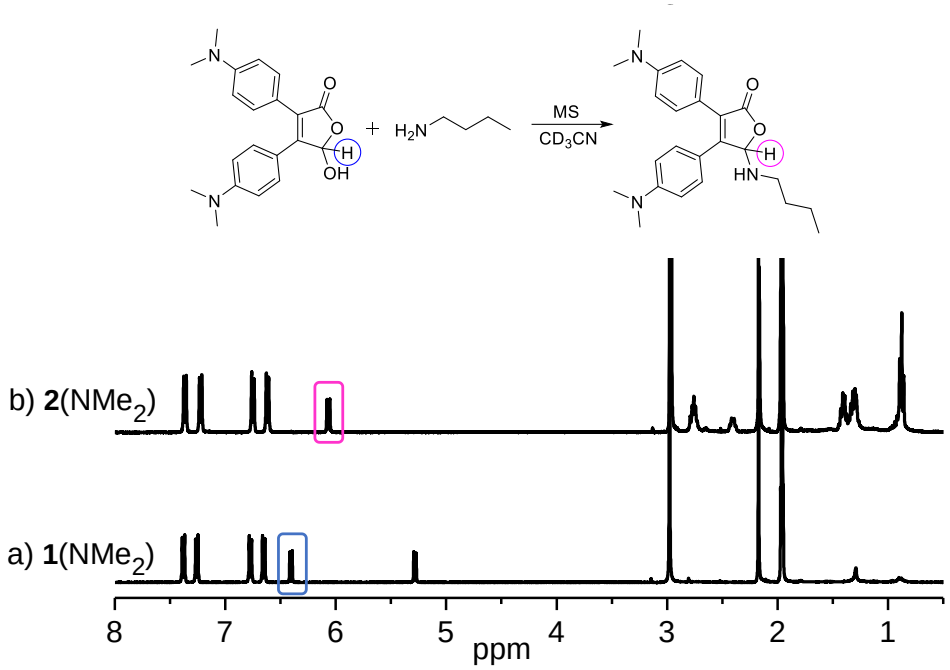

Figure S26. ^{1}H NMR spectra of **1**(NMe$_2$) (a) and its reaction with 1-butylamine (1.2 equiv., b) in CD_3CN.

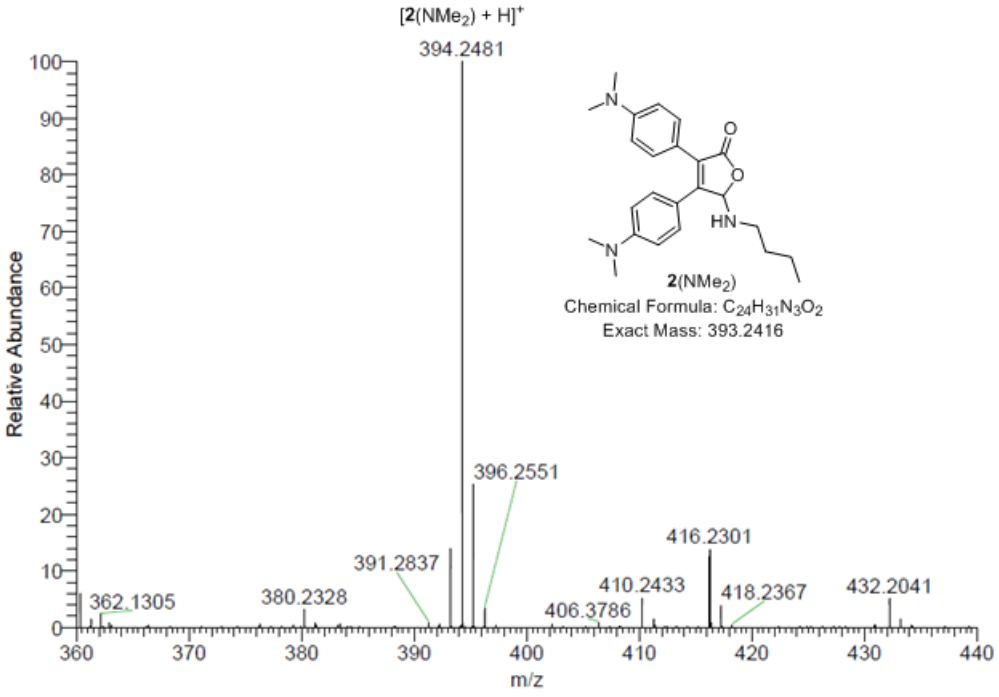

Figure S27. ESI mass spectrum of the reaction of **1**(NMe$_2$) and 1-butylamine in CH_3CN.

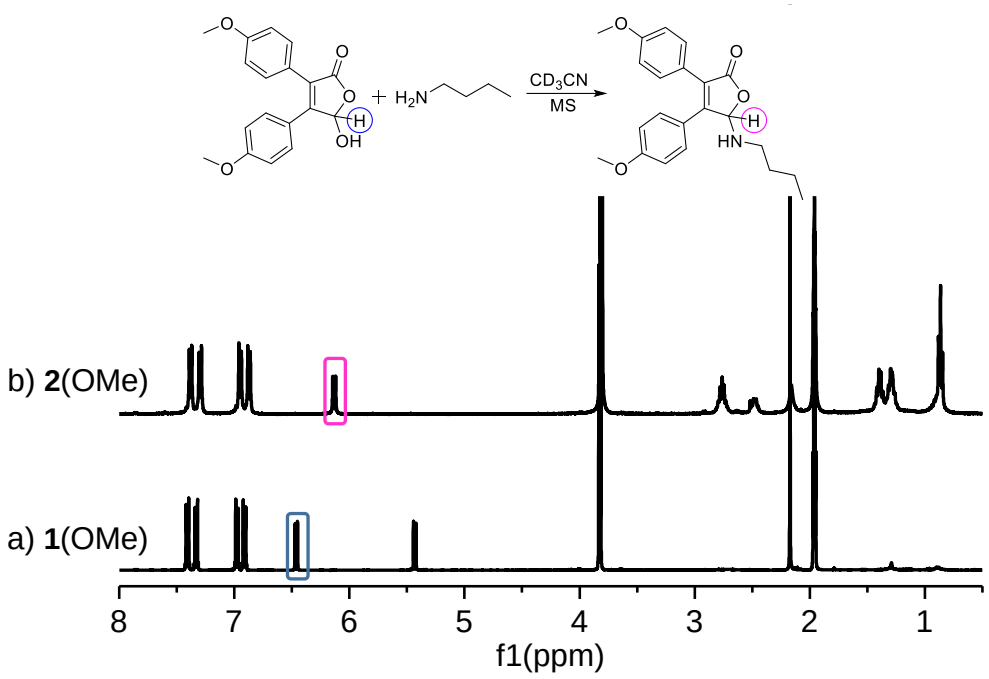

Figure S28. ^{1}H NMR spectra of **1**(OMe) (a) and its reaction with 1-butylamine (1.2 equiv., b) in CD_3CN.

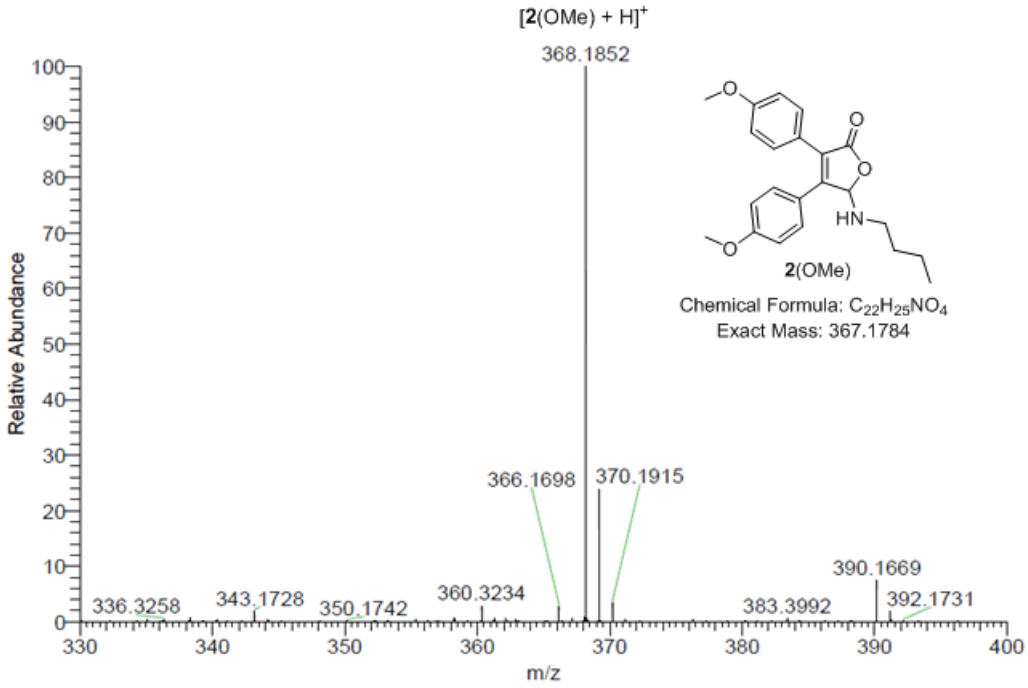

Figure S29. ESI mass spectrum of the reaction of **1**(OMe) and 1-butylamine in CH_3CN.

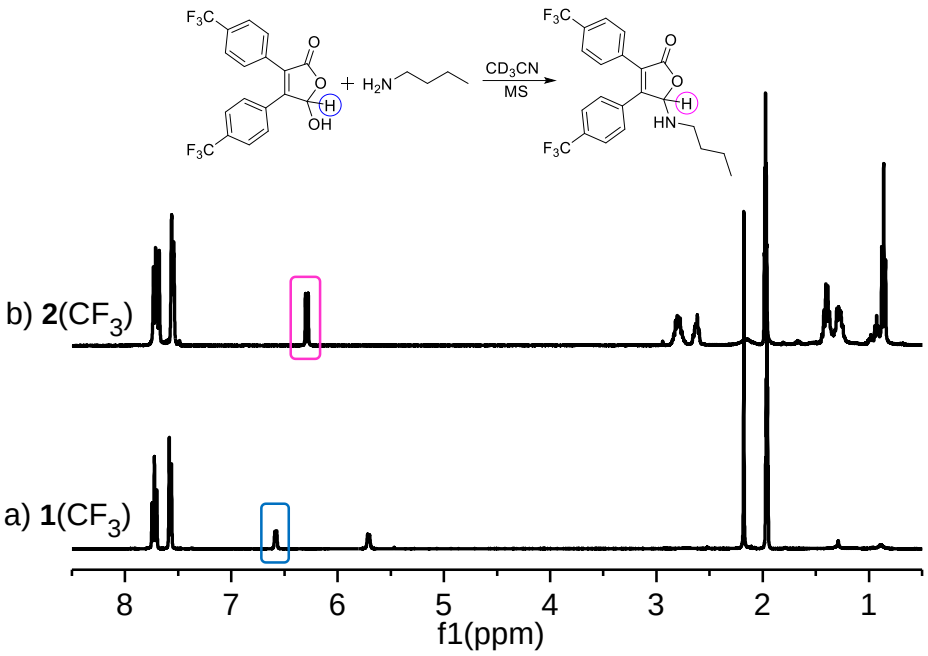

Figure S30. ^{1}H NMR spectra of **1**(CF_3) (a) and its reaction with 1-butylamine (1.2 equiv., b) in CD_3CN.

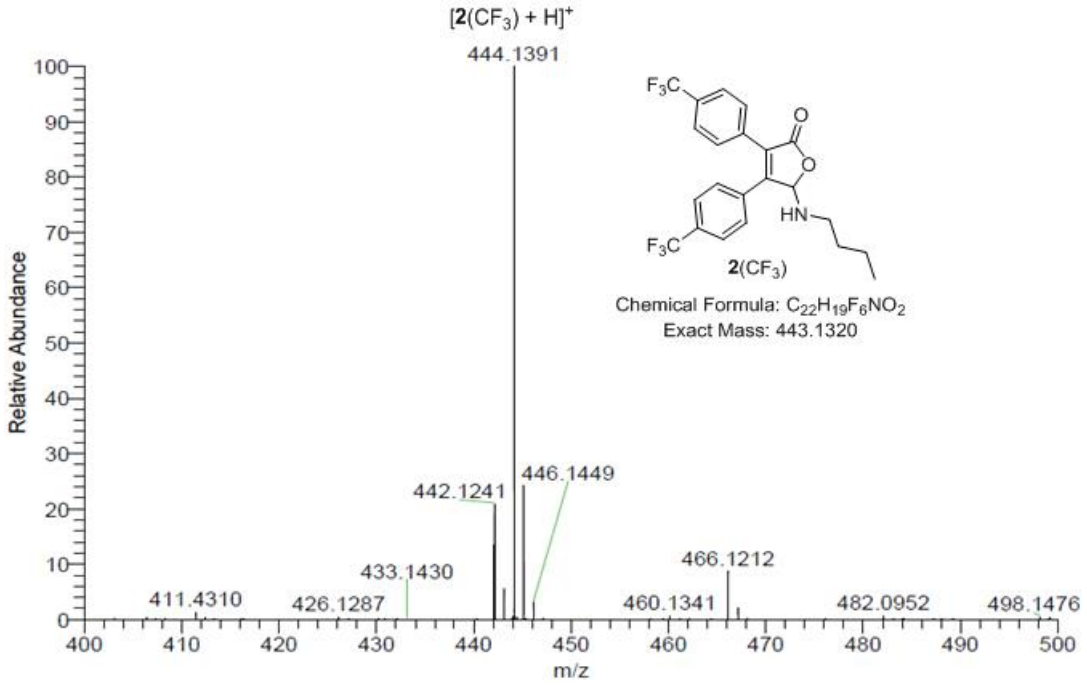

Figure S31. ESI mass spectrum of the reaction of **1**(CF_3) and 1-butylamine in CH_3CN.

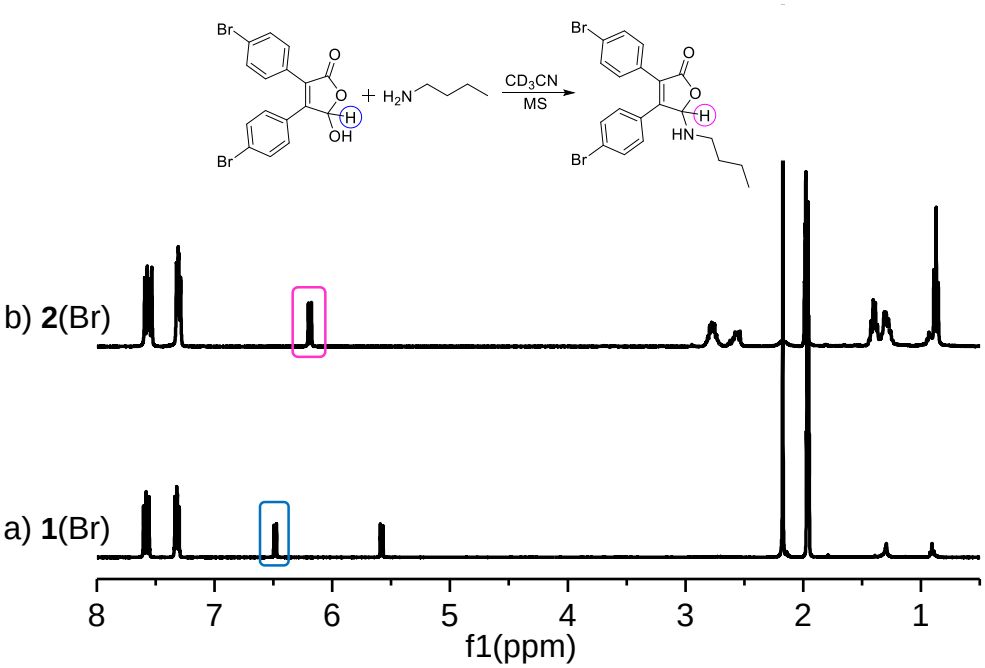

Figure S32. ^{1}H NMR spectra of **1**(Br) (a) and its reaction with 1-butylamine (1.2 equiv., b) in CD_3CN.

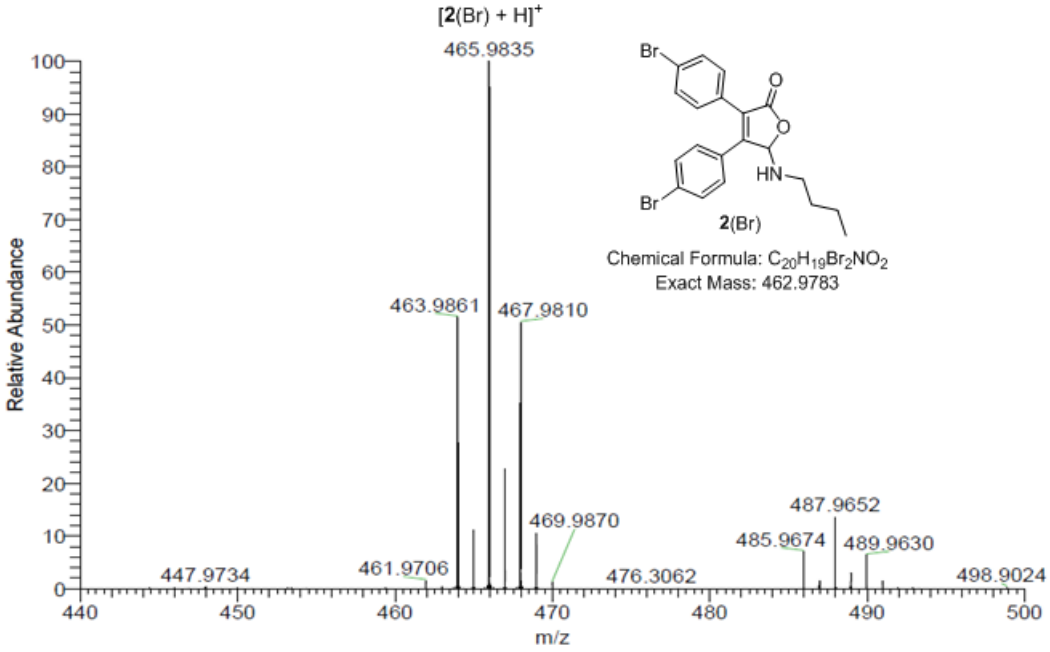

Figure S33. ESI mass spectrum of the reaction of **1**(Br) and 1-butylamine in CH_3CN.

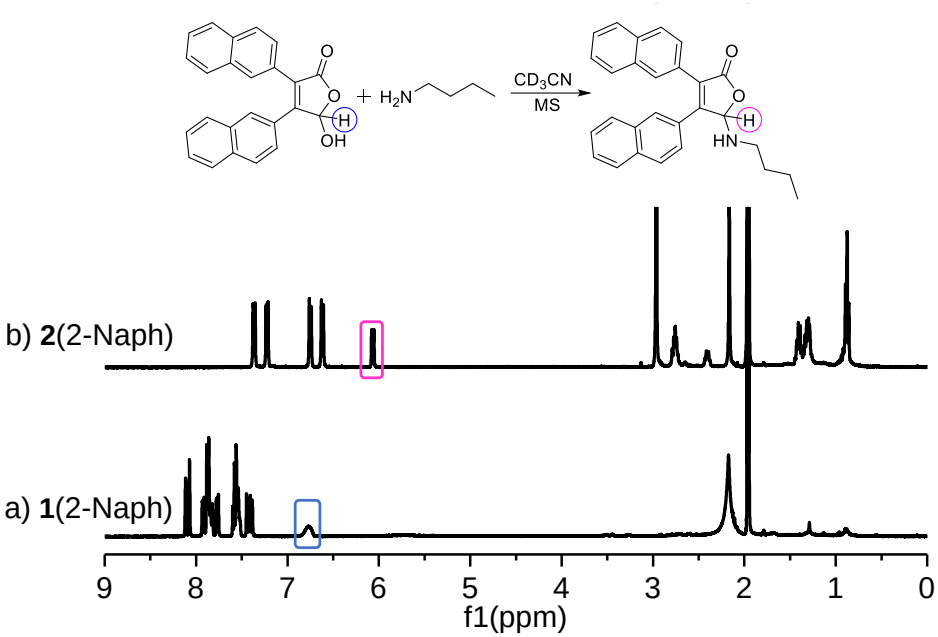

Figure S34. ^{1}H NMR spectra of **1**(2-Naph) (a) and its reaction with 1-butylamine (1.2 equiv., b) in CD_3CN.

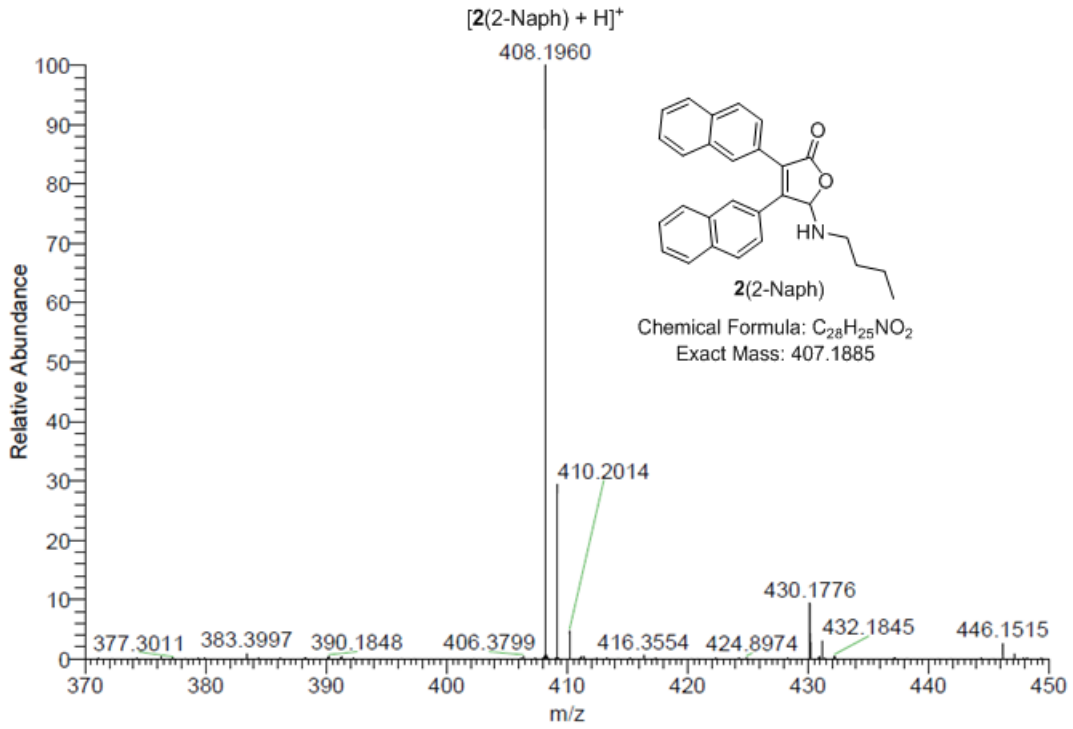

Figure S35. ESI mass spectrum of the reaction of **1**(2-Naph) and 1-butylamine in CH_3CN.

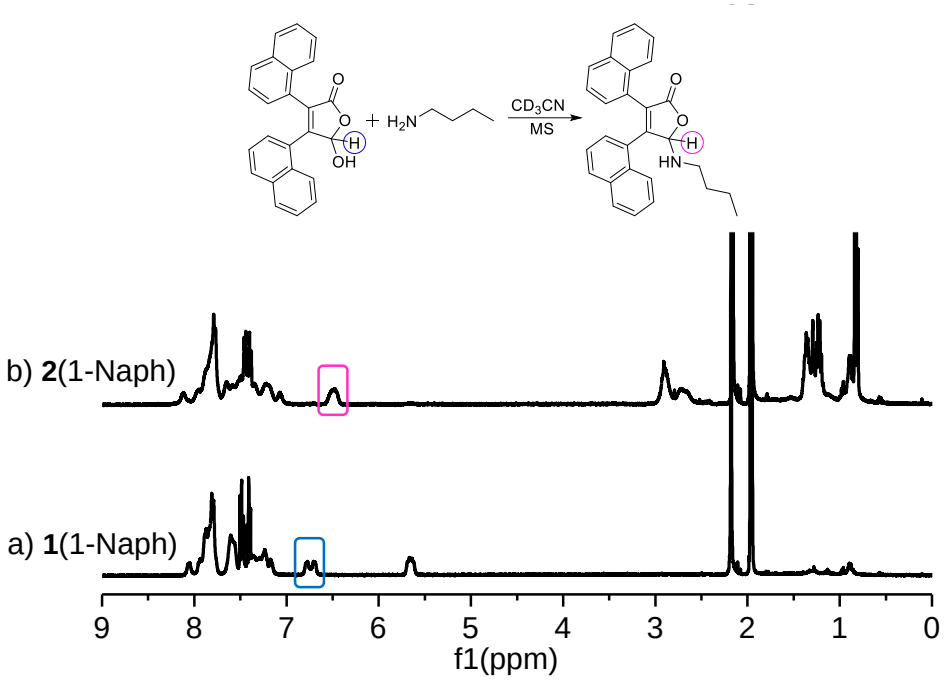

Figure S36. ^{1}H NMR spectra of **1**(1-Naph) (a) and its reaction with 1-butylamine (1.2 equiv., b) in CD_3CN.

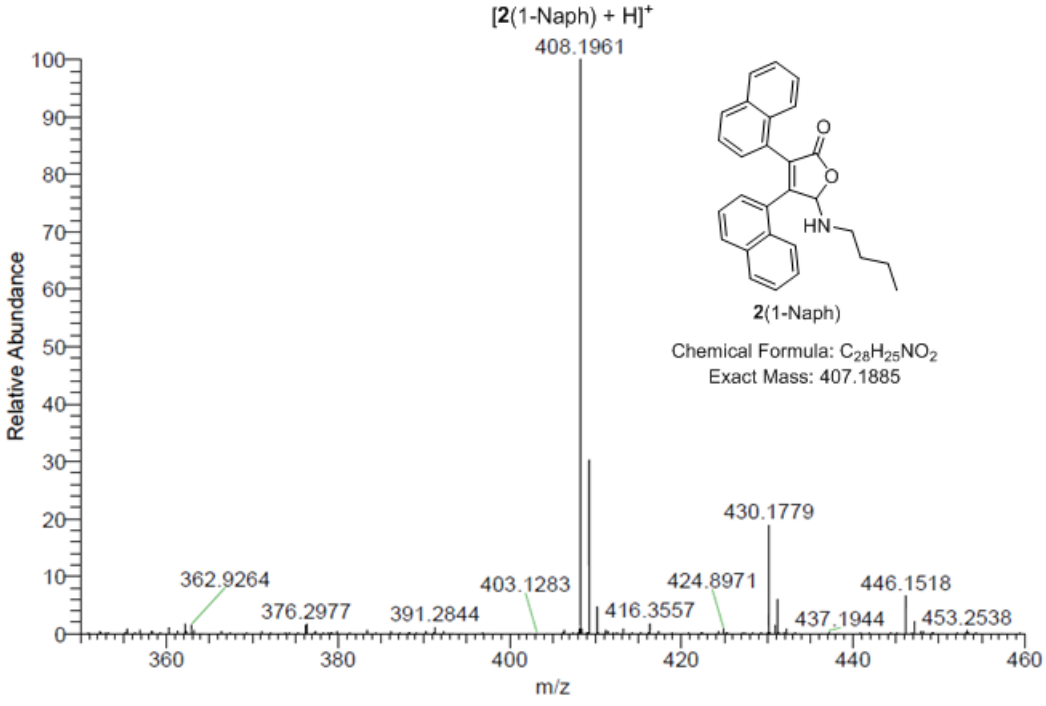

Figure S37. ESI mass spectrum of the reaction of **1**(1-Naph) and 1-butylamine in CH_3CN.

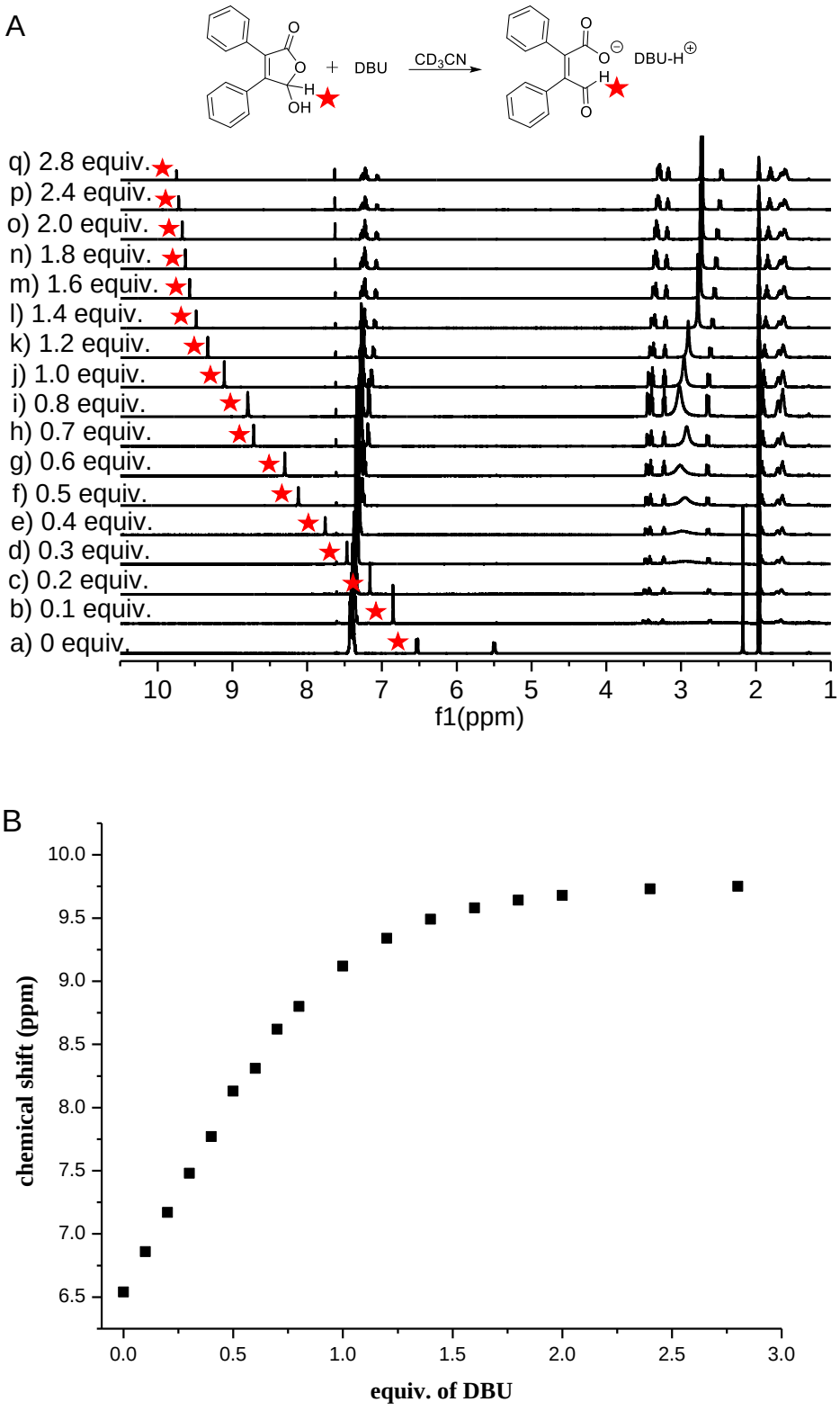

Figure S38. ^{1}H NMR spectra (A) as well as titration curve (B) of **1**(H) (16.7 mM) with DBU (0-2.8 equiv.) in CD_3CN. The tracked proton is marked with a star.

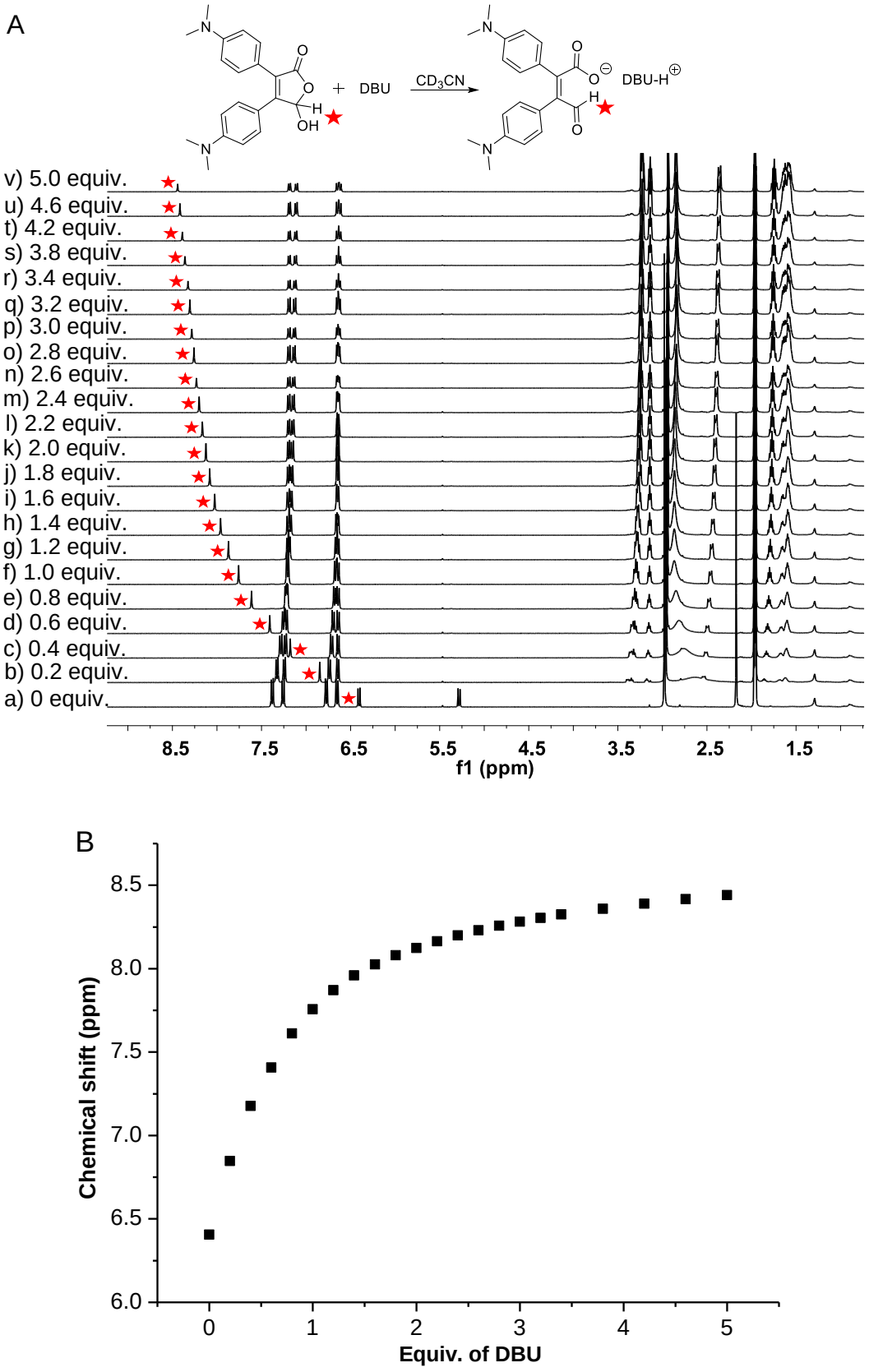

Figure S39. ^{1}H NMR spectra (A) as well as titration curve (B) of **1**(NMe_2) (16.7 mM) with DBU (0-5.0 equiv.) in CD_3CN. The tracked proton is marked with a star.

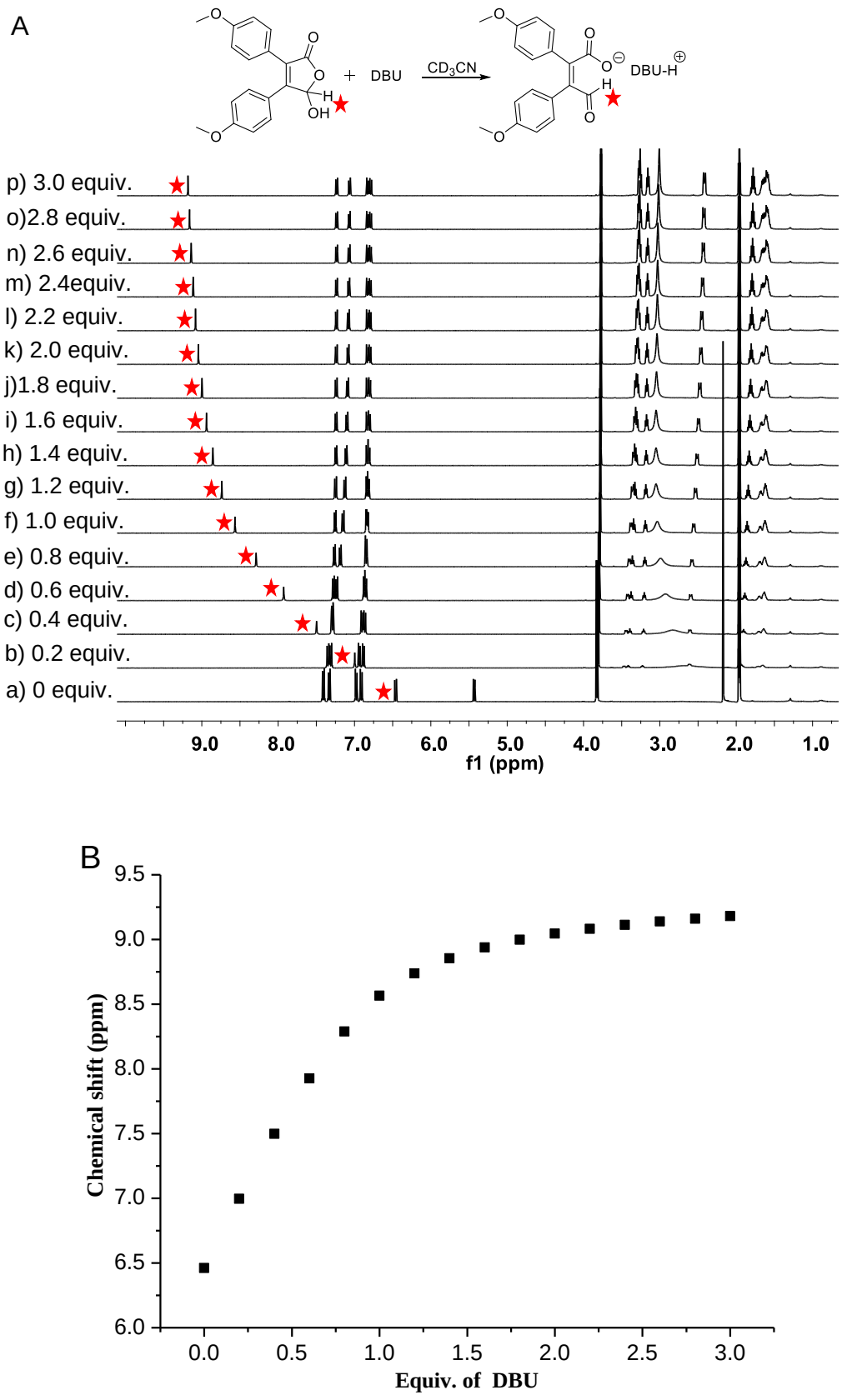

Figure S40. ^{1}H NMR spectra (A) as well as titration curve (B) of **1**(OMe) (16.7 mM) with DBU (0-3.0 equiv.) in CD_3CN. The tracked proton is marked with a star.

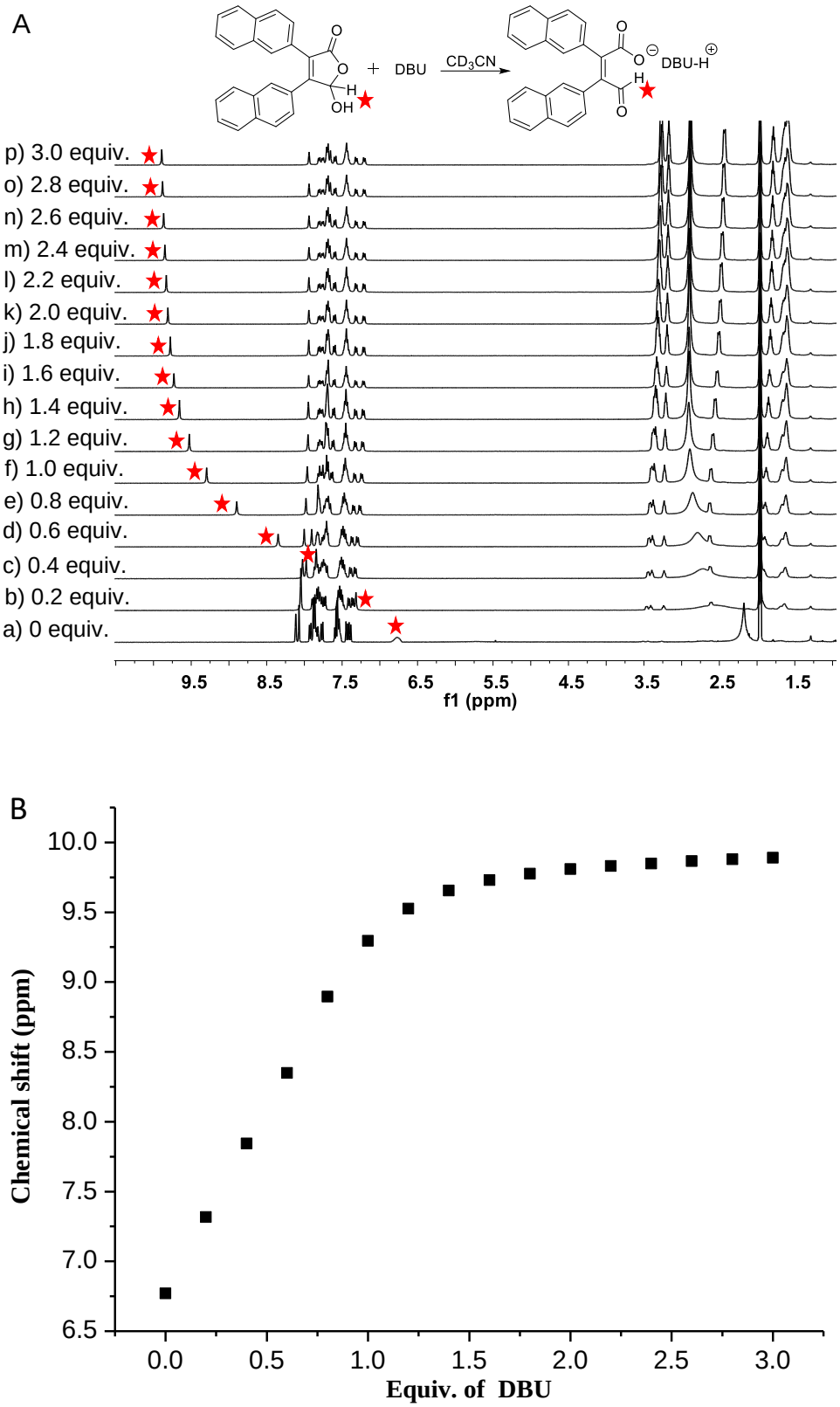

Figure S41. ^{1}H NMR spectra (A) as well as titration curve (B) of **1**(2-Naph) (16.7 mM) with DBU (0-3.0 equiv.) in CD_3CN. The tracked proton is marked with a star.

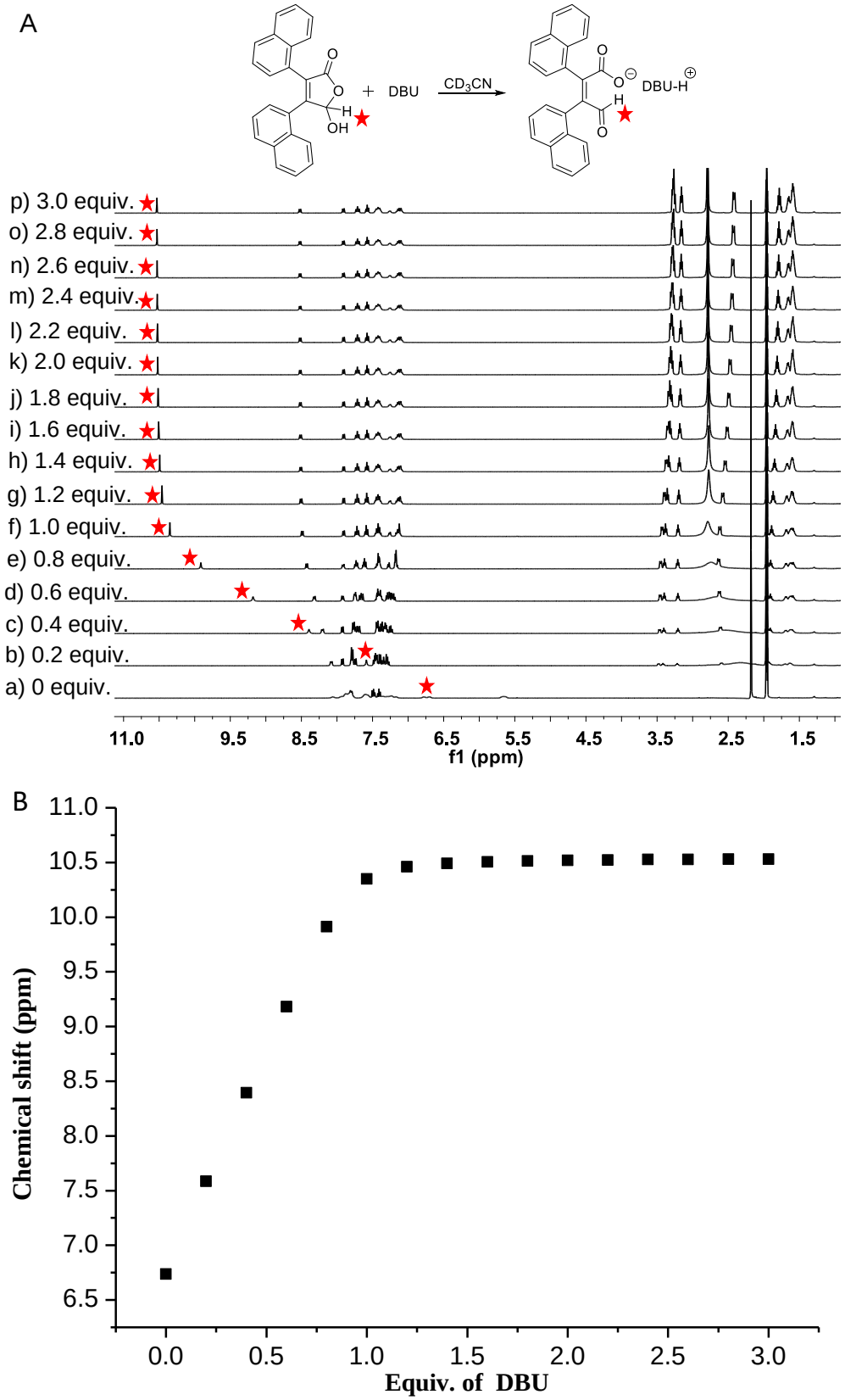

Figure S42. ^{1}H NMR spectra (A) as well as titration curve (B) of **1**(1-Naph) (16.7 mM) with DBU (0-3.0 equiv.) in CD_3CN. The tracked proton is marked with a star.

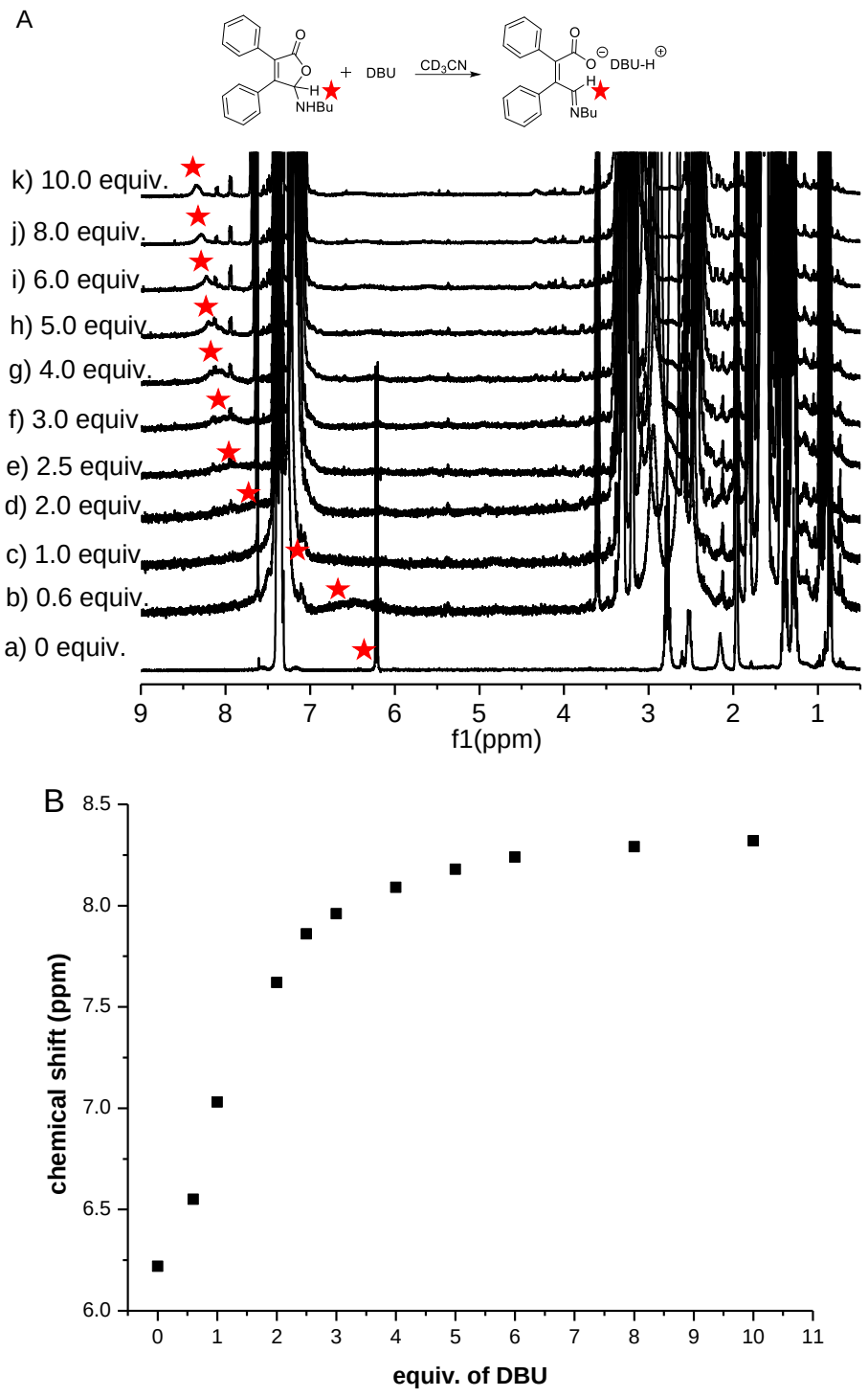

Figure S43. ^{1}H NMR spectra (A) as well as titration curve (B) of **2**(H) (16.7 mM) with DBU (0-10 equiv.) in CD_3CN. The tracked proton is marked with a star.

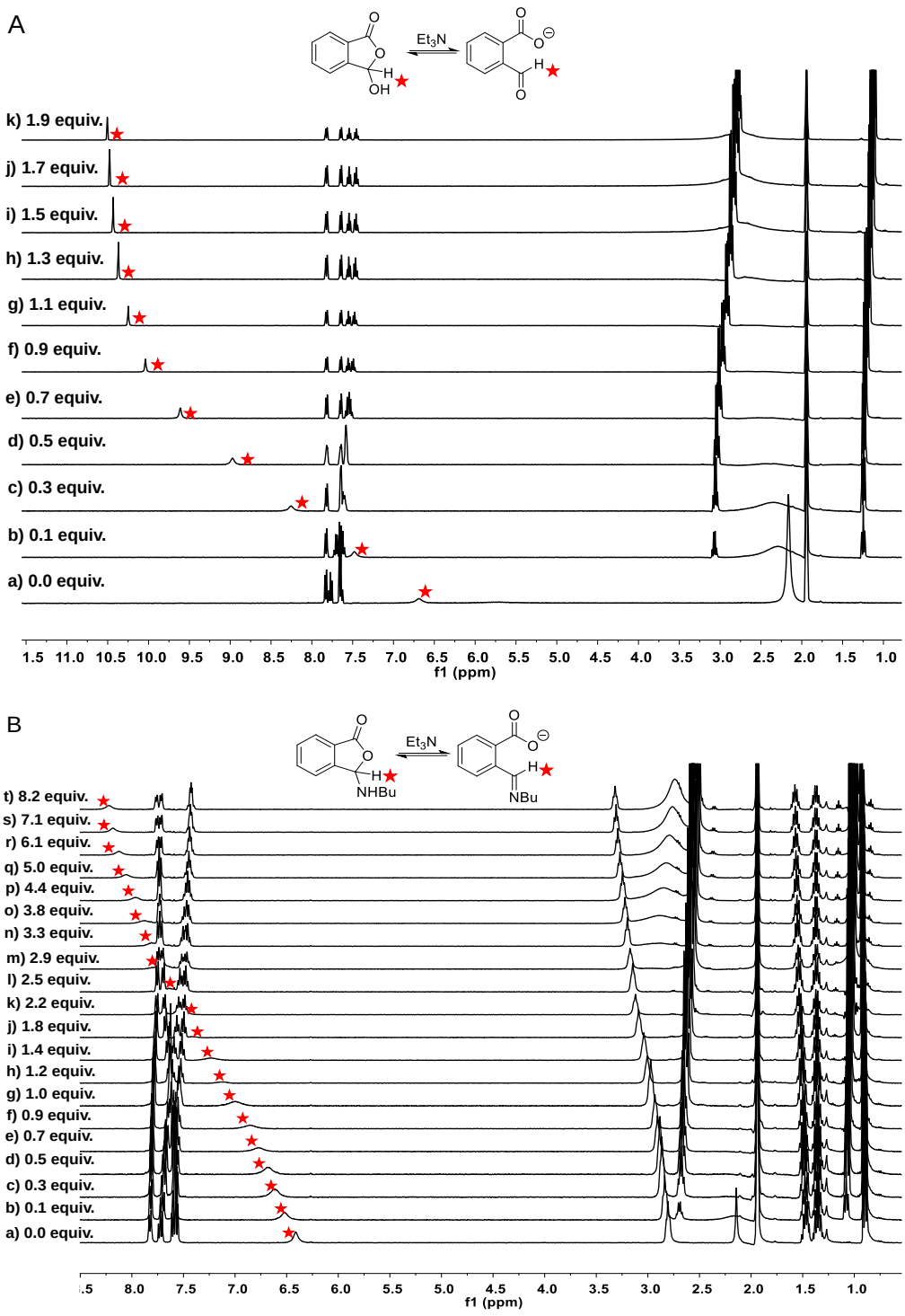

Figure S44. ^{1}H NMR spectra of 2-formylbenzoic acid (16.7 mM, A) as well as its 1-butylamine adduct (B) with triethylamine (0-1.9 equiv. for panel A, 0-8.2 equiv. for panel B) in CD_3CN. The tracked proton is marked with a star.

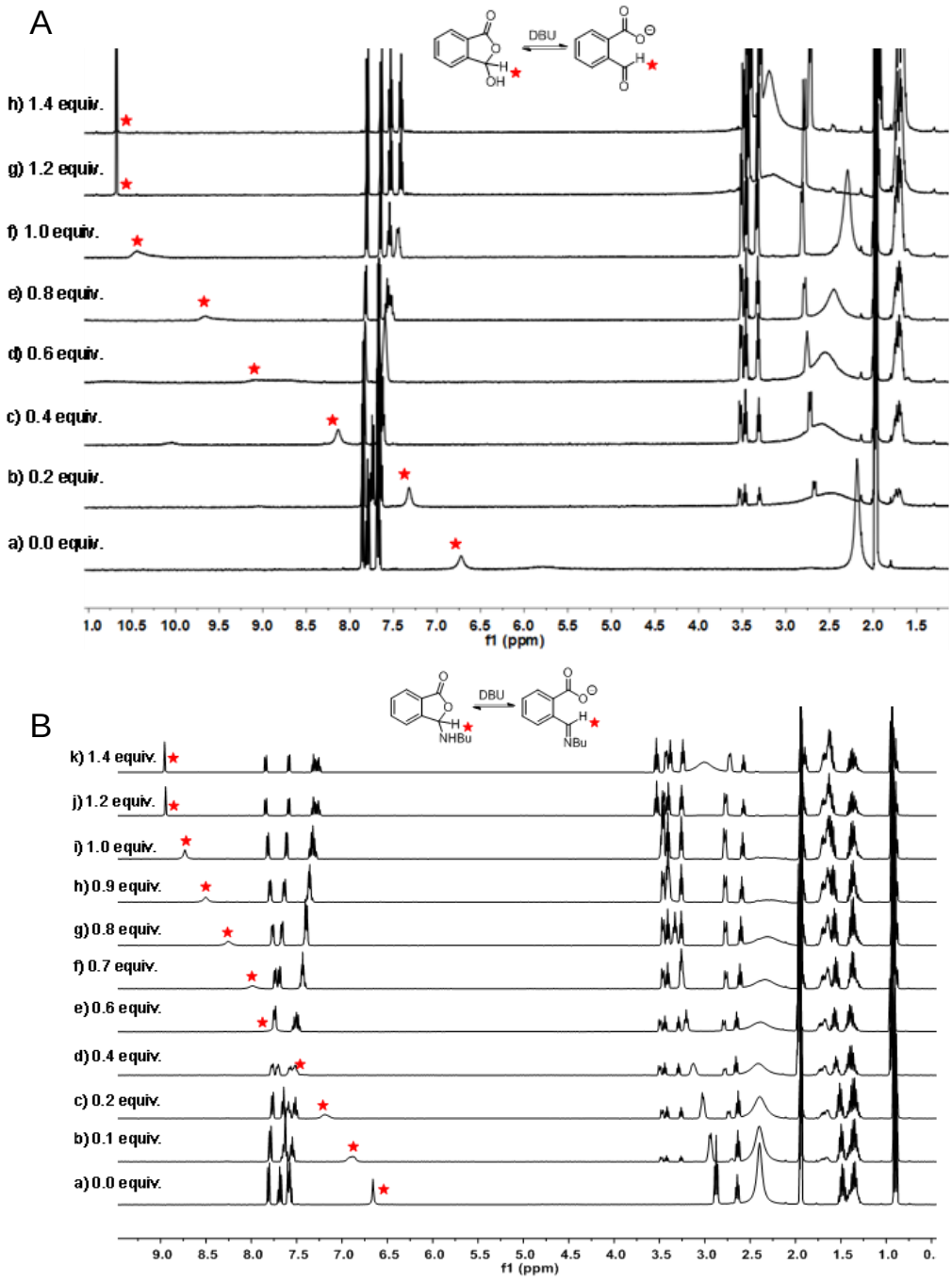

Figure S45. ^{1}H NMR spectra of 2-formylbenzoic acid (16.7 mM, A) as well as its 1-butylamine adduct (B) with DBU (0-1.4 equiv.) in CD_3CN. The tracked proton is marked with a star.

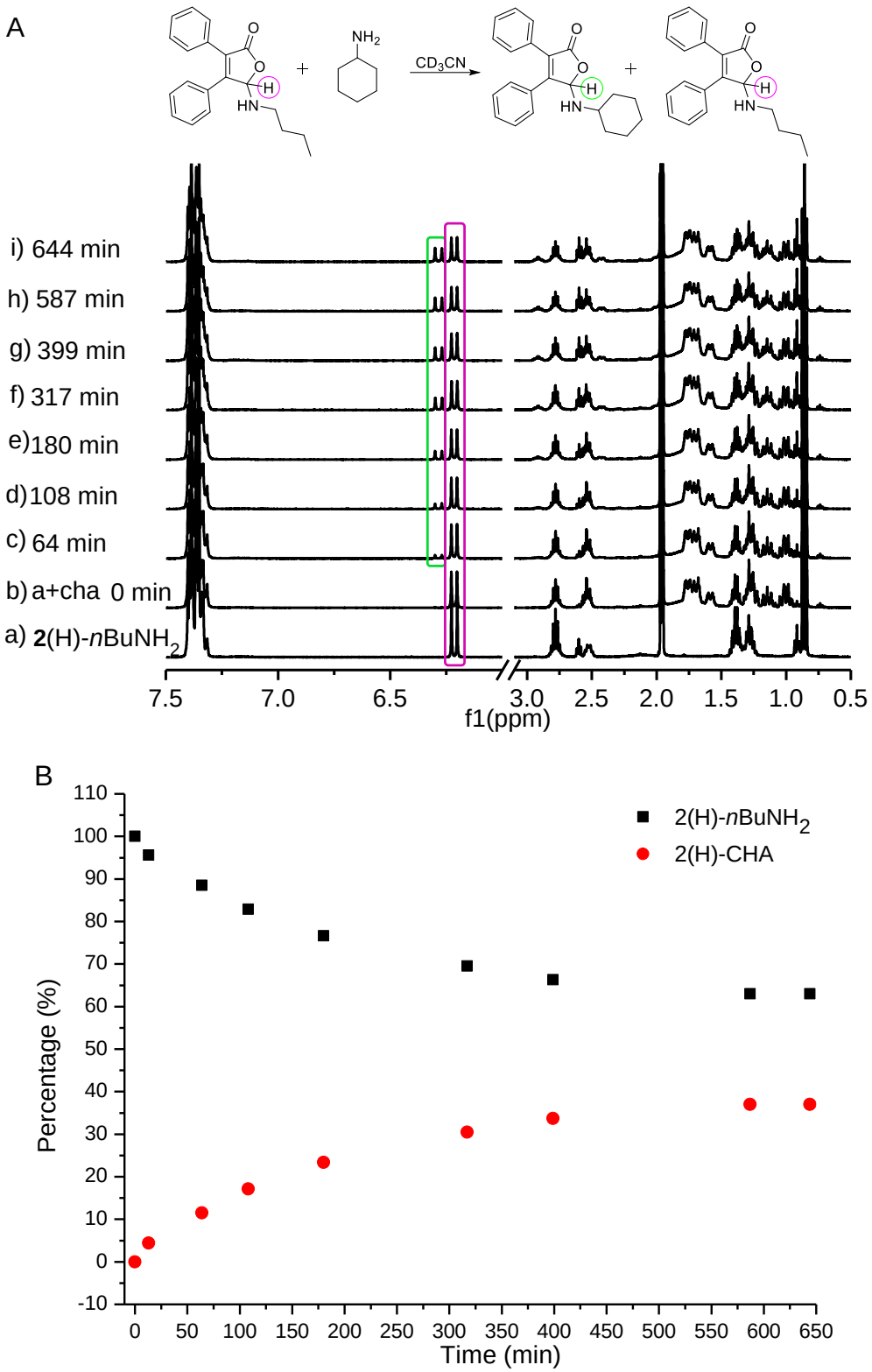

Figure S46. (A) ^{1}H NMR spectra of **2**(H)-*n*BuNH$_2$ (16.7 mM) and its dynamic amine exchange with cyclohexylamine (CHA, 1.2 equiv.) in CD$_3$CN at varied time. (B) The change in the percentage of **2**(H)-*n*BuNH$_2$ and **2**(H)-CHA. The equilibrium was reached after 10 h, with 63 % of **2**(H)-*n*BuNH$_2$ and 37 % of **2**(H)-CHA (K = 0.35).

4. Solution and Solid-State Luminescence

The influence of solvent environment on the PL property of the compounds can be understood using the Lippert-Mataga equation, a model that describes the interactions between the solvent and the dipole moment of solute. The Lippert-Mataga equation is as follows:

$$hc(\nu_a - \nu_f) = hc(\nu_a^0 - \nu_f^0) + \frac{2(\mu_e - \mu_g)^2}{a^3} f(\varepsilon, n)$$

where μ_e is the dipole moment of excited state, μ_g is the dipole moment of ground state, h is the Plank constant, c is the light speed in vacuum, a is the solvent Onsager cavity radius derived from the Avogadro number (N), molecular weight (M), and density (d = 1.0 g/cm^3), $\nu_a - \nu_f$ is the Stokes shift, $f(\varepsilon, n)$ is the orientational polarizability of solvents, ε is the solvent dielectric constant, and n is the solvent refractive index.[S6] μ_g can be estimated by DFT calculation. $f(\varepsilon, n)$ and a can be calculated respectively as follows:

$$f(\varepsilon, n) = \left[\frac{\varepsilon - 1}{2\varepsilon + 1} - \frac{n^2 - 1}{2n^2 + 1}\right], \; a = (3M \; / \; 4N\pi d)^{1/3}$$

All DFT calculations were carried out with the Gaussian 09 D.01 Package.[S7] The ground states of **1**(NMe_2), **1**(OMe), **1**(2-Naph) and **1**(1-Naph) were calculated at the level of B3LYP/6-31G (d, p), a commonly used level for the precise geometry optimization. The excited states are then calculated with time-dependent DFT (TDDFT) method in different solutions (PCM: DMSO, THF, hexane) at the M06-2X/6-31G (d, p) level.

Table S2. Detailed absorption and emission peak positions of **1**(NMe_2) in different solvents.

Solvents	ε	n	f (ε, n)	λ_a [nm]	λ_f [nm]	ν_a-ν_f [cm^{-1}]
hexane	1.9	1.3751	0.0012	377	488	6033
toluene	2.38	1.4969	0.0133	387	504	5999
$CHCl_3$	4.7	1.4467	0.145	396	529	6349
ethyl acetate	6.03	1.3718	0.2	384	511	6472
THF	7.39	1.4073	0.2073	379	508	6700
dichloromethane	8.9	1.4242	0.2168	391	535	6884
DMSO	48.9	1.4795	0.2637	392	545	7162
CH_3CN	37.5	1.3442	0.3054	385	543	7558

Table S3. Detailed absorption and emission peak positions of **1**(OMe) in different solvents.

Solvents	ε	n	f (ε, n)	λ_a [nm]	λ_f [nm]	ν_a-ν_f [cm^{-1}]
hexane	1.9	1.3751	0.0012	321	431	7951
toluene	2.38	1.4969	0.0133	327	441	7905
$CHCl_3$	4.7	1.4467	0.145	328	448	8166
ethyl acetate	6.03	1.3718	0.2	321	445	8533
THF	7.39	1.4073	0.2073	323	441	8284
dichloromethane	8.9	1.4242	0.2168	326	448	8353
DMSO	48.9	1.4795	0.2637	326	448	8353
CH_3CN	37.5	1.3442	0.3054	320	445	8778

Table S4. Detailed absorption and emission peak positions of **1**(2-Naph) in different solvents.

Solvents	ε	n	f (ε, n)	λ_a [nm]	λ_f [nm]	ν_a-ν_f [cm^{-1}]
hexane	1.9	1.3751	0.0012	316	418	7722
toluene	2.38	1.4969	0.0133	321	429	7843
$CHCl_3$	4.7	1.4467	0.145	324	437	7981
ethyl acetate	6.03	1.3718	0.2	319	434	8306
THF	7.39	1.4073	0.2073	318	427	8027
dichloromethane	8.9	1.4242	0.2168	321	438	8322
DMSO	48.9	1.4795	0.2637	323	443	8386
CH_3CN	37.5	1.3442	0.3054	319	440	8620

Table S5. Detailed absorption and emission peak positions of **1**(1-Naph) in different solvents.

Solvents	ε	n	f (ε, n)	λ_a [nm]	λ_f [nm]	ν_a-ν_f [cm^{-1}]
hexane	1.9	1.3751	0.0012	284	436	1227
toluene	2.38	1.4969	0.0133	284	440	1248
$CHCl_3$	4.7	1.4467	0.145	284	443	1264
ethyl acetate	6.03	1.3718	0.2	283	447	1296
THF	7.39	1.4073	0.2073	291	443	1215
dichloromethane	8.9	1.4242	0.2168	283	449	1306
DMSO	48.9	1.4795	0.2637	285	459	1272
CH_3CN	37.5	1.3442	0.3054	283	447	1355

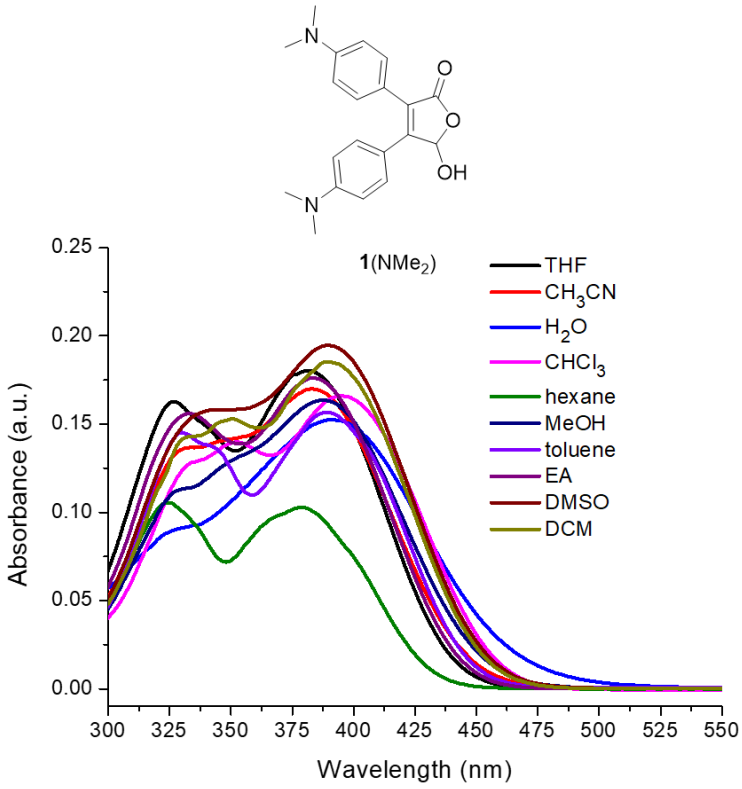

Figure S47. Absorption spectra of **1**(NMe_2) (10 μM) in different solvents.

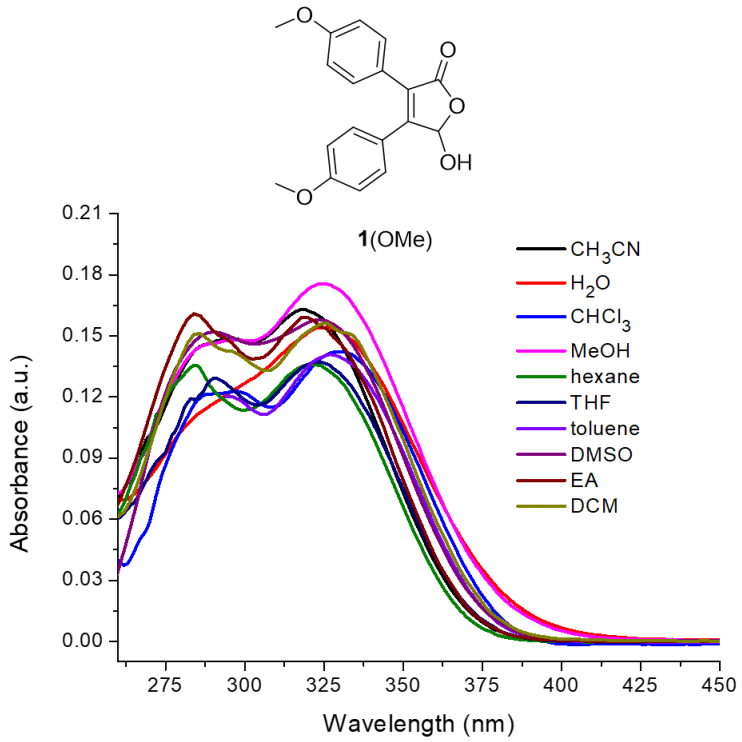

Figure S48. Absorption spectra of **1**(OMe) (10 μM) in different solvents.

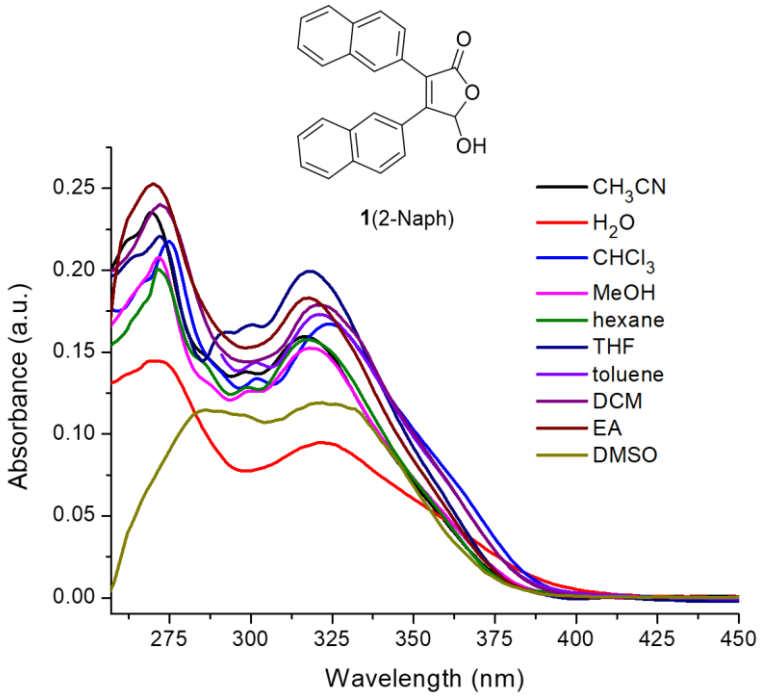

Figure S49. Absorption spectra of **1**(2-Naph) (10 μM) in different solvents.

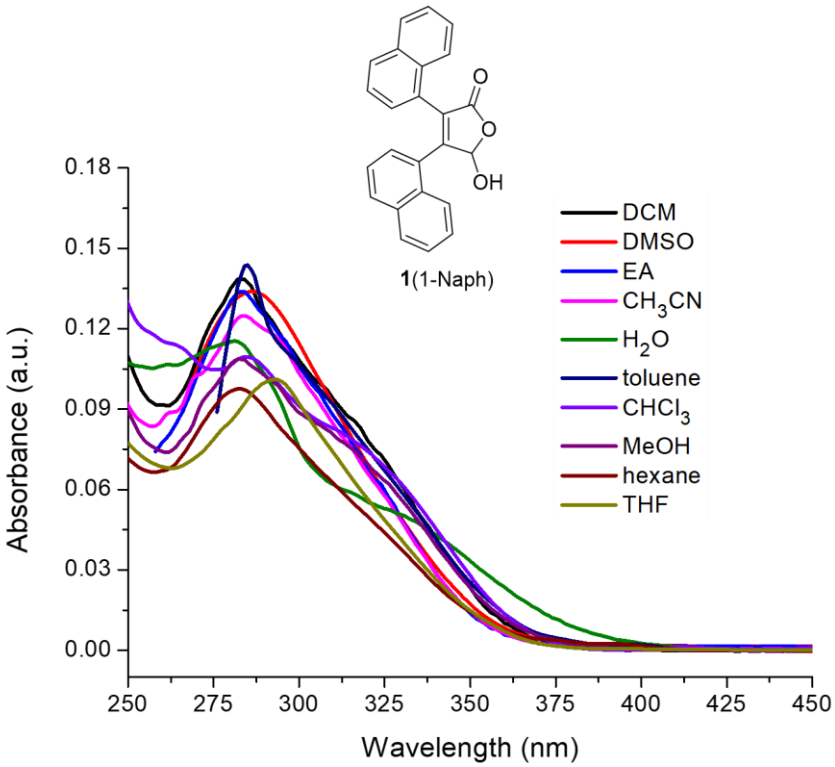

Figure S50. Absorption spectra of **1**(1-Naph) (10 μM) in different solvents.

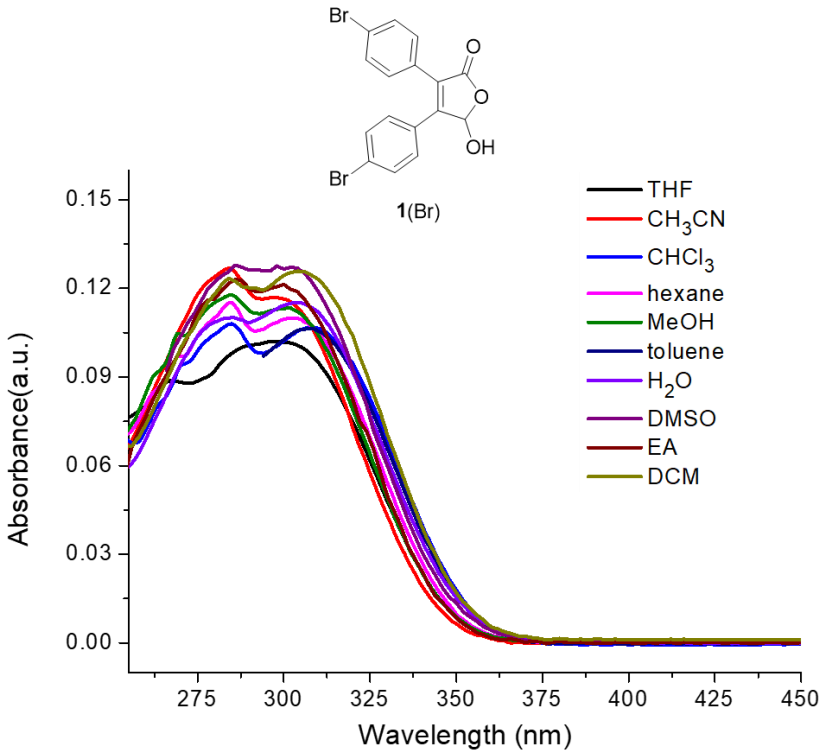

Figure S51. Absorption spectra of **1**(Br) (10 μM) in different solvents.

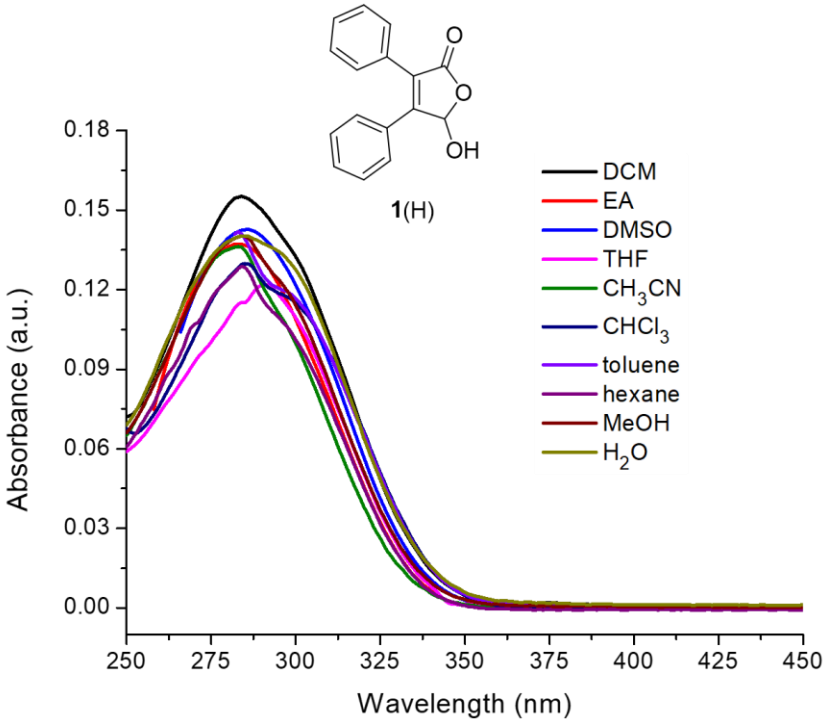

Figure S52. Absorption spectra of **1**(H) (10 μM) in different solvents.

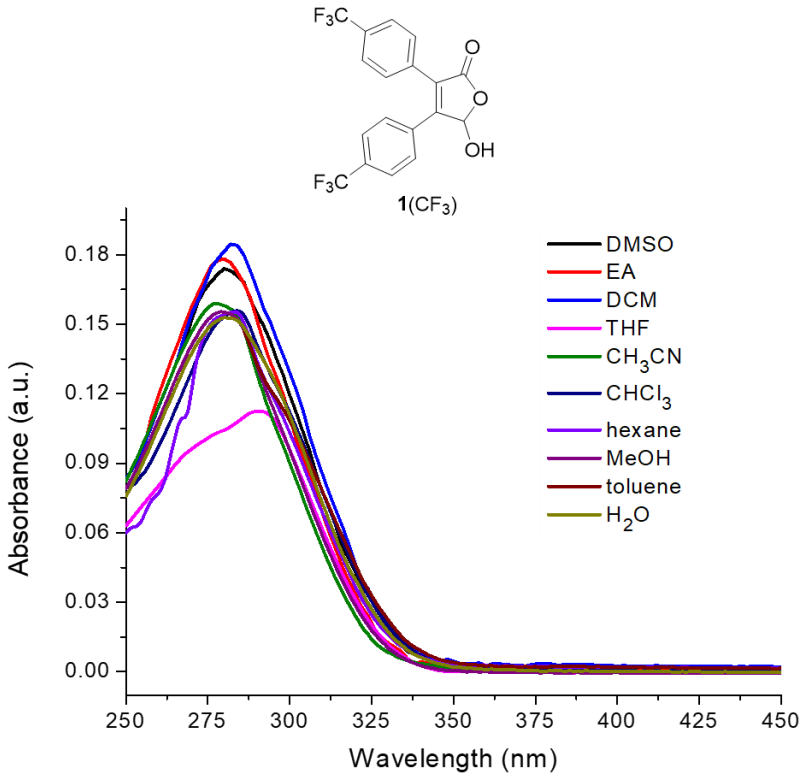

Figure S53. Absorption spectra of **1**(CF_3) (10 μM) in different solvents.

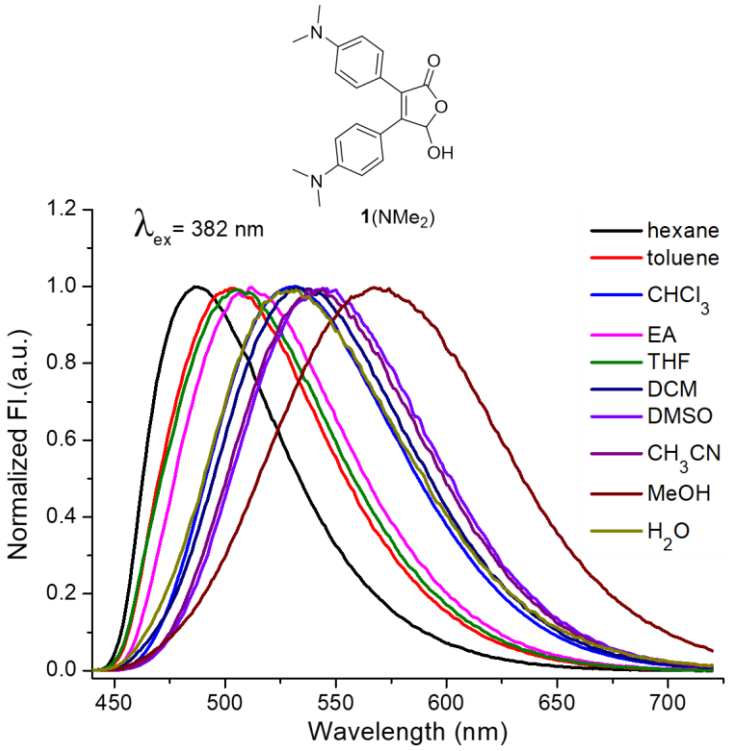

Figure S54. Normalized fluorescence spectra of **1**(NMe_2) (10 μM) in different solvents with excitation at 382 nm.

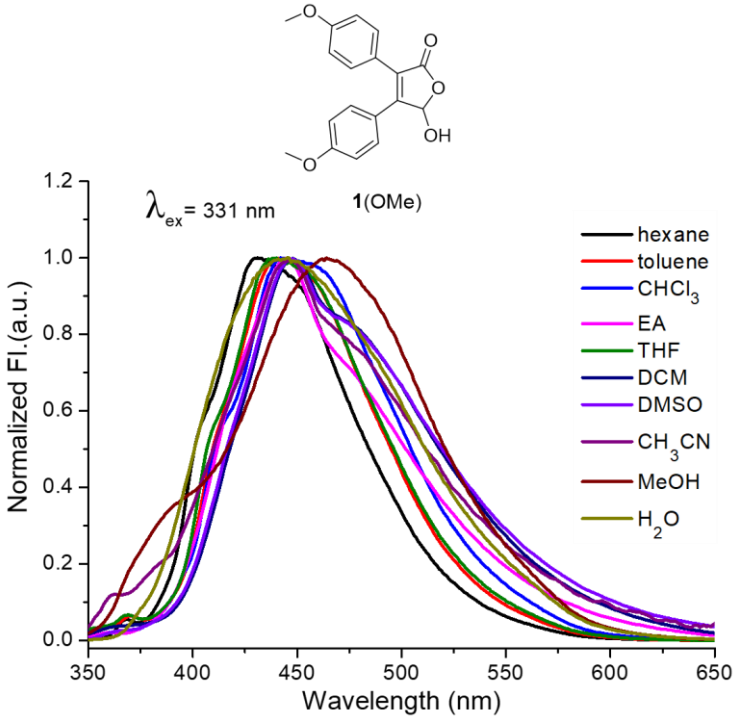

Figure S55. Normalized fluorescence spectra of **1**(OMe) (10 μM) in different solvents with excitation at 331 nm.

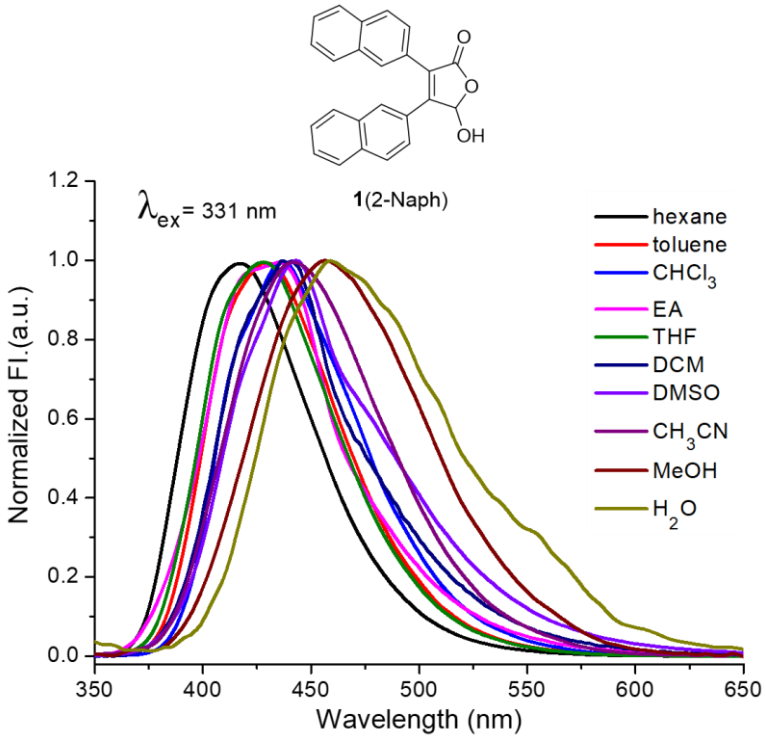

Figure S56. Normalized fluorescence spectra of **1**(2-Naph) (10 μM) in different solvents with excitation at 331 nm.

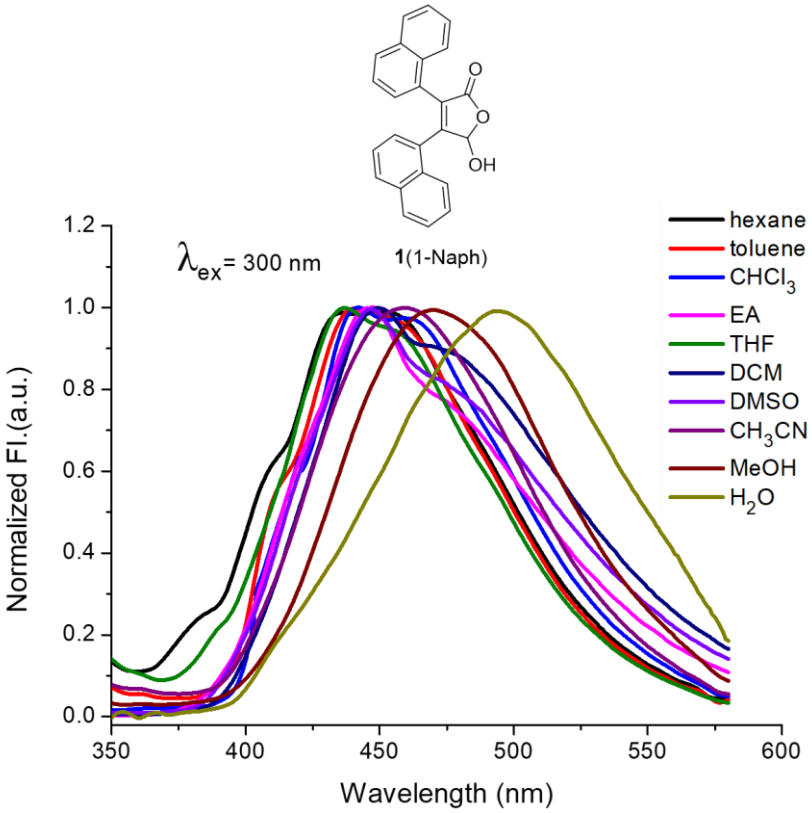

Figure S57. Normalized fluorescence spectra of **1**(1-Naph) (10 μM) in different solvents with excitation at 300 nm.

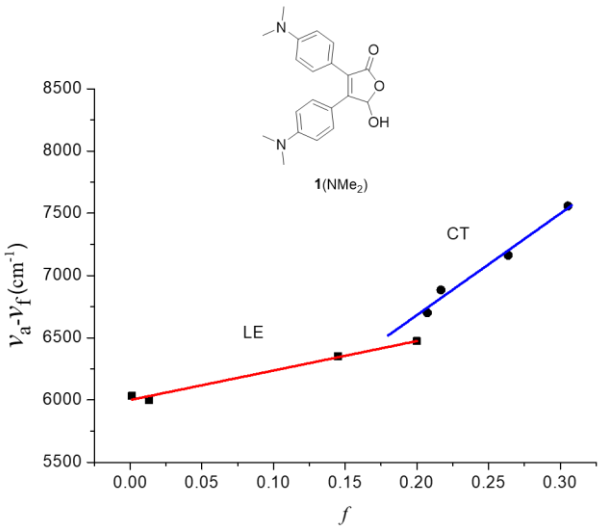

Figure S58. Solvatochromic Lippert–Mataga model of **1**(NMe_2). The fitted result of **1**(NMe_2) reflects a non-linear relationship between Stokes shift and solvent polarity. The slope of the fit is 8153 cm^{-1} (R^2 = 0.97) for high-polarity solvents and 2366 cm^{-1} (R^2 = 0.98) for low-polarity solvents. μ_e-μ_g were found to be 10.4 D in high-polarity solvents and 5.6 D in low-polarity solvents, respectively, according to the Lippert–Mataga equation. The dipole moments μ_e were found to be 19.0 D in high-polarity solvents and 14.2 D in low-polarity solvents, respectively. The smaller μ_e of 14.2 D can be attributed to a LE-like state, while the larger μ_e of 19.0 D should be treated as a CT-like state. The μ_e values obtained by theoretical calculations are 13.6 D in hexane (low-polarity solvent) and 17.4 D in DMSO (high-polarity solvent) respectively, and the results support experimental findings.

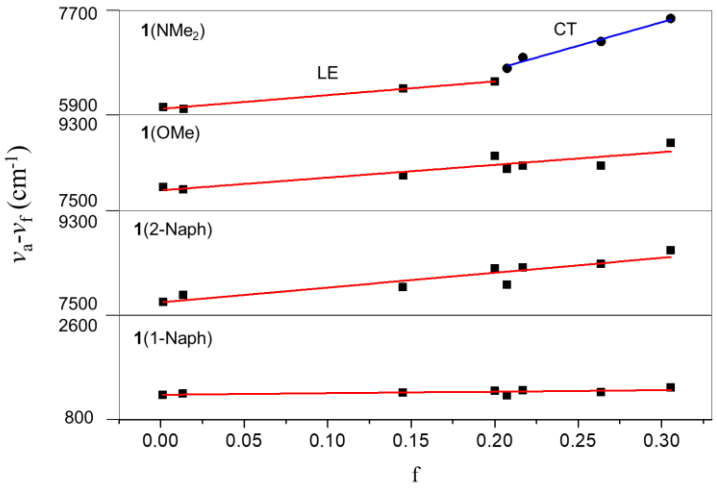

Figure S59. Solvatochromic Lippert–Mataga models of **1**(NMe_2), **1**(OMe), **1**(2-Naph), and **1**(1-Naph). Obviously, the overall fitted result of **1**(NMe_2) reflects a non-linear relationship between Stokes shift and solvent polarity. As for **1**(OMe), **1**(2-Naph), and **1**(1-Naph) a poor linear relationship between Stokes shift and solvent polarity (R^2 = 0.80, 0.84, and 0.33, respectively) and a small slope (2377 cm^{-1}, 2562 cm^{-1}, and 270 cm^{-1}, respectively) were observed, suggesting that the emission is dominated by LE state.

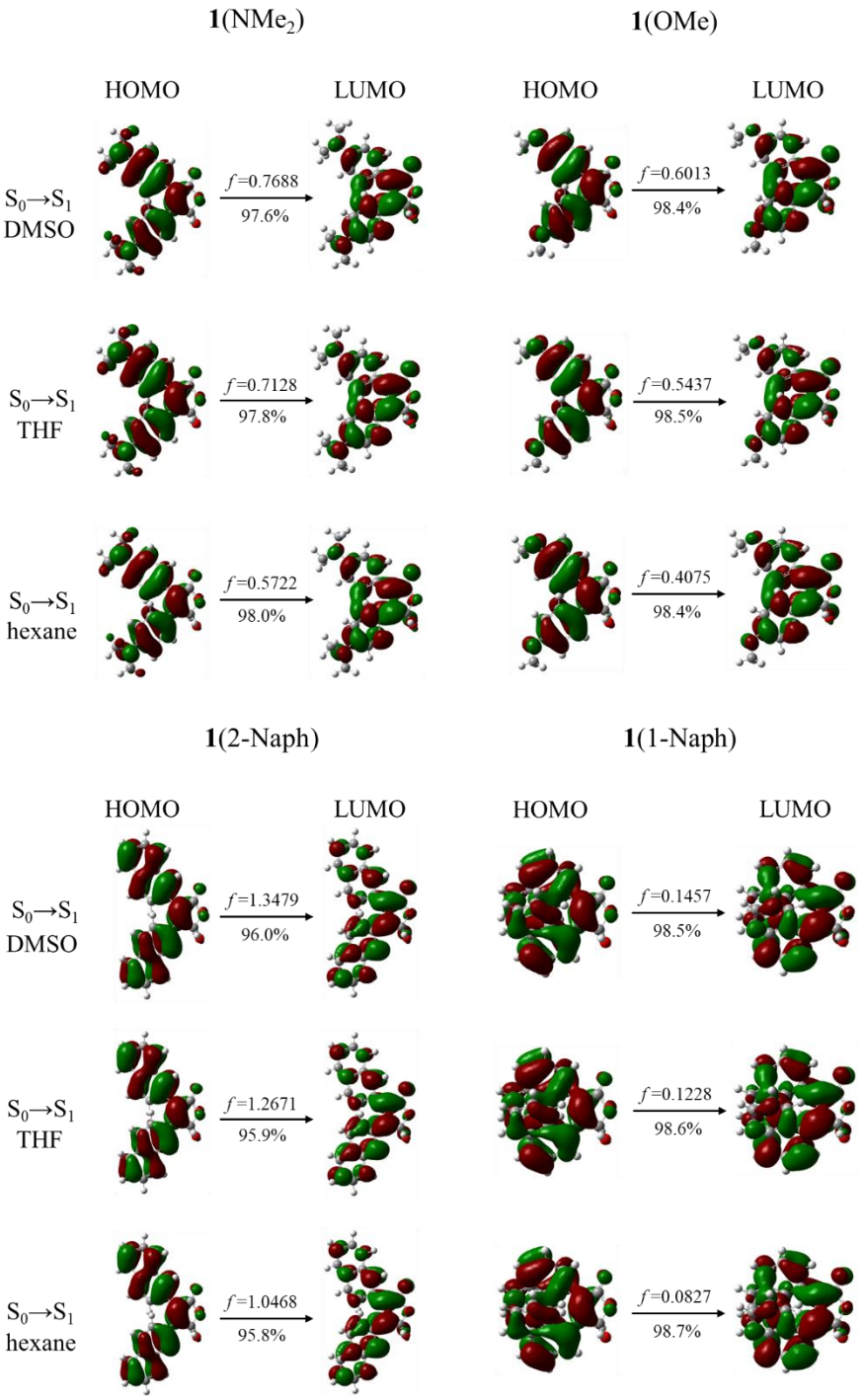

Figure S60. TD-DFT calculation of $S_0 \rightarrow S_1$ excitation of **1**(NMe_2), **1**(OMe), **1**(2-Naph), and **1**(1-Naph), with the oscillator strength *f* and the weight of the HOMO-LUMO contribution to the excitation also included. As shown in the figure, the lowest energy electronic transition ($S_0 \rightarrow S_1$) is essentially described as HOMO to LUMO excitation with more than 95% participation. The $S_0 \rightarrow S_1$ transition is dominated by LE character, which is in good agreement with those evaluated from the Lippert–Mataga equation.

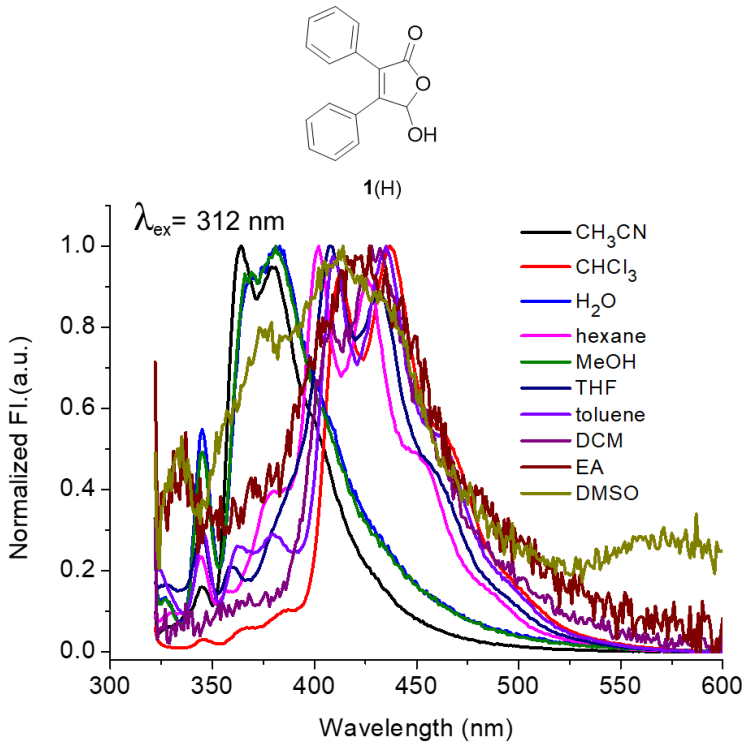

Figure S61. Normalized fluorescence spectra of **1**(H) (10 μM) in different solvents with excitation at 312 nm and weak fluorescence emission.

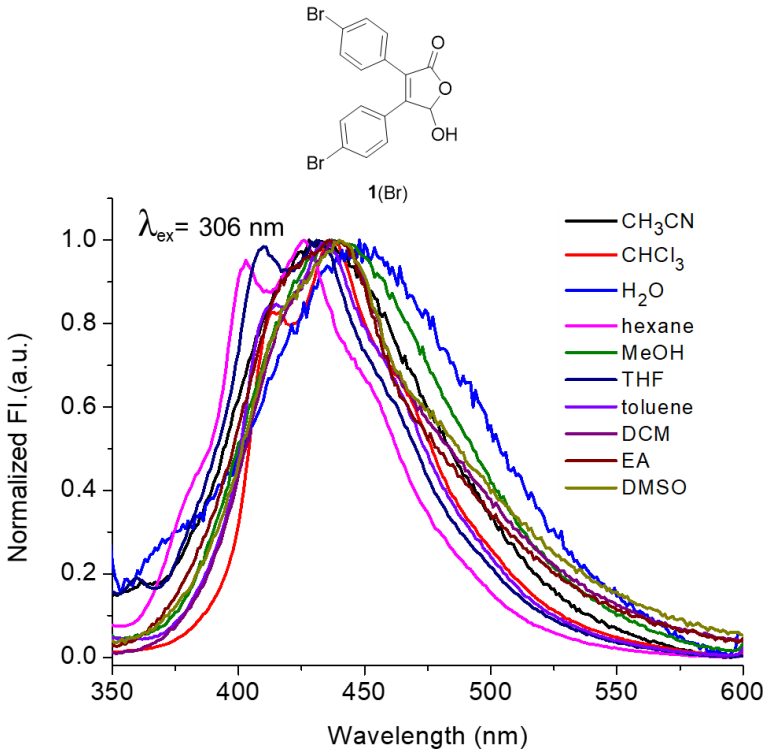

Figure S62. Normalized fluorescence spectra of **1**(Br) (10 μM) in different solvents with excitation at 306 nm and weak fluorescence emission.

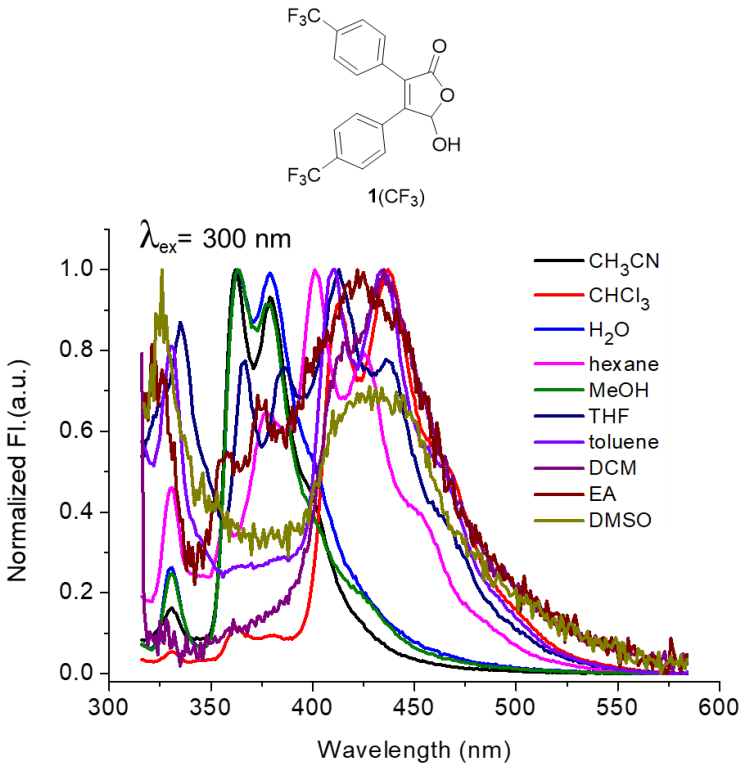

Figure S63. Fluorescence spectra of **1**(CF_3) (10 μM) in different solvents with excitation at 300 nm and weak fluorescence emission.

Table S6. Photophysical data of **1** and **3** in CH_3CN: PL quantum yields (Φ_F), lifetimes (τ_F), radiative and nonradiative rates (k_r, k_{nr}).

name	Φ_F (%) [a]	τ_F (ns) [b]	k_r (s^{-1}) [c]	k_{nr} (s^{-1}) [c]
1(NMe_2)	55	4.4	$1.25*10^8$	$1.02*10^8$
1(OMe)	29	1.3	$2.23*10^8$	$5.46*10^8$
1(2-Naph)	7	1.3	$5.38*10^7$	$7.15*10^8$
1(1-Naph)	3	1.4	$2.14*10^7$	$6.93*10^8$
1(Br)	<1	1.7	$<5.88*10^6$	$>5.82*10^8$
1(H)	<1	1.5	$<6.67*10^6$	$>6.60*10^8$
1(CF_3)	<1	2.1	$<4.76*10^6$	$>4.71*10^8$
3(OMe)	60	5.2	$1.15*10^8$	$7.69*10^7$
3(H)	23	0.3	$7.67*10^8$	$2.57*10^9$

[a] From absolute measurements in an integrating sphere; [b] From single-exponential fitting or intensity averages from double-exponential fitting; [c] From $\tau_F = 1/ (k_r + k_{nr})$, $\Phi_F = k_r \cdot \tau_F$.

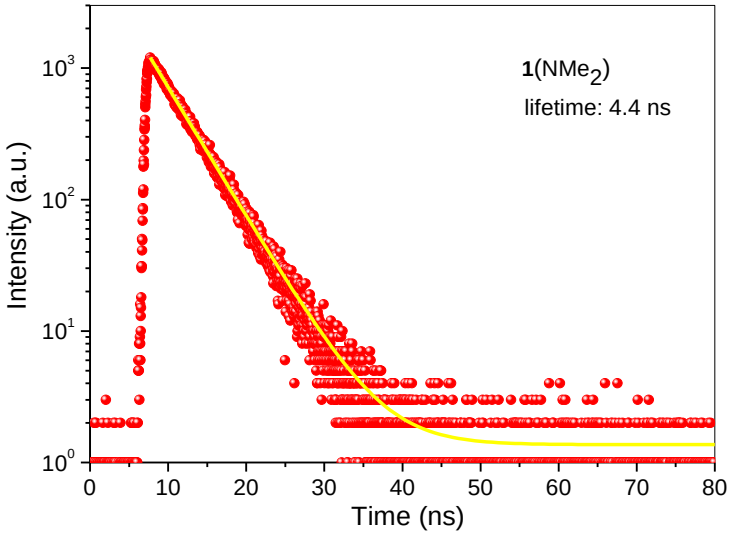

Figure S64. PL decay profile of **1**(NMe_2) in CH_3CN recorded at 543 nm, by using time-correlated single photon counting method under the excitation of a laser (375 nm).

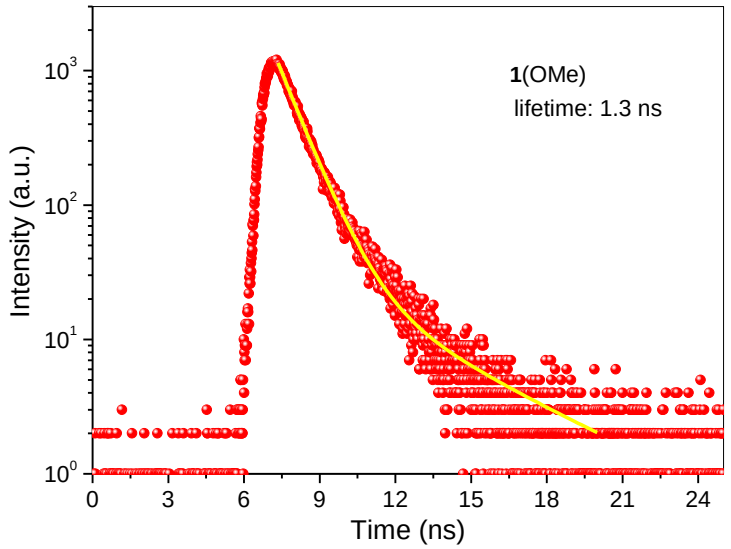

Figure S65. PL decay profile of **1**(OMe) in CH_3CN recorded at 445 nm, by using time-correlated single photon counting method under the excitation of a laser (375 nm).

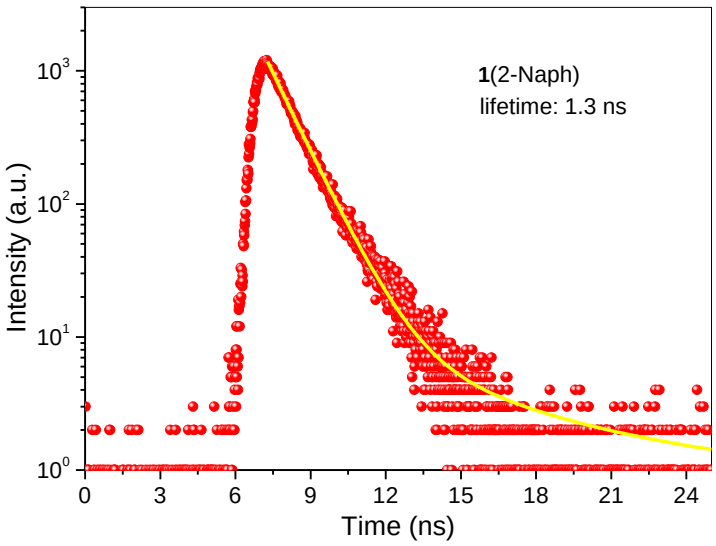

Figure S66. PL decay profile of **1**(2-Naph) in CH_3CN recorded at 440 nm, by using time-correlated single photon counting method under the excitation of a laser (375 nm).

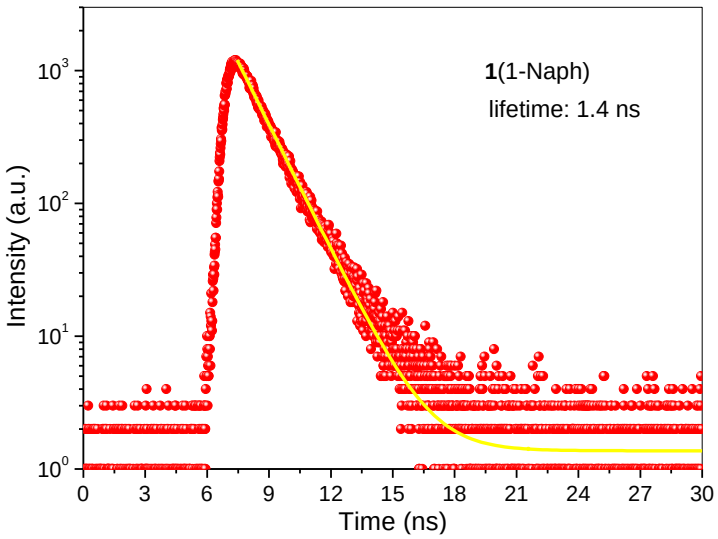

Figure S67. PL decay profile of **1**(1-Naph) in CH_3CN recorded at 447 nm, by using time-correlated single photon counting method under the excitation of a laser (375 nm).

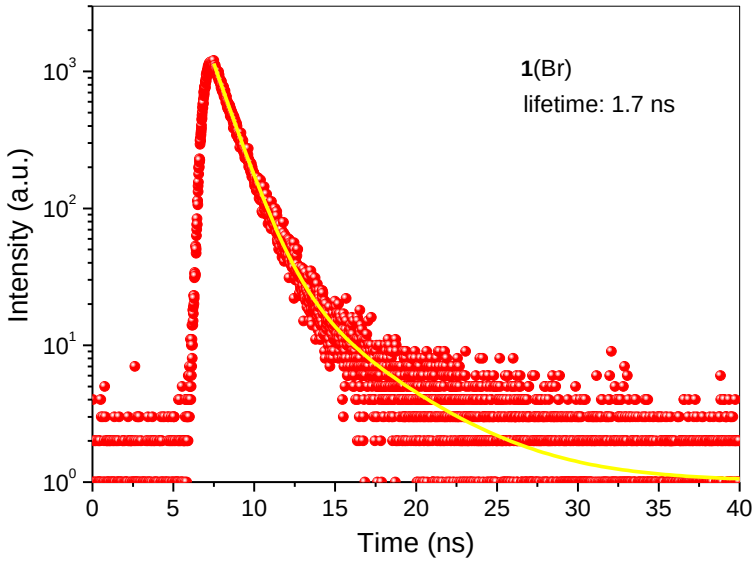

Figure S68. PL decay profile of **1**(Br) in CH_3CN recorded at 432 nm, by using time-correlated single photon counting method under the excitation of a laser (375 nm).

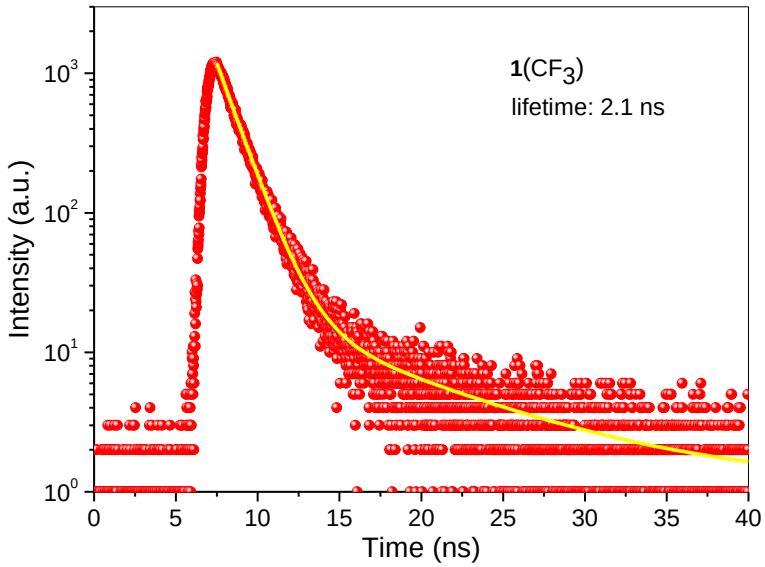

Figure S69. PL decay profile of **1**(CF_3) in CH_3CN recorded at 450 nm, by using time-correlated single photon counting method under the excitation of a laser (375 nm).

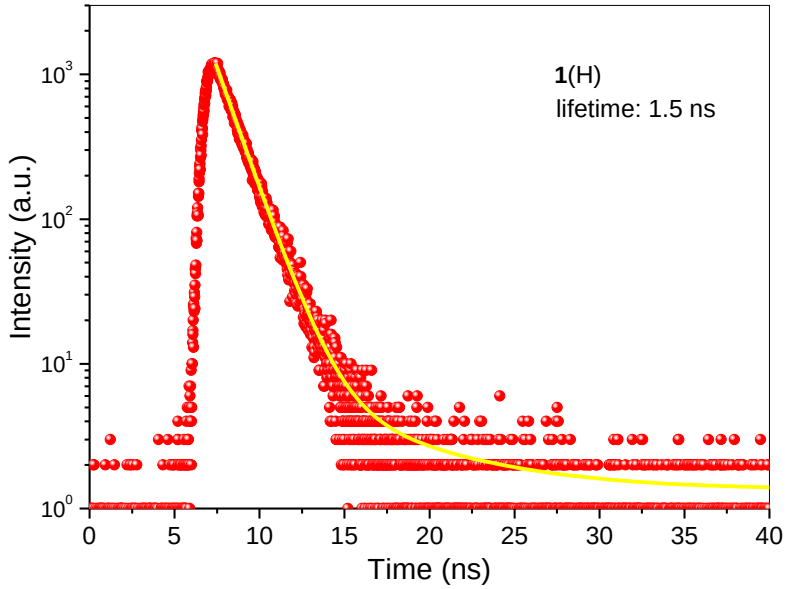

Figure S70. PL decay profile of **1**(H) in CH_3CN recorded at 450 nm, by using time-correlated single photon counting method under the excitation of a laser (375 nm).

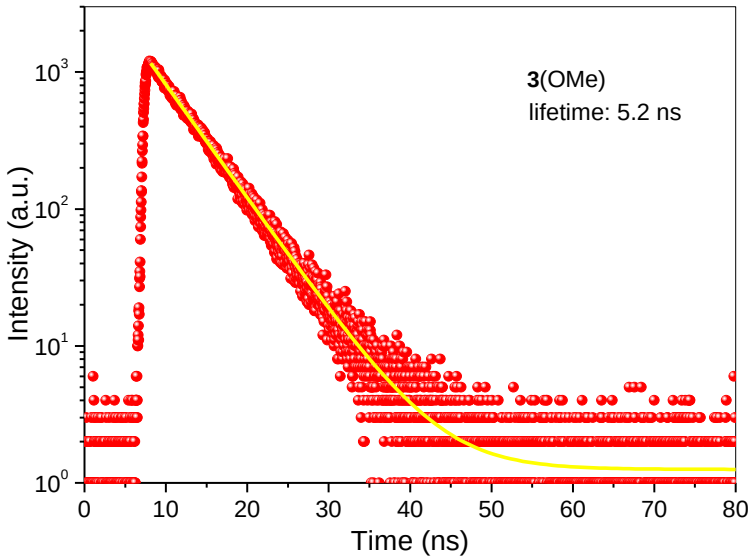

Figure S71. PL decay profile of **3**(OMe) in CH_3CN recorded at 388 nm, by using time-correlated single photon counting method under the excitation of a laser (375 nm).

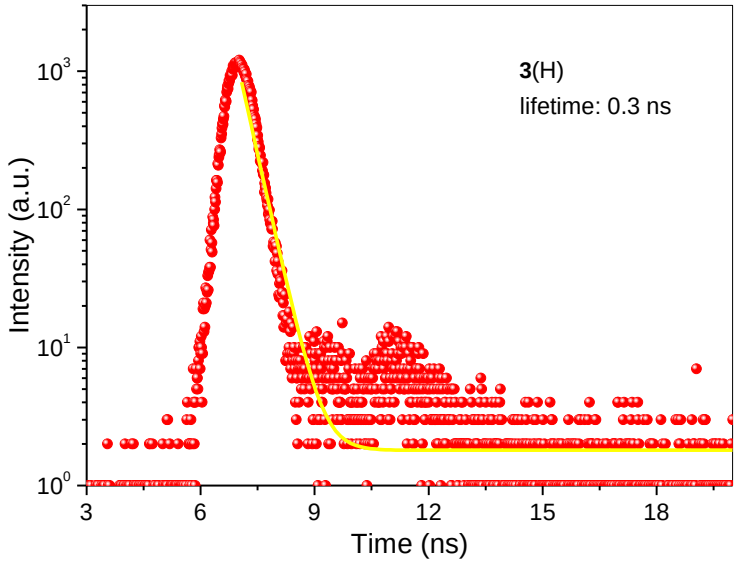

Figure S72. PL decay profile of **3**(H) in CH_3CN recorded at 385 nm, by using time-correlated single photon counting method under the excitation of a laser (375 nm).

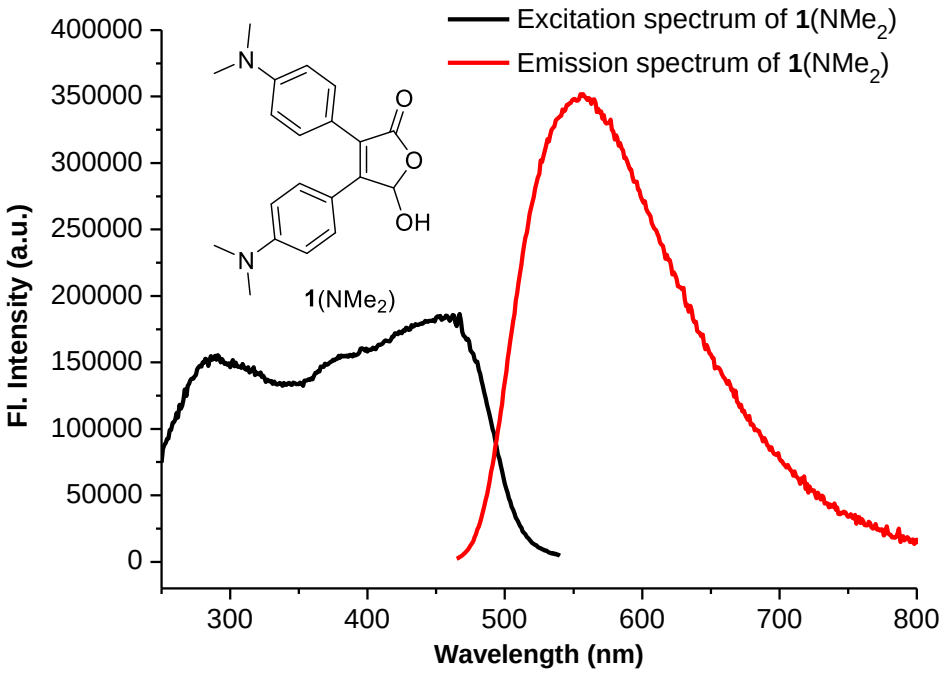

Figure S73. Excitation and PL spectra of **1**(NMe_2) in solid state.

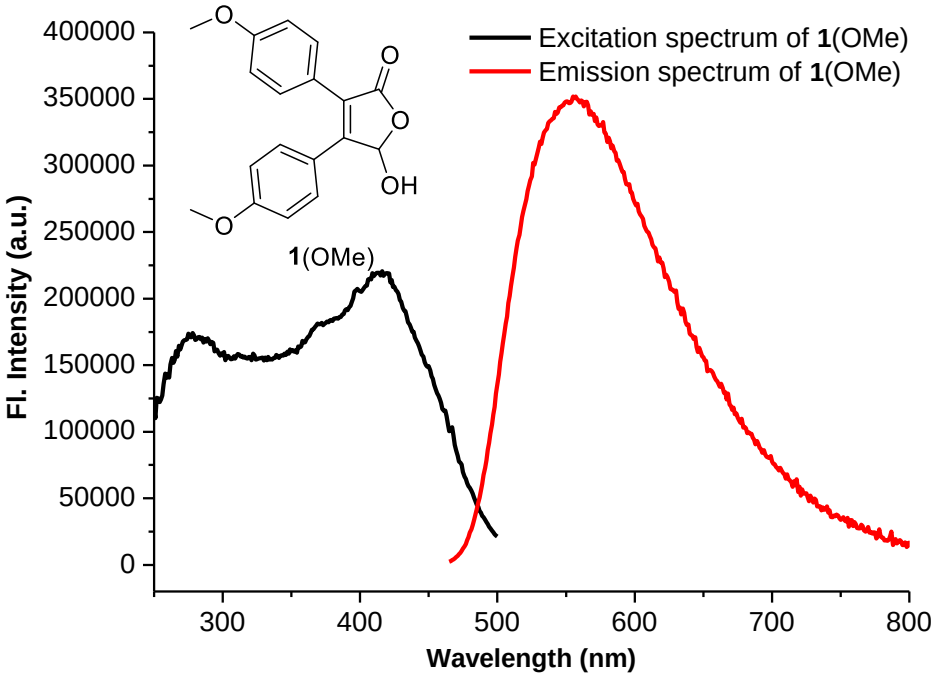

Figure S74. Excitation and PL spectra of **1**(OMe) in solid state.

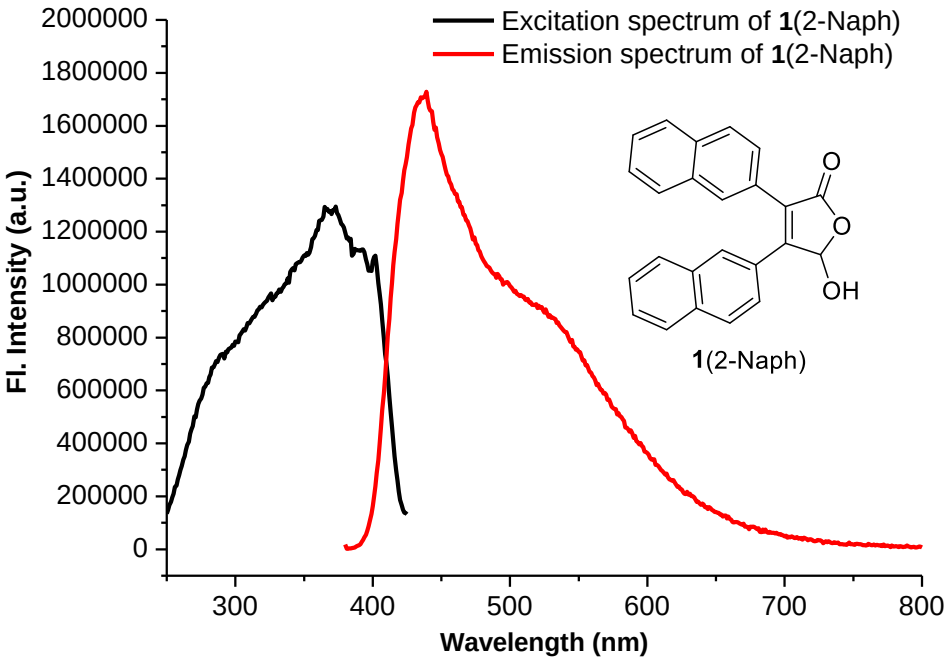

Figure S75. Excitation and PL spectra of **1**(2-Naph) in solid state.

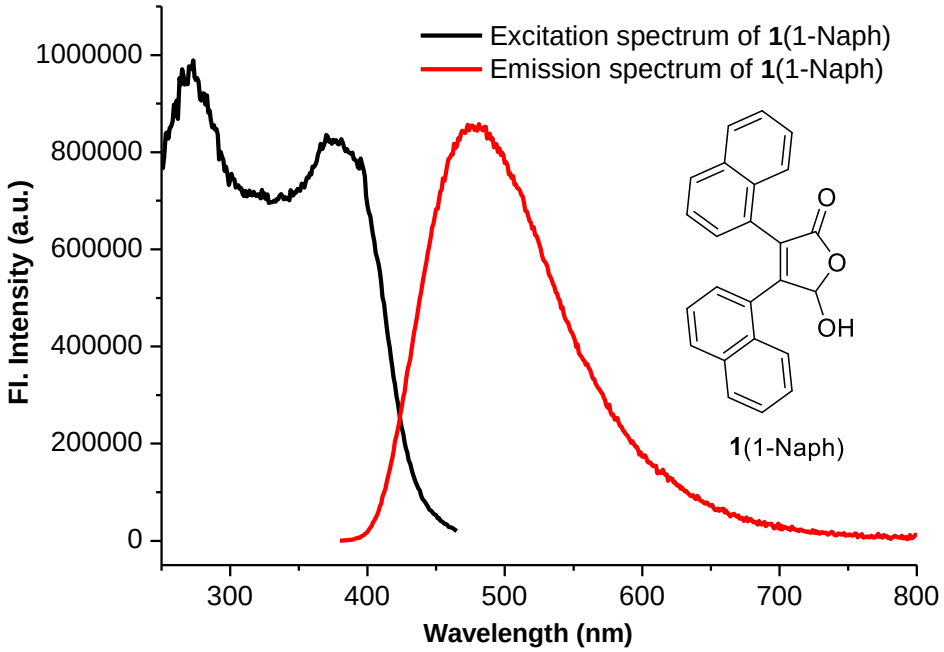

Figure S76. Excitation and PL spectra of **1**(1-Naph) in solid state.

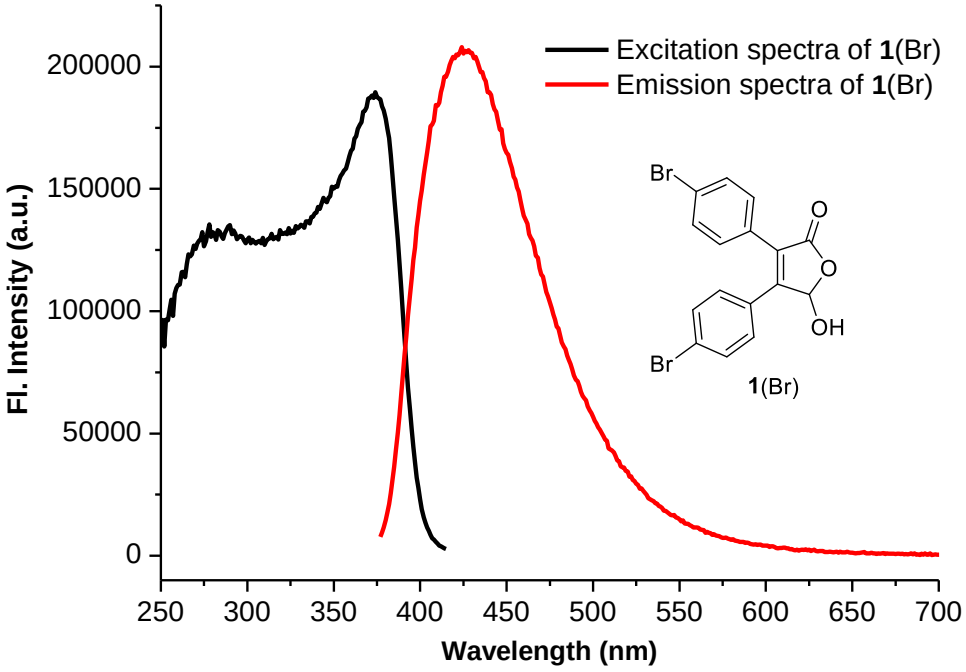

Figure S77. Excitation and PL spectra of **1**(Br) in solid state.

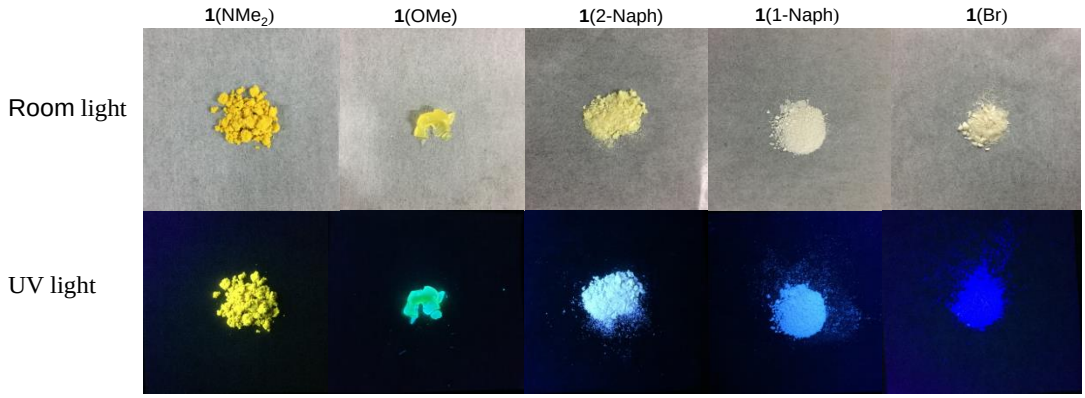

Figure S78. Photographs of **1**(NMe_2), **1**(MeO), **1**(2-Naph), **1**(1-Naph), and **1**(Br) in the solid state taken under room light and UV light (365 nm) irradiation.

5. Regulation of PL with DCC

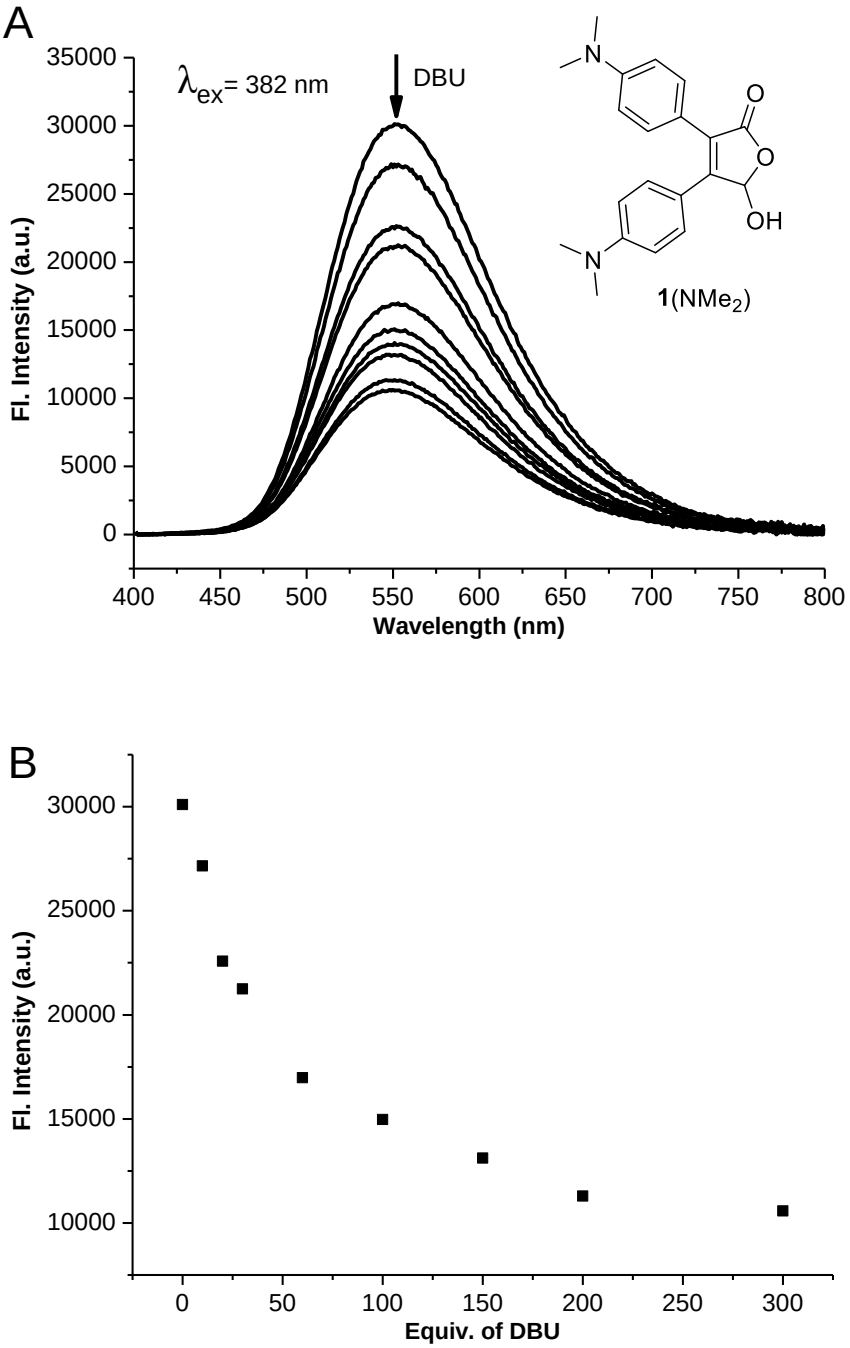

Figure S79. Fluorescence titration (A) as well as titration curve at 551 nm (B) of **1**(NMe_2) (10 μM) with DBU (0-300 equiv.) in CH_3CN with excitation at 382 nm.

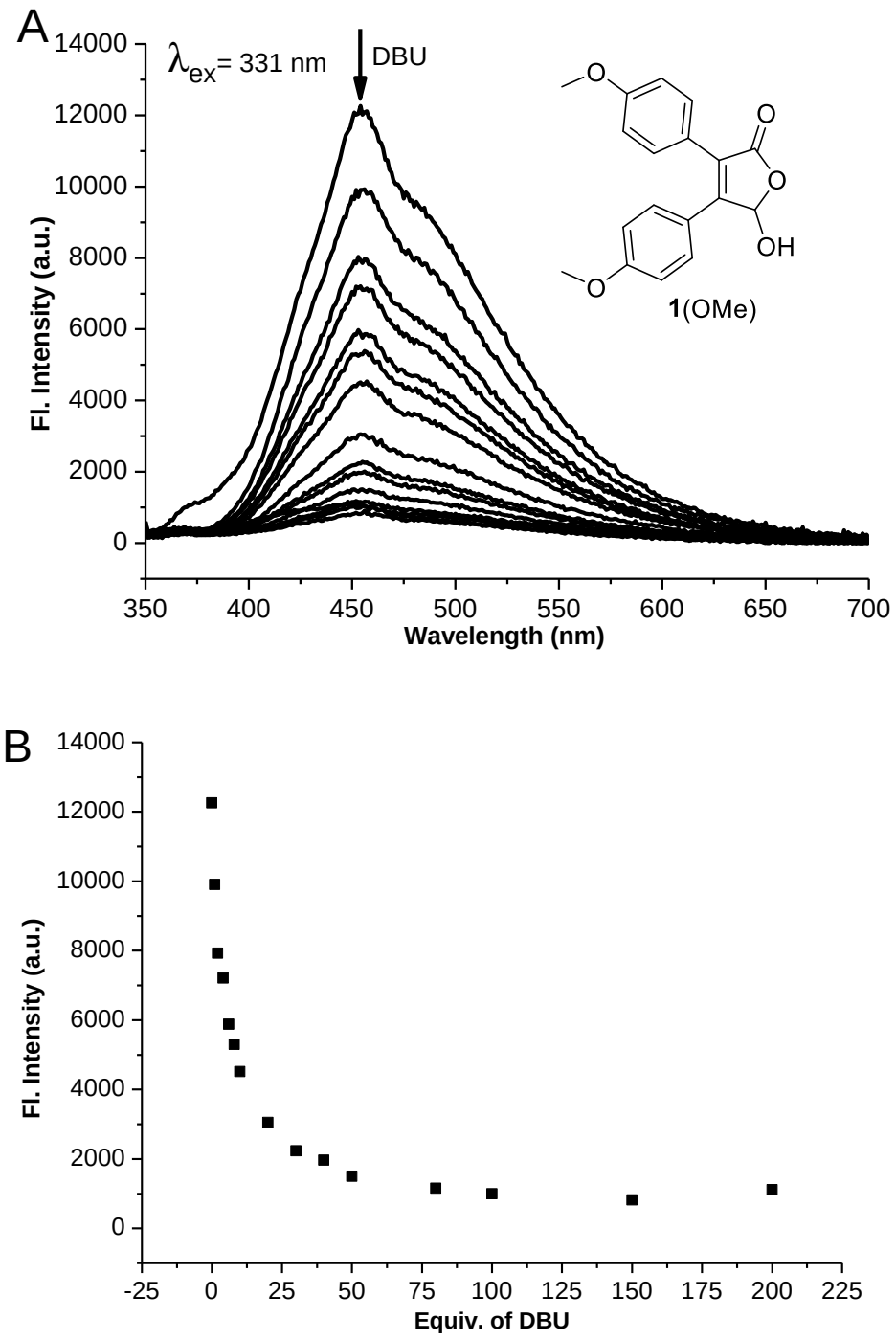

Figure S80. Fluorescence titration (A) as well as titration curve at 454 nm (B) of **1**(OMe) (10 μM) with DBU (0-200 equiv.) in CH_3CN with excitation at 331 nm.

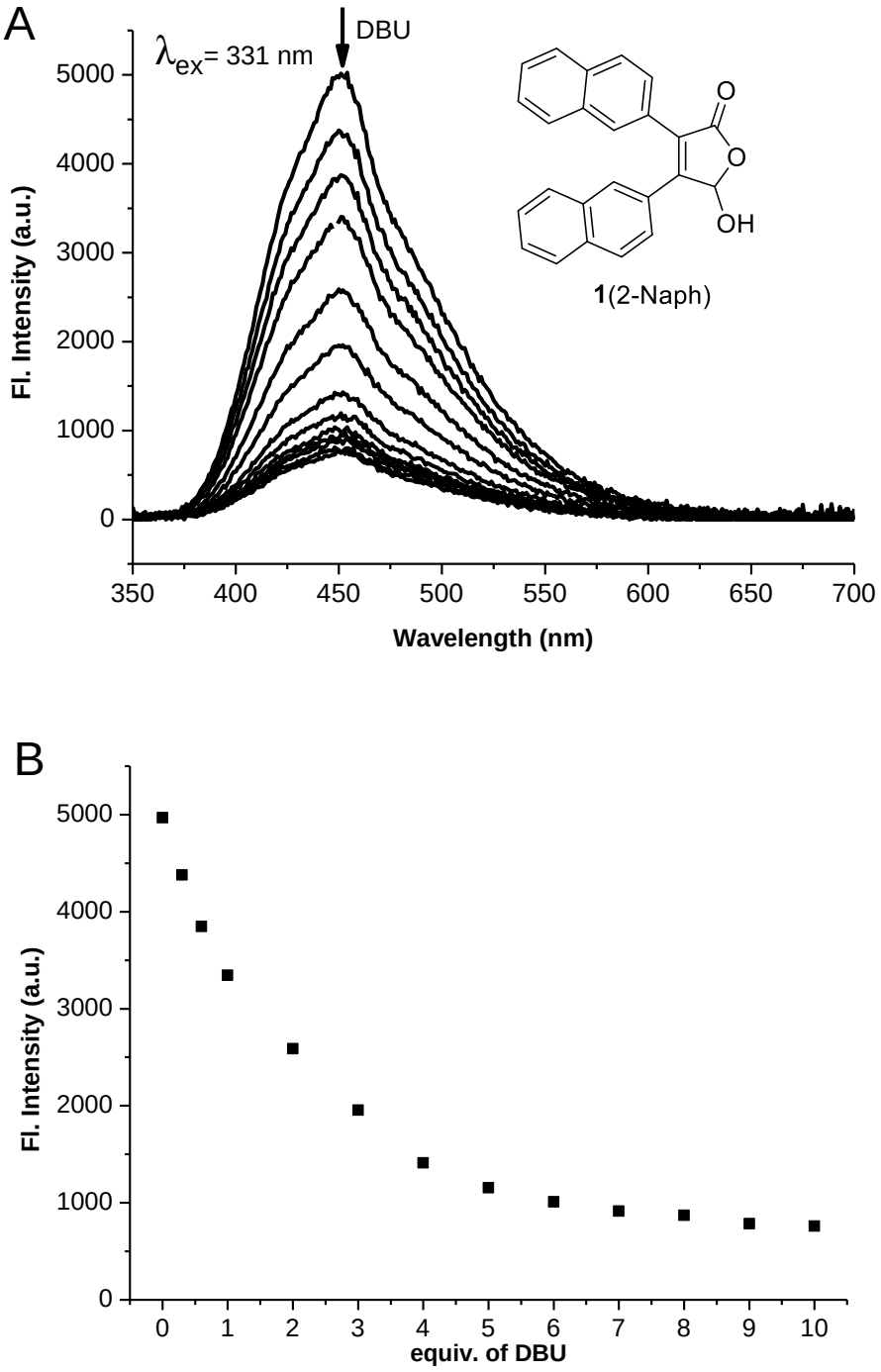

Figure S81. Fluorescence titration (A) as well as titration curve at 451 nm (B) of **1**(2-Naph) (10 μM) with DBU (0-10 equiv.) in CH_3CN with excitation at 331 nm.

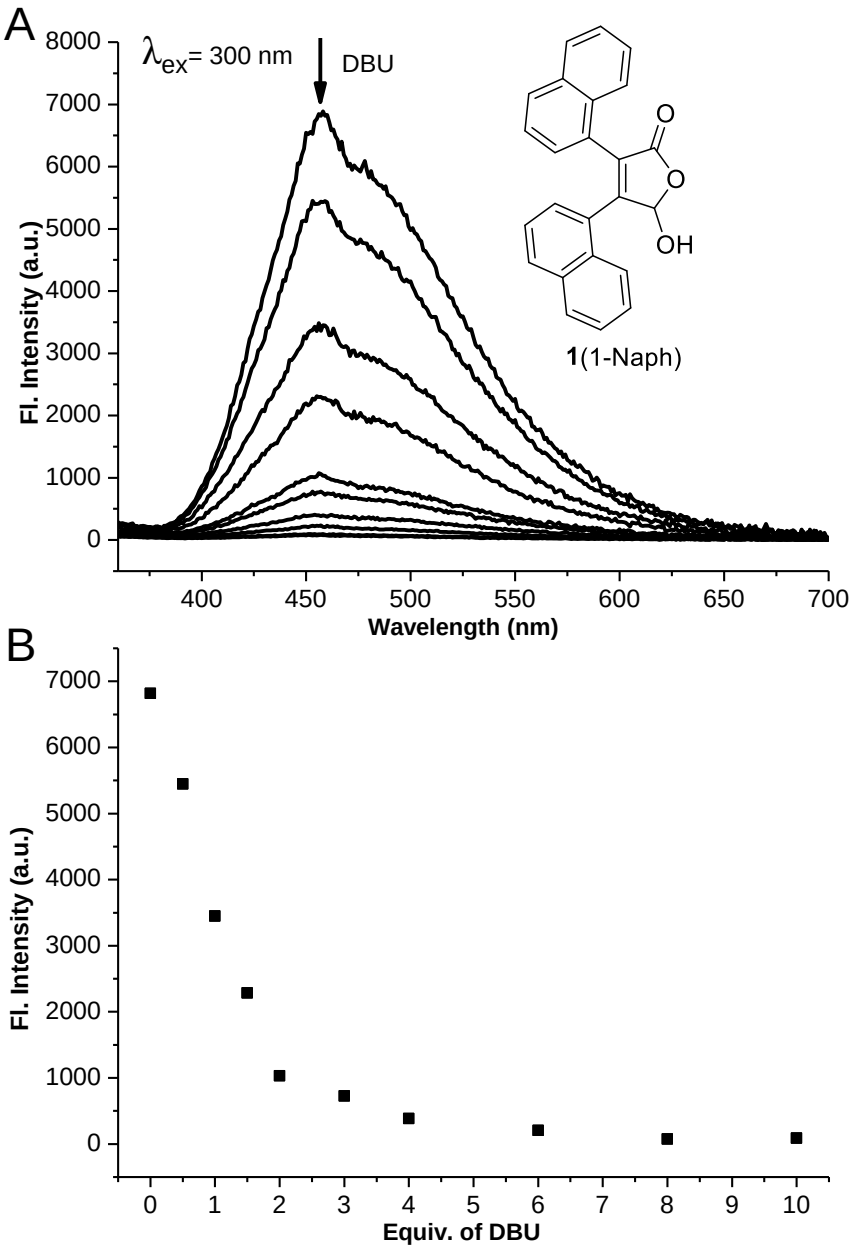

Figure S82. Fluorescence titration (A) as well as titration curve at 457 nm (B) of **1**(1-Naph) (10 μM) with DBU (0-10 equiv.) in CH_3CN with excitation at 300 nm.

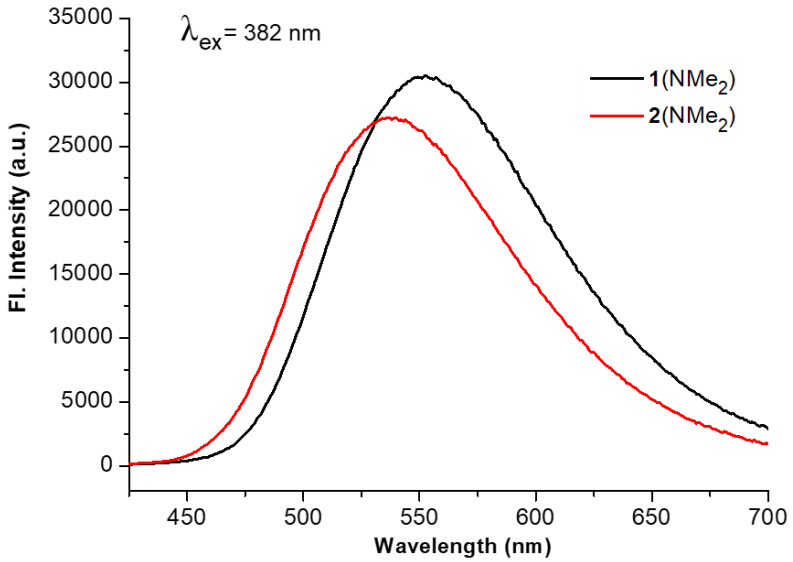

Figure S83. Fluorescence spectra of **1**(NMe_2) and **2**(NMe_2) in CH_3CN (10 μM) with excitation at 382 nm.

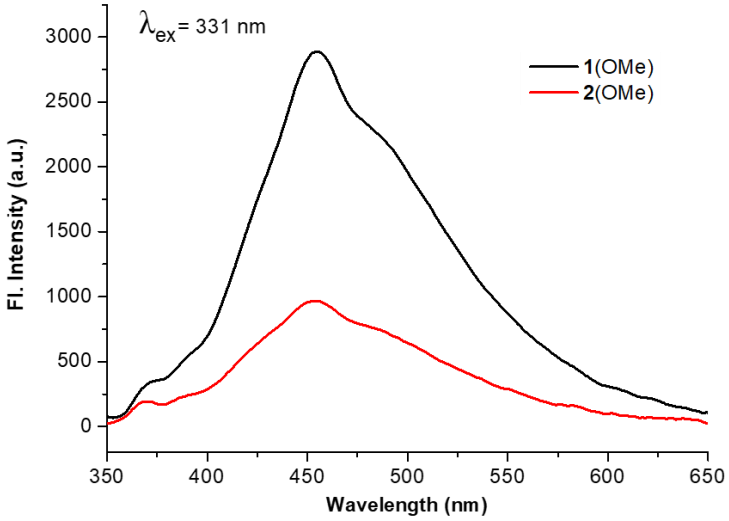

Figure S84. Fluorescence spectra of **1**(OMe) and **2**(OMe) in CH_3CN (10 μM) with excitation at 331 nm.

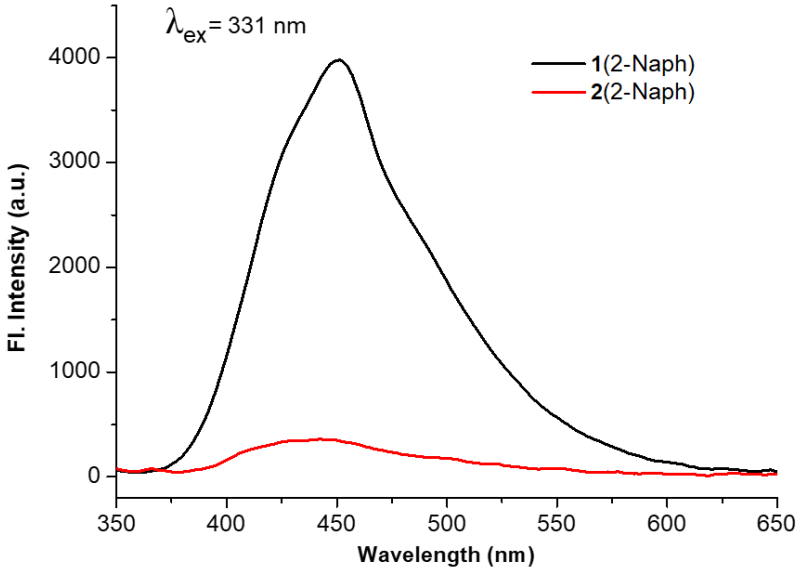

Figure S85. Fluorescence spectra of **1**(2-Naph) and **2**(2-Naph) in CH_3CN (10 μM) with excitation at 331 nm.

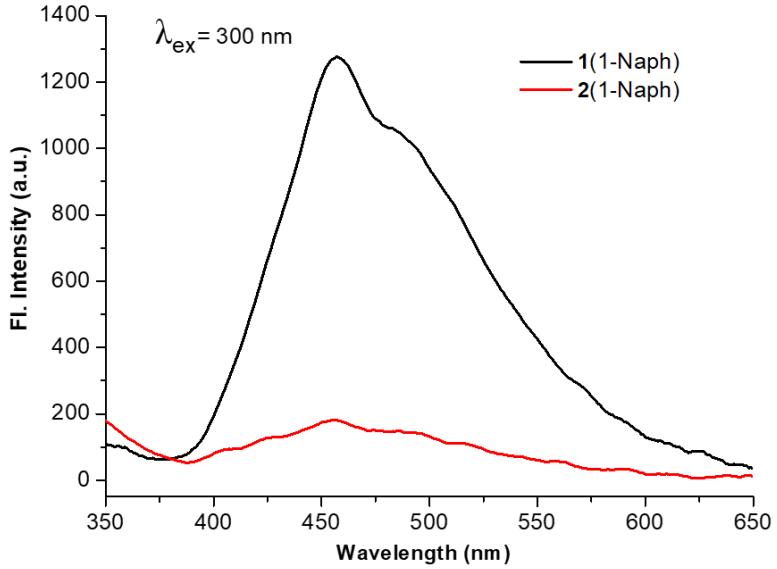

Figure S86. Fluorescence spectra of **1**(1-Naph) and **2**(1-Naph) in CH_3CN (10 μM) with excitation at 300 nm.

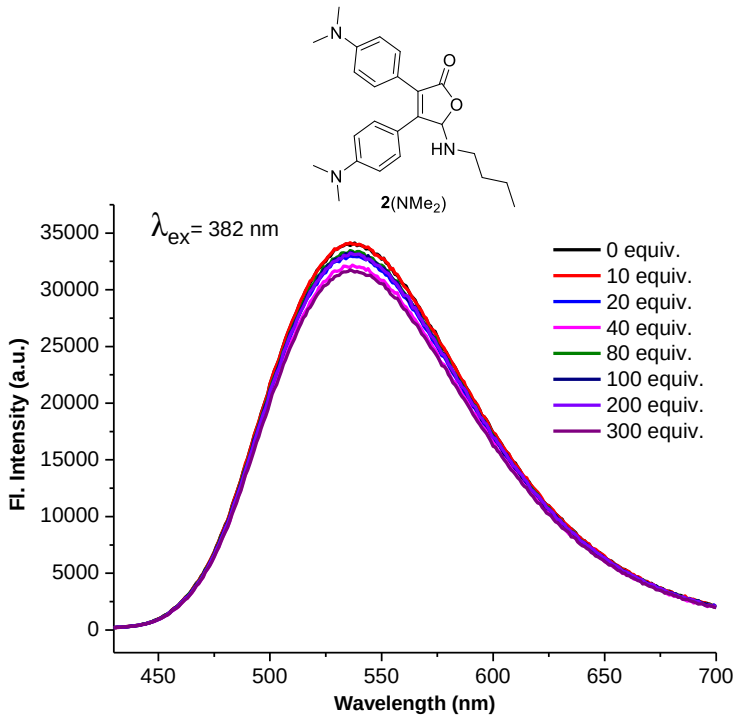

Figure S87. Fluorescence titration of **2**(NMe_2) (10 μM) with DBU (0-300 equiv.) in CH_3CN with excitation at 382 nm.

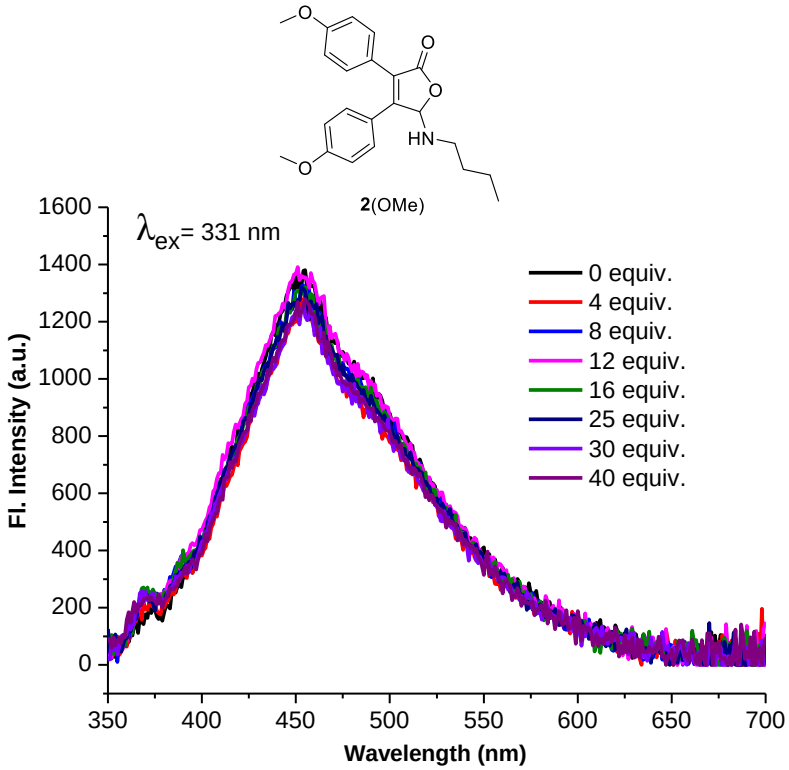

Figure S88. Fluorescence titration of **2**(OMe) (10 μM) with DBU (0-40 equiv.) in CH_3CN with excitation at 331 nm.

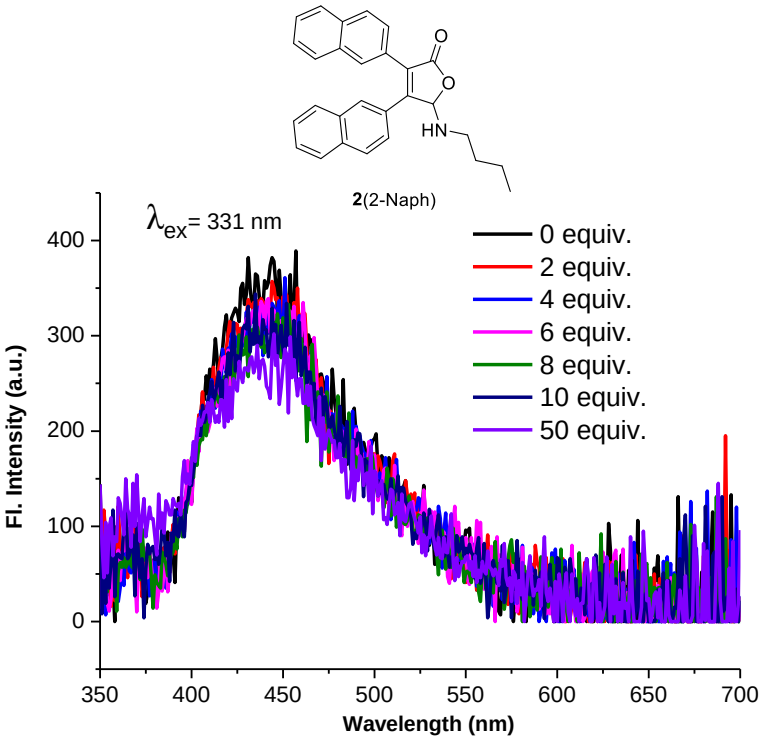

Figure S89. Fluorescence titration of **2**(2-Naph) (10 μM) with DBU (0-50 equiv.) in CH_3CN with excitation at 331 nm.

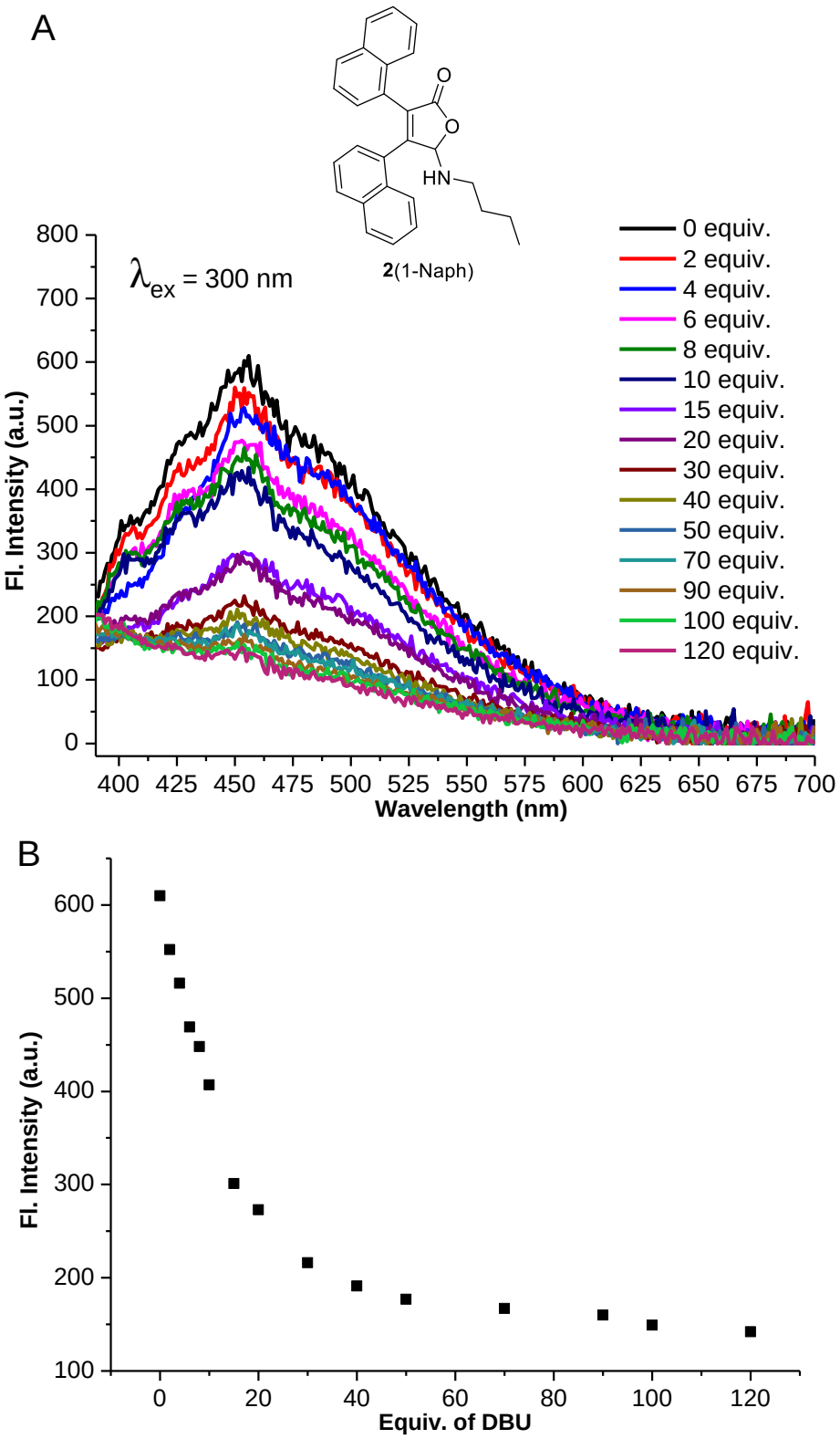

Figure S90. Fluorescence titration (A) as well as titration curve at 457 nm (B) of **2**(1-Naph) (10 μM) with DBU (0-120 equiv.) in CH_3CN with excitation at 300 nm.

6. Effects of Multi-Stimuli

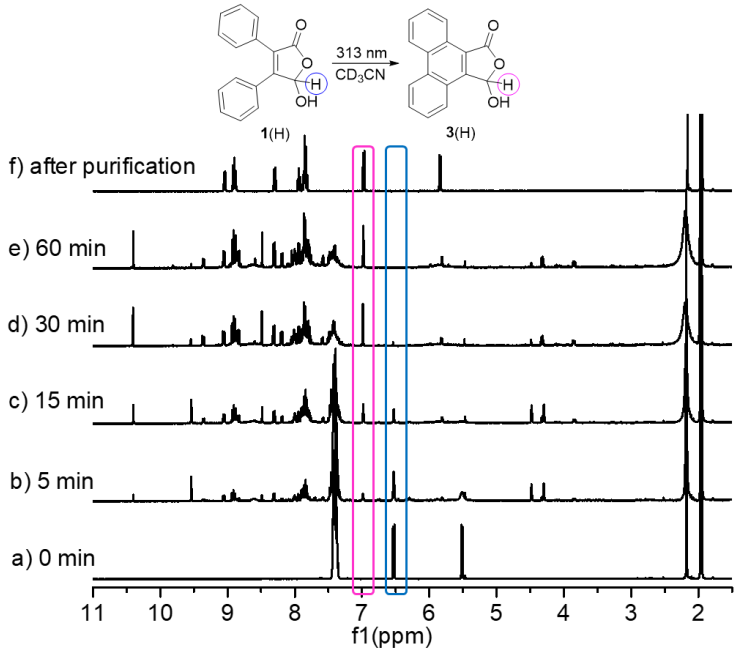

Figure S91. ^{1}H NMR spectra of **1**(H) (16.7 mM in CD_3CN) under 313 nm light at varied time. The desired product was confirmed with isolation and characterization.

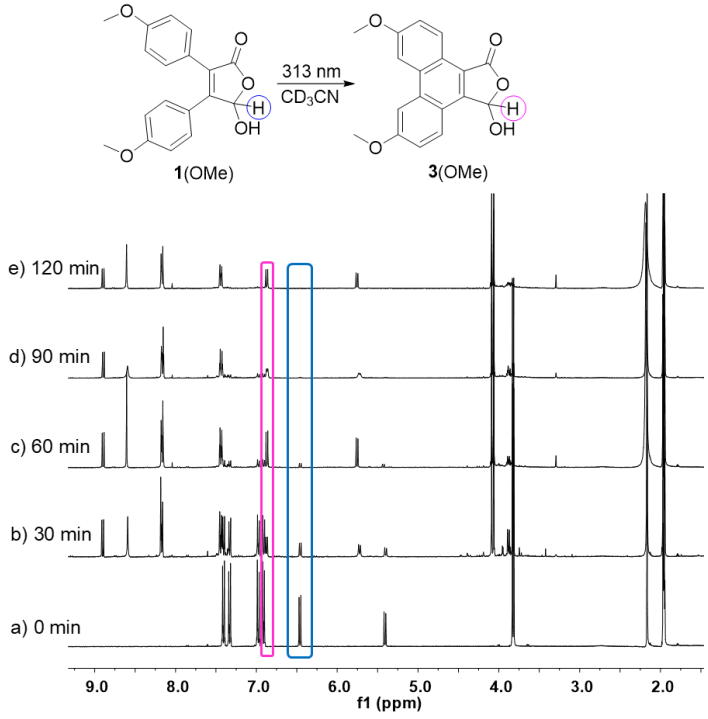

Figure S92. ^{1}H NMR spectra of **1**(OMe) (16.7 mM in CD_3CN) under 313 nm light at varied time. The desired product was confirmed with isolation and characterization.

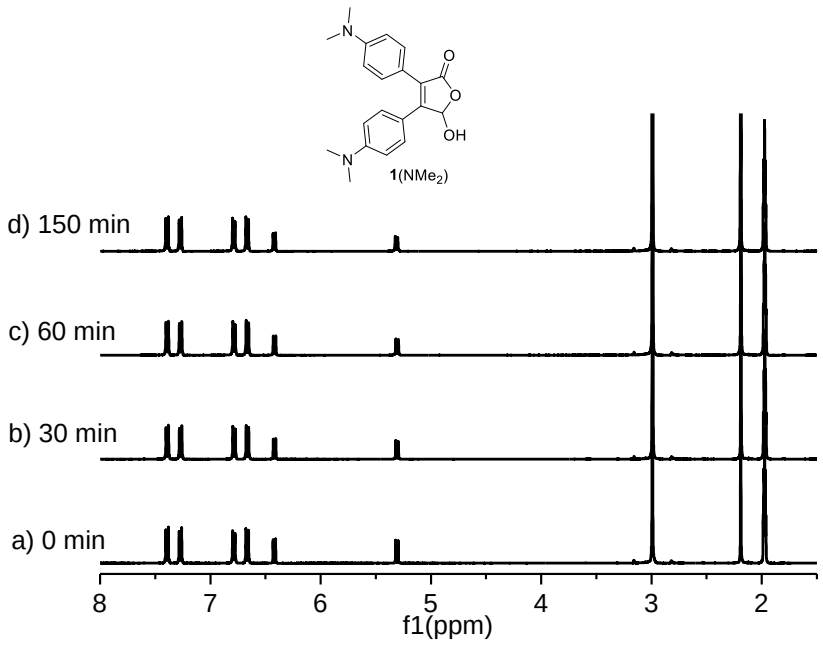

Figure S93. ^{1}H NMR spectra of **1**(NMe_2) (16.7 mM in CD_3CN) under 313 nm light at varied time. No reaction occurred under this condition.

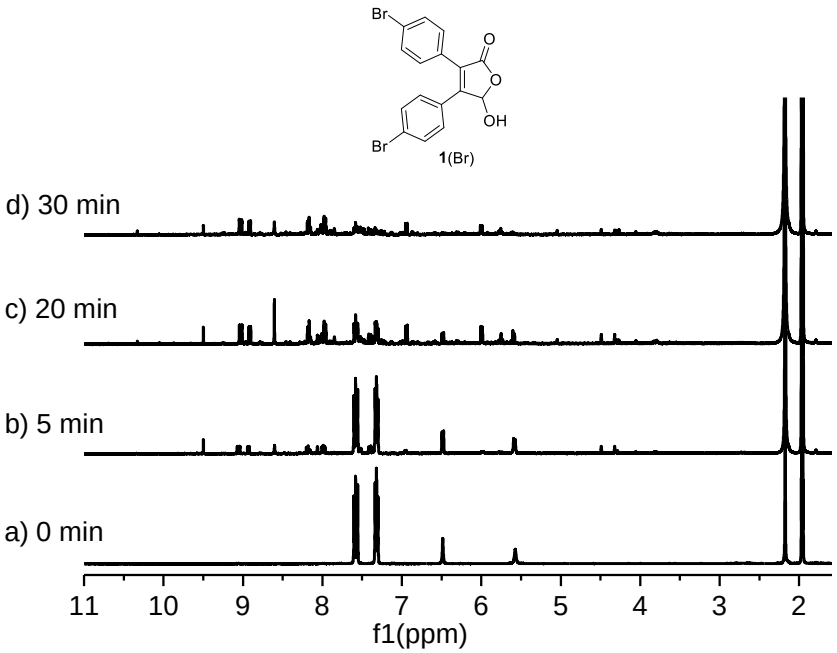

Figure S94. ^{1}H NMR spectra of **1**(Br) (16.7 mM in CD_3CN) under 313 nm light at varied time. A complex mixture was obtained.

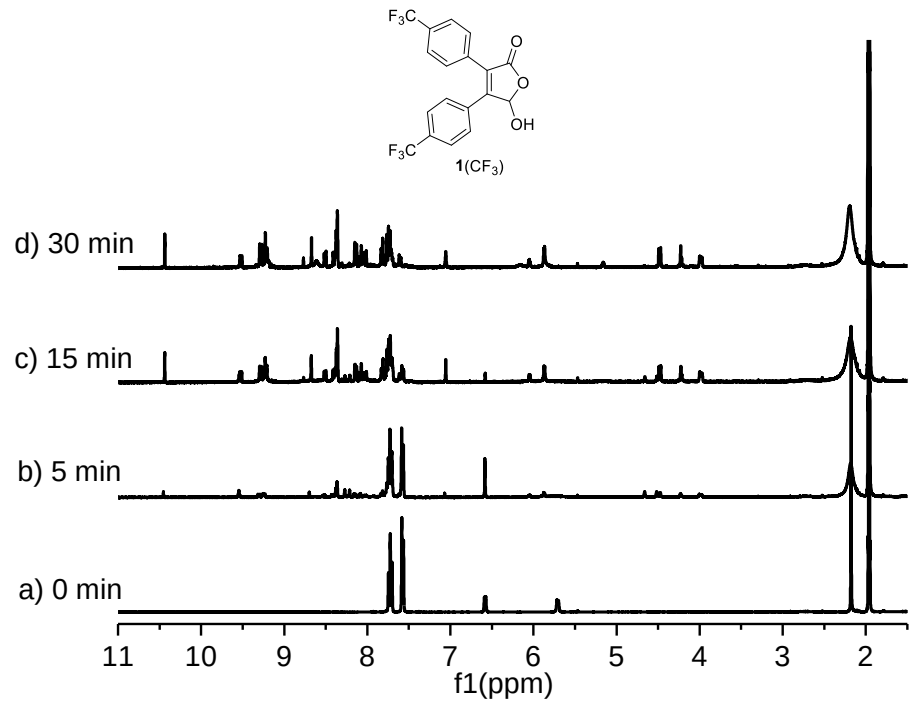

Figure S95. ^{1}H NMR spectra of **1**(CF_3) (16.7 mM in CD_3CN) under 313 nm light at varied time. A complex mixture was obtained.

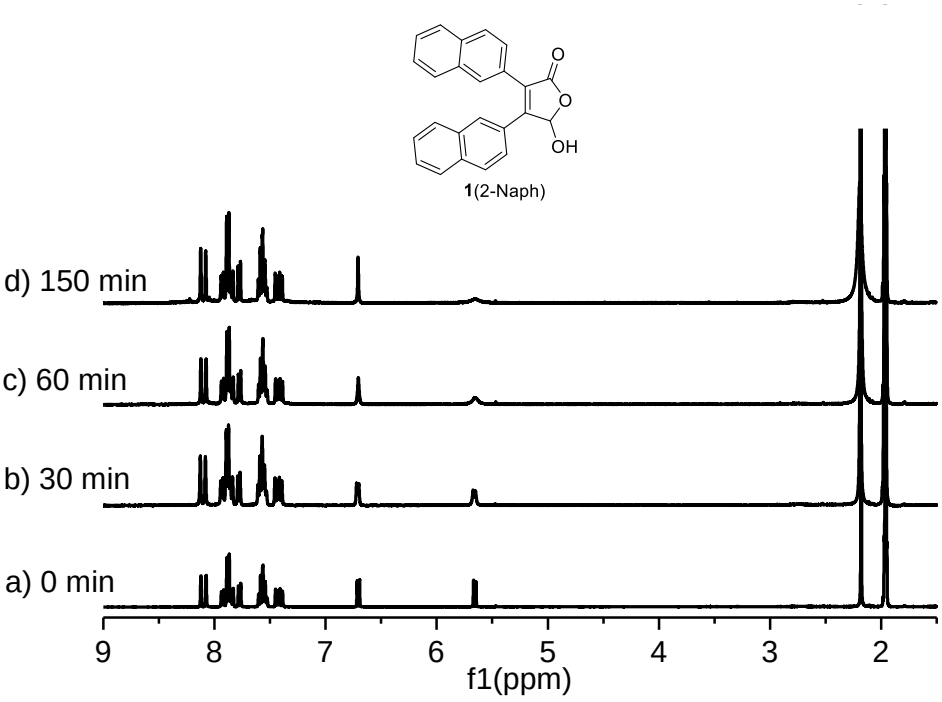

Figure S96. ^{1}H NMR spectra of **1**(2-Naph) (16.7 mM in CD_3CN) under 313 nm light at varied time. No reaction occurred under this condition.

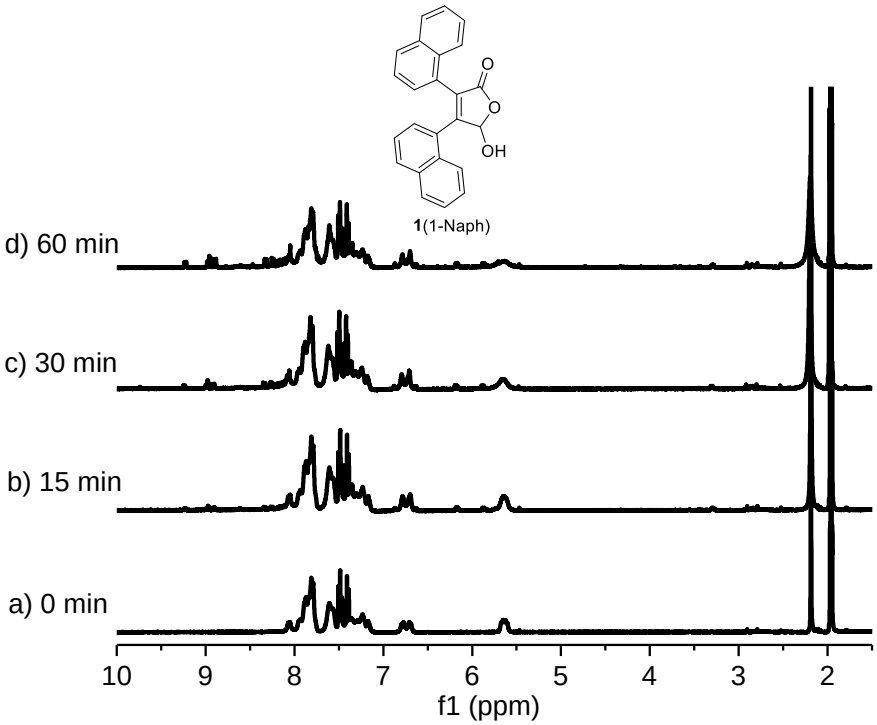

Figure S97. ^{1}H NMR spectra of **1**(1-Naph) (16.7 mM in CD_3CN) under 313 nm light at varied time. A complex mixture was obtained.

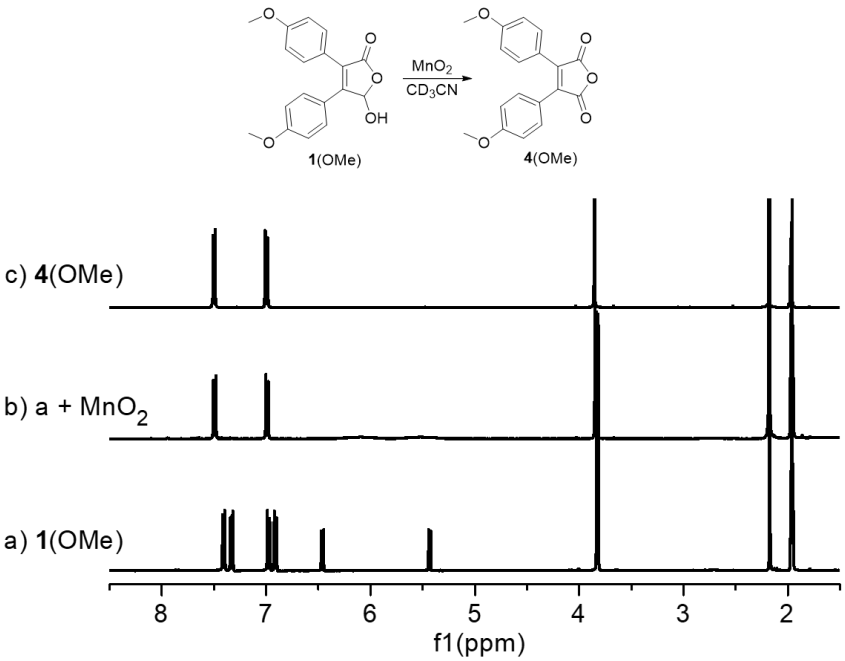

Figure S98. ^{1}H NMR spectra of **1**(OMe) (16.7 mM in CD_3CN, a) and its oxidation (b) with MnO_2 (10 equiv.). The spectrum of **4**(OMe) (c) is included for the comparison.

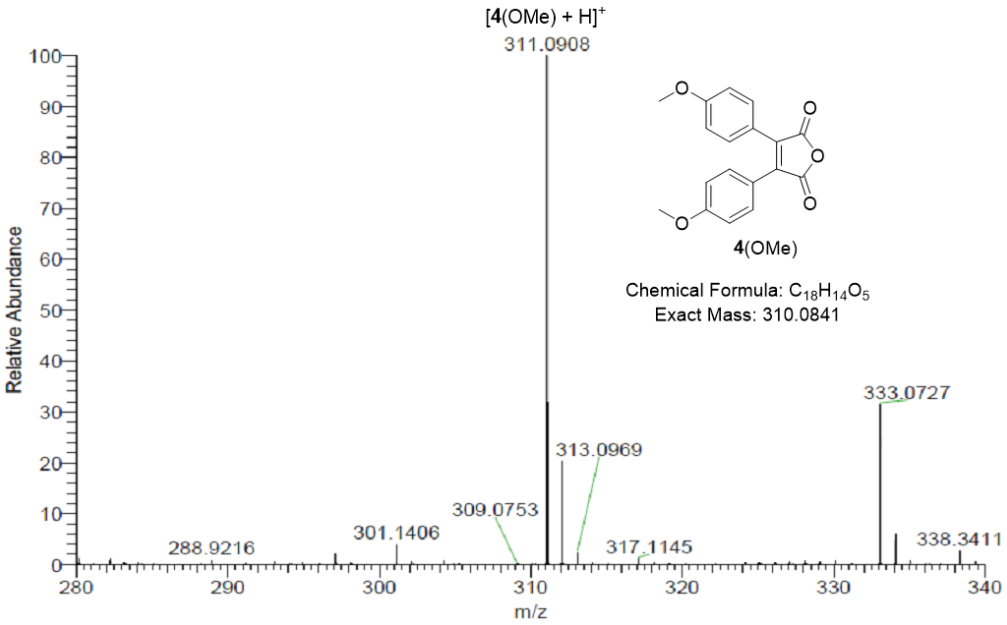

Figure S99. ESI mass spectrum of the reaction of **1**(OMe) and MnO_2 in CH_3CN.

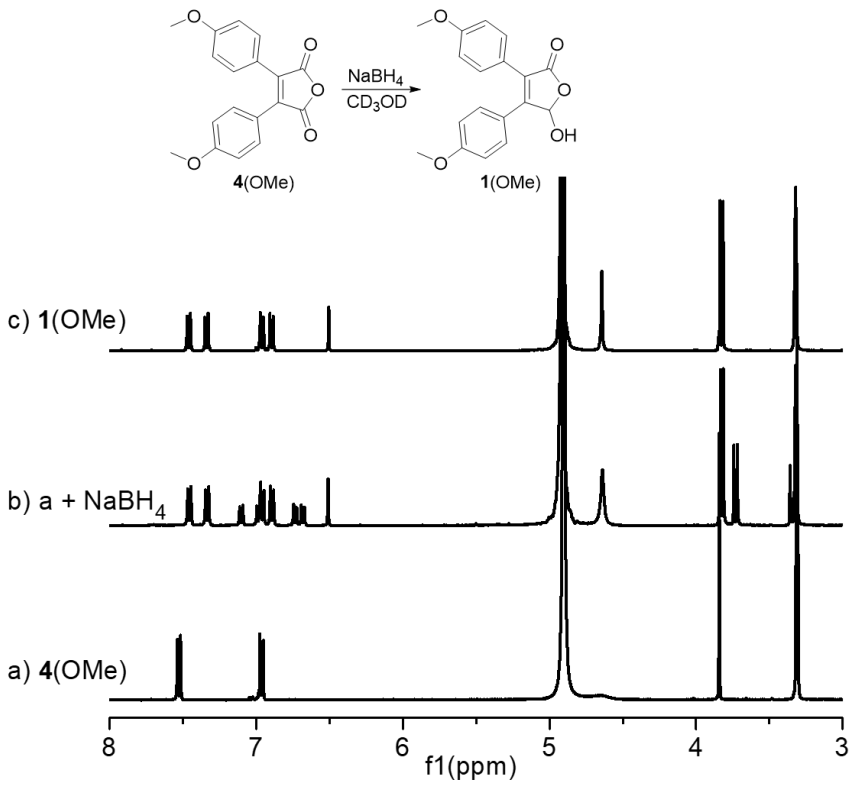

Figure S100. ^{1}H NMR spectra of **4**(OMe) (16.7 mM in CD_3OD, a) and its reduction (b) with $NaBH_4$ (1 equiv.). The spectrum of **1**(OMe) (c) is included for the comparison.

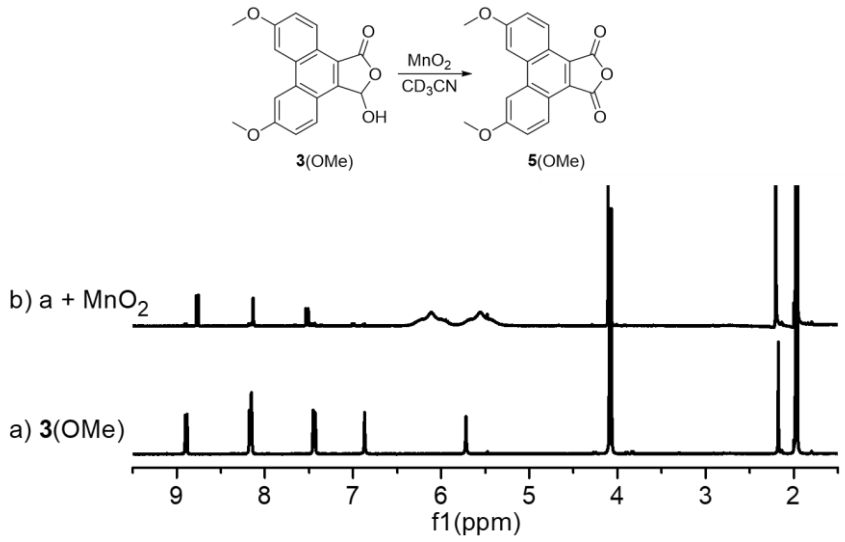

Figure S101. ^{1}H NMR spectra of **3**(OMe) (16.7 mM in CD_3CN, a) and its oxidation (b) with MnO_2 (10 equiv.).

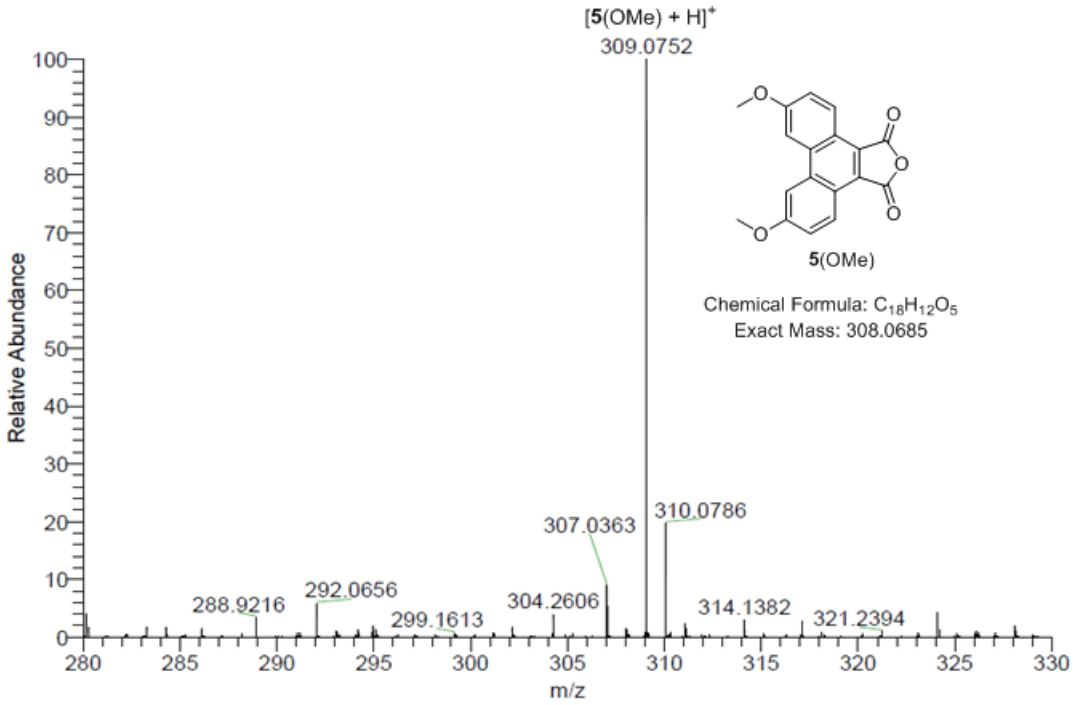

Figure S102. ESI mass spectrum of the reaction of **3**(OMe) and MnO_2 in CH_3CN.

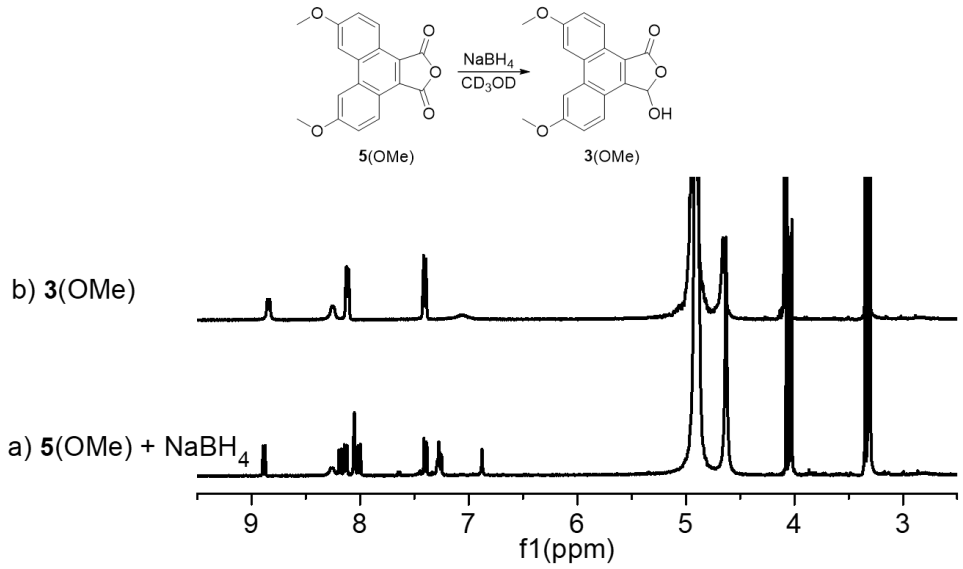

Figure S103. ^1H NMR spectra of the reduction of **5**(OMe) (16.7 mM, created by oxidation of **3**(OMe)) with $NaBH_4$ (1.0 equiv.) in CD_3OD (a) and the spectra of **3**(OMe) in CD_3OD (b).

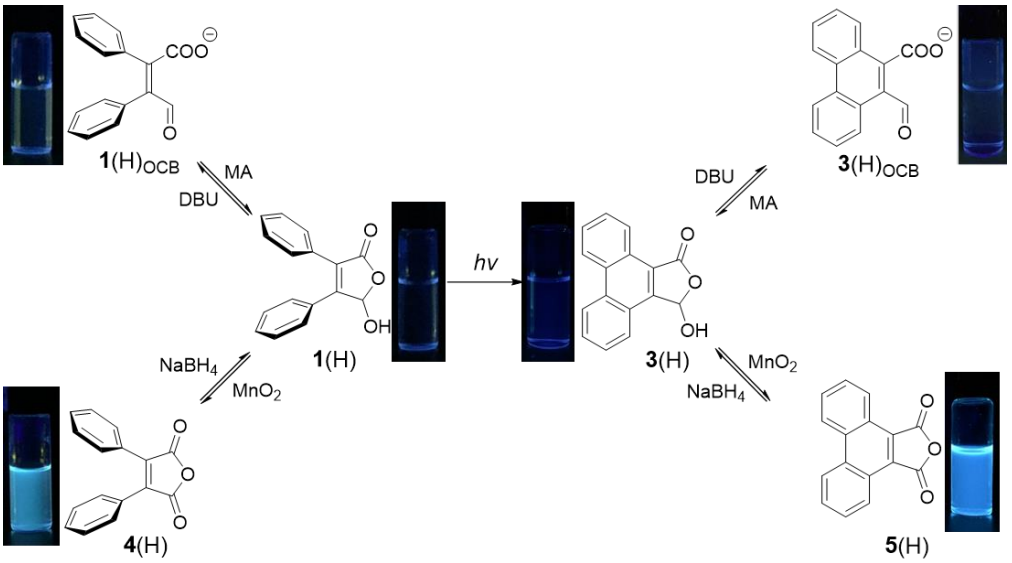

Figure S104. Luminescence photographs of **1**(H) and **3**(H) in CH_3CN in response to pH and redox stimuli under a 365 nm UV lamp.

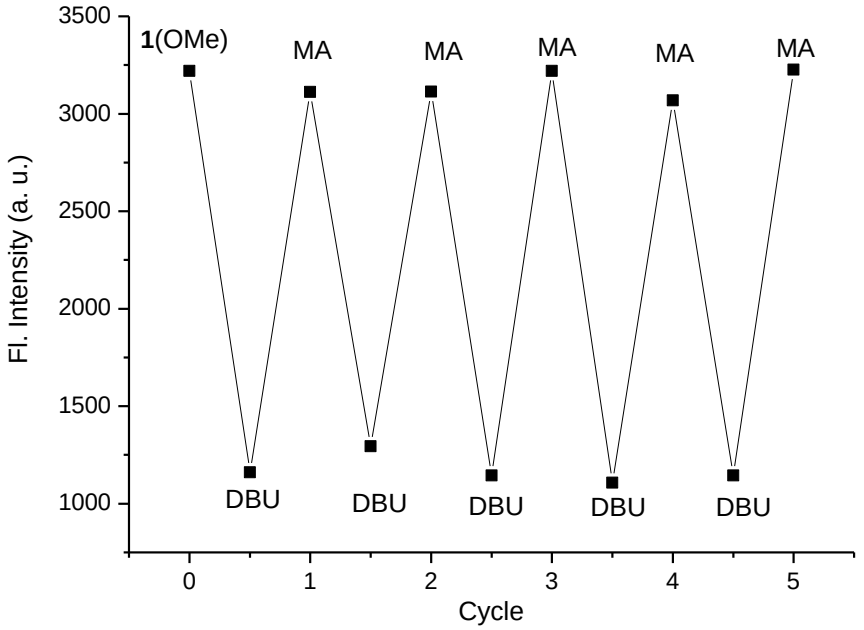

Figure S105. Fluorescence response of **1**(OMe) (10 μM) at 455 nm upon consecutive addition of DBU (10 equiv) and MA (10 equiv) in CH_3CN (λ_{ex} = 331 nm). The quantum yield of **1**(OMe) decreased from 29% to 5 % with the addition of DBU.

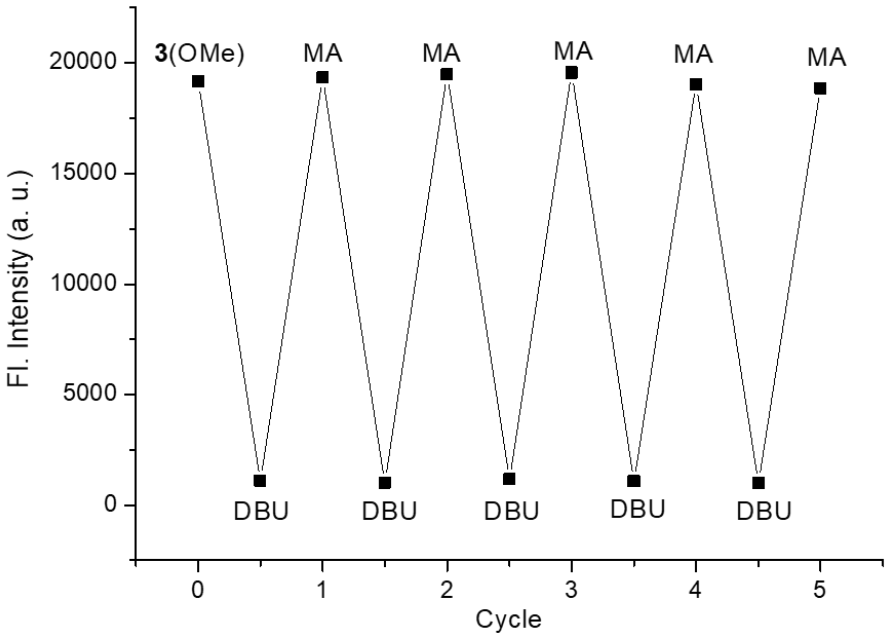

Figure S106. Fluorescence response of **3**(OMe) (10 μM) at 389 nm upon consecutive addition of DBU (10 equiv) and MA (10 equiv) in CH_3CN (λ_{ex} = 331 nm). The quantum yield of **3**(OMe) decreased from 60% to 11% with the addition of DBU.

Table S7. Excitation wavelength, emission wavelength, and quantum yield of **1**(OMe), **1**$(OMe)_{ocb}$, **3**(OMe), **3**$(OMe)_{ocb}$, **4**(OMe), and **5**(OMe) in CH_3CN (10 μM).

name	λ_{ex} (nm)	λ_{em} (nm)	Φ_F (%)
1(OMe)	331	445	29
1$(OMe)_{ocb}$	331	445	5
3(OMe)	331	388	60
3$(OMe)_{ocb}$	331	389	11
4(OMe)	400	556	64
5(OMe)	400	499	64

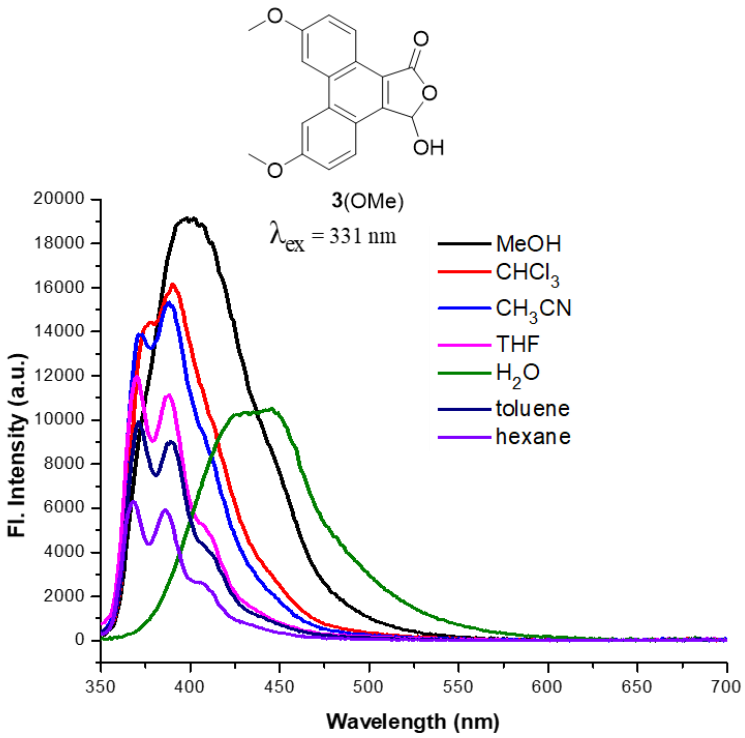

Figure S107. Fluorescence spectra of **3**(OMe) (10 μM) in different solvents with excitation at 331 nm.

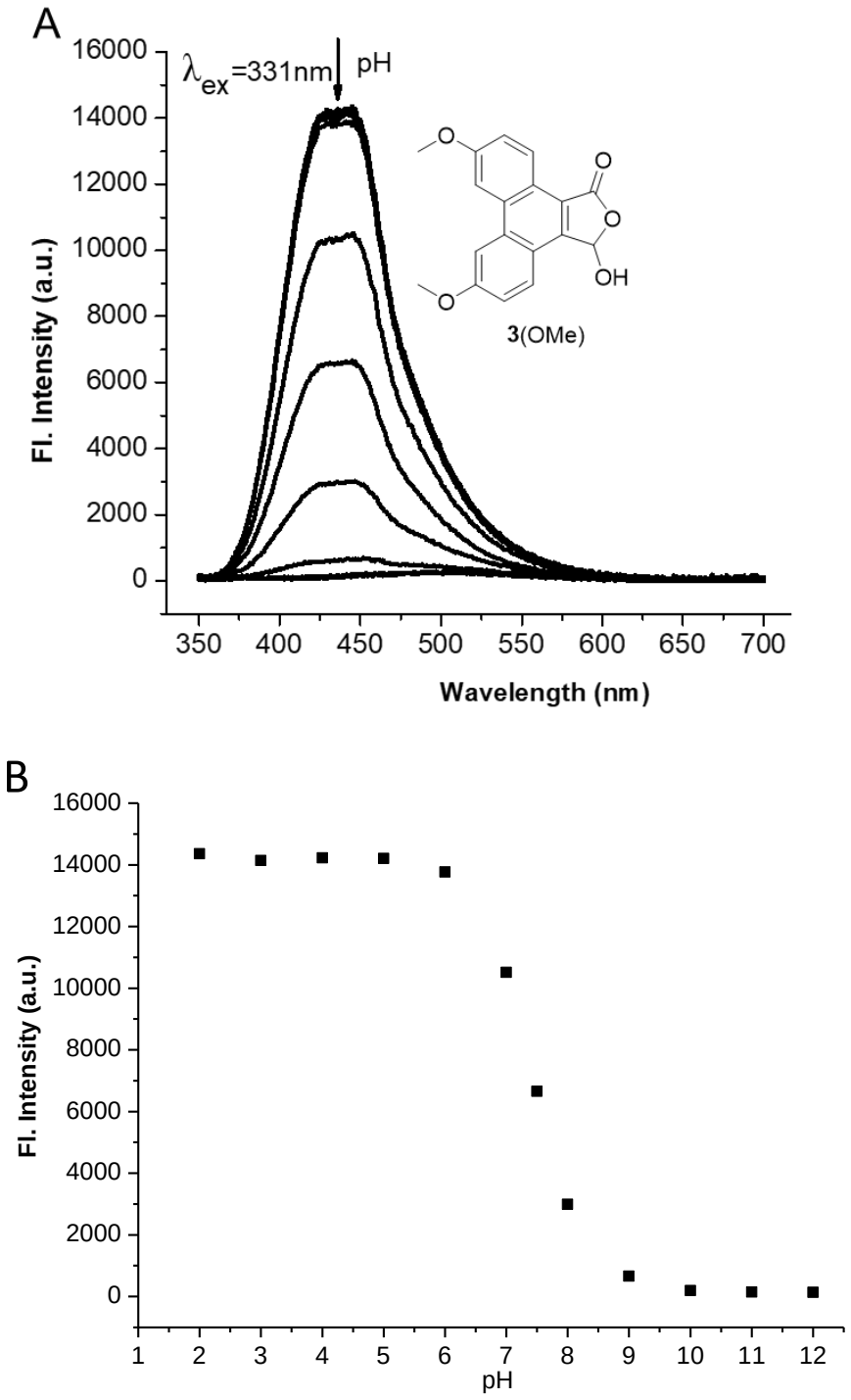

Figure S108. Fluorescence titration (A) as well as titration curve at 445 nm (B) of **3**(OMe) (10 μM) in PBS buffer (40 mM) with different pH (excitation at 331 nm).

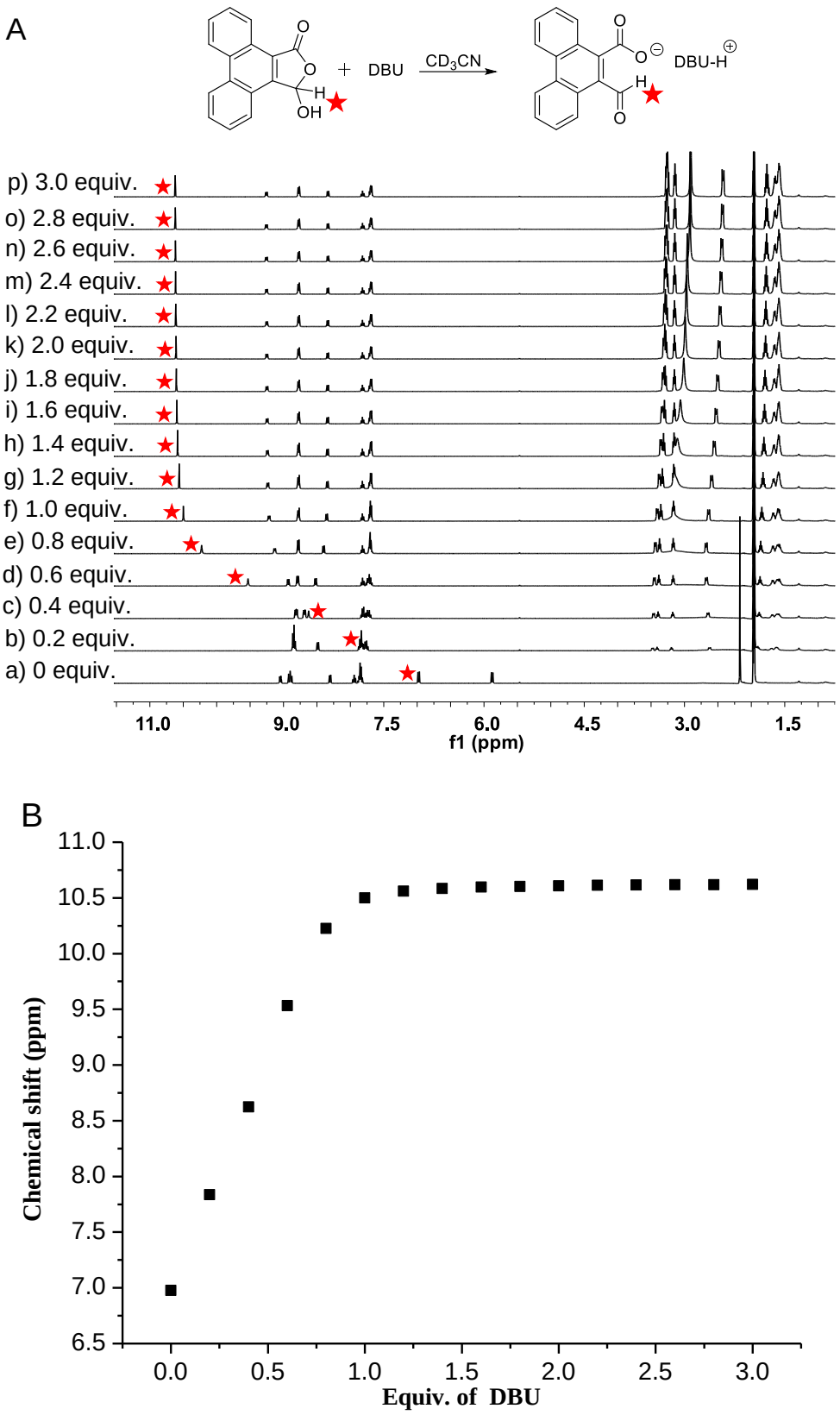

Figure S109. ^{1}H NMR spectra (A) as well as titration curve (B) of **3**(H) (16.7 mM) with DBU (0-3.0 equiv.) in CD_3CN. The tracked proton is marked with a star.

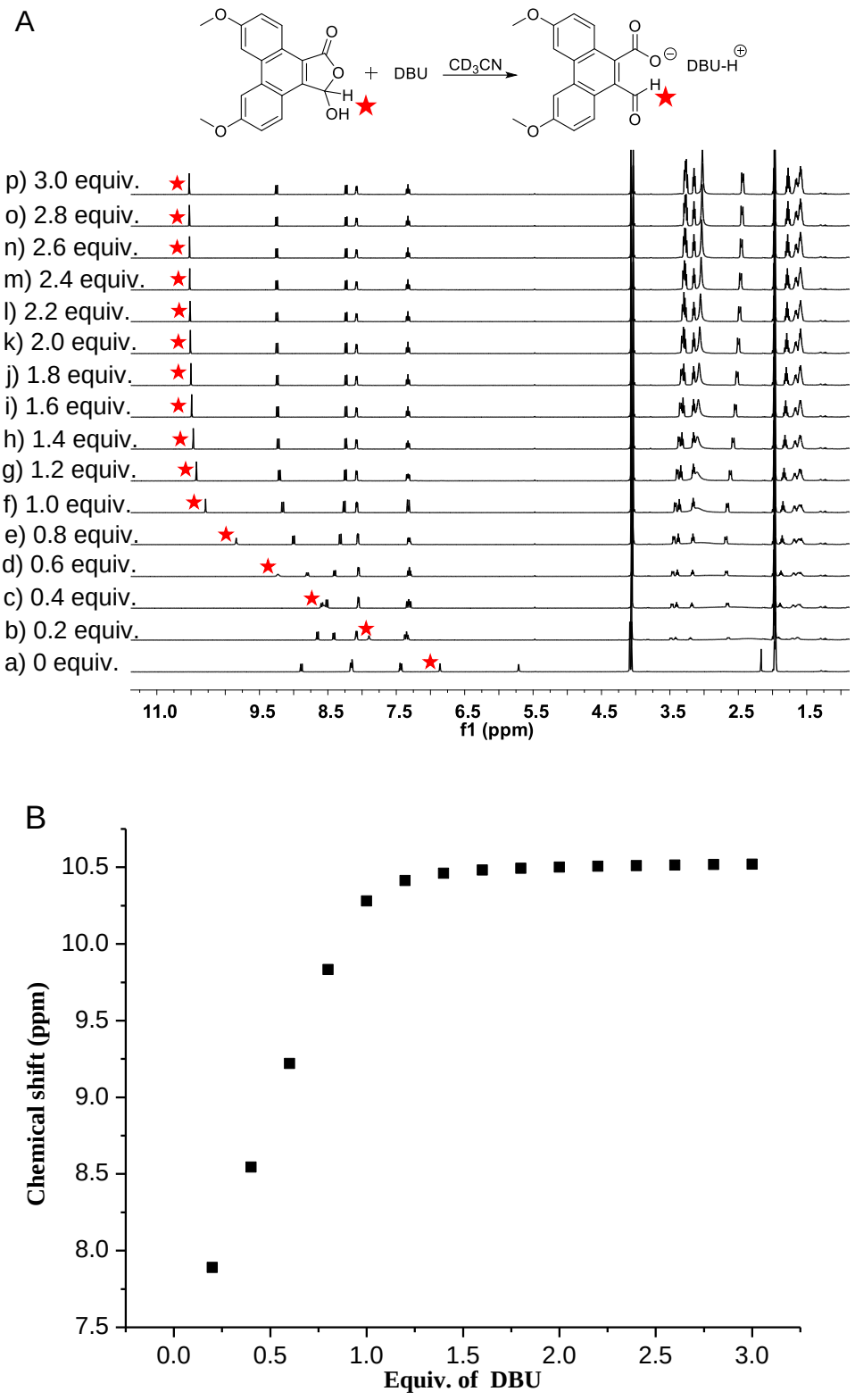

Figure S110. ^{1}H NMR spectra (A) as well as titration curve (B) of **3**(OMe) (16.7 mM) with DBU (0-3.0 equiv.) in CD_3CN. The tracked proton is marked with a star.

7. DCC and PL in the Solid State

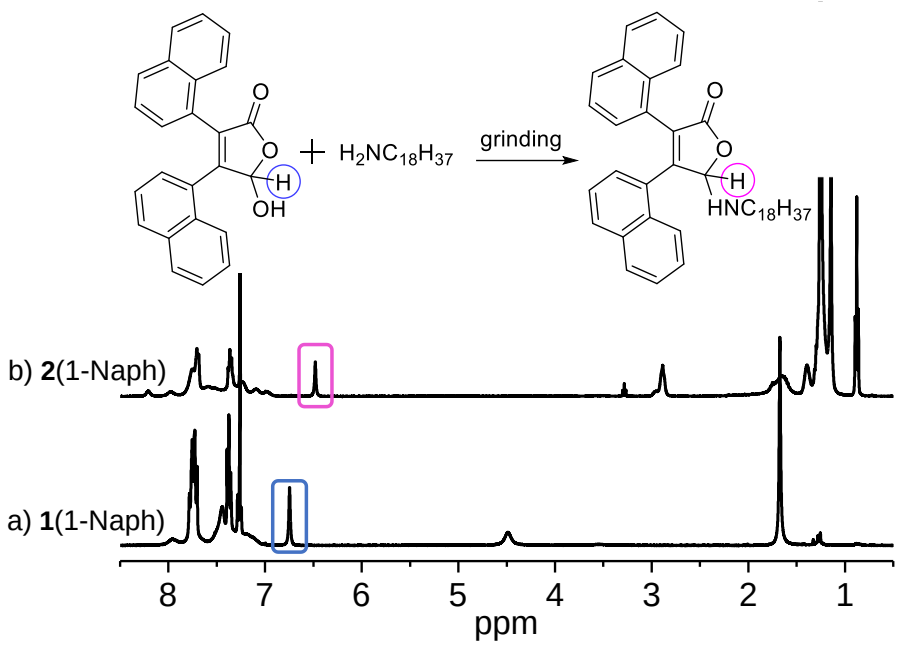

Figure S111. ^{1}H NMR spectra of **1**(1-Naph) (a) and its reaction with 1-octadecylamine (1.2 equiv., b) in the solid state, checked in $CDCl_3$. **2**(1-Naph) was obtained by grinding the solid mixture of **1**(1-Naph) (~10 mg, 1.0 equiv.) and 1-octadecylamine (1.2 equiv.) in a quartz mortar for 10 min.

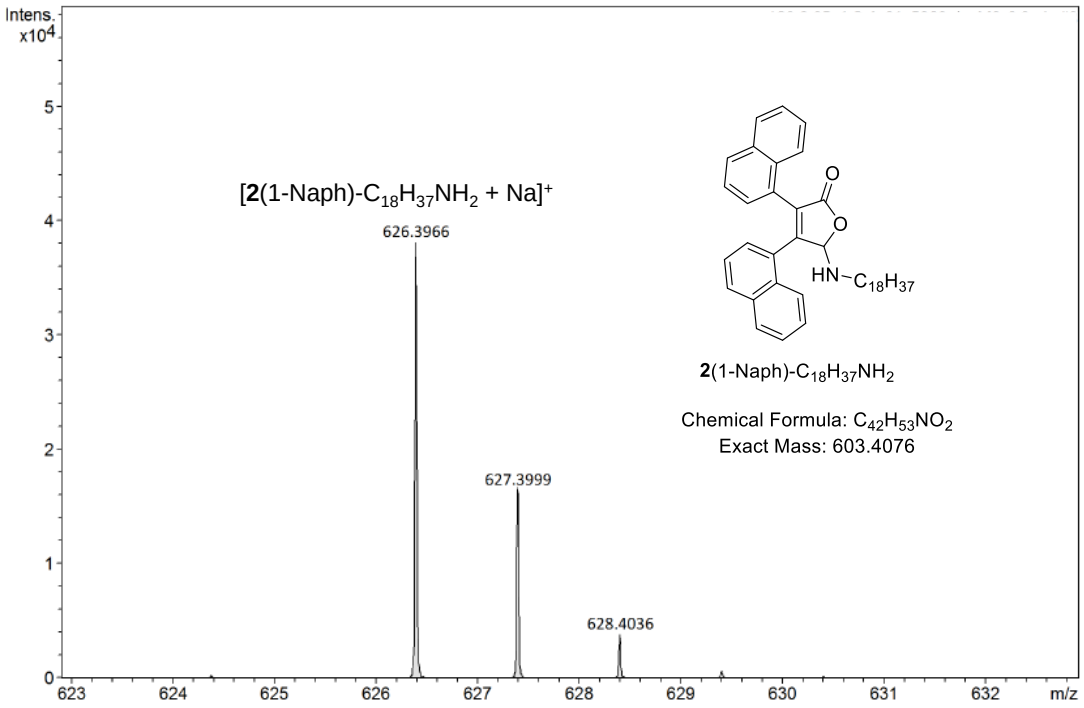

Figure S112. ESI mass spectrum of the solid-state reaction of **1**(1-Naph) and 1-octadecylamine.

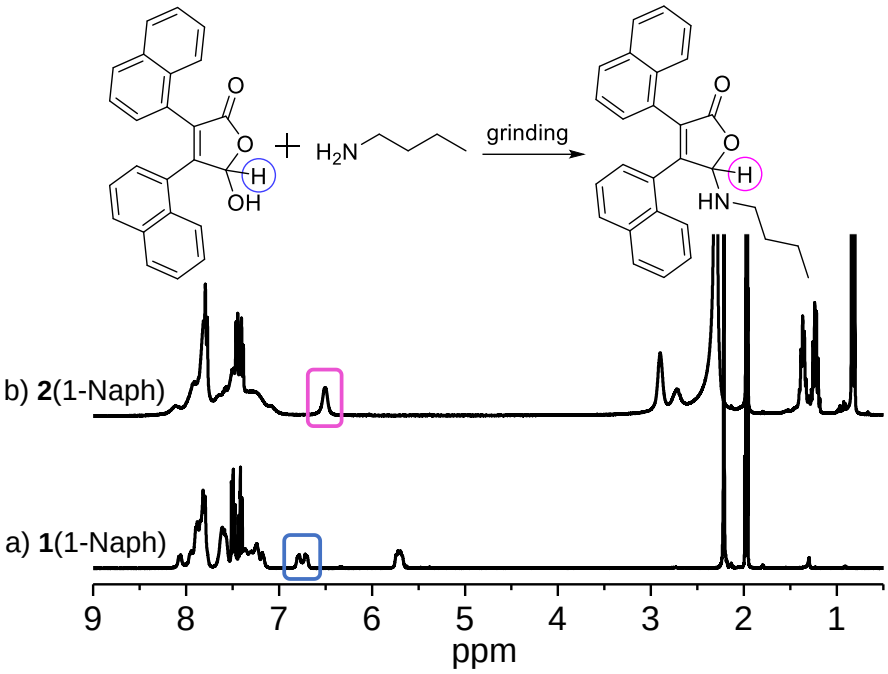

Figure S113. ^{1}H NMR spectra of **1**(1-Naph) (a) and its reaction with 1-butylamine (1.2 equiv., b) in the solid state, checked in CD_3CN. **2**(1-Naph) was obtained by grinding the solid mixture of **1**(1-Naph) (~10 mg, 1.0 equiv.) and 1- butylamine (1.2 equiv.) in a quartz mortar for 20 min.

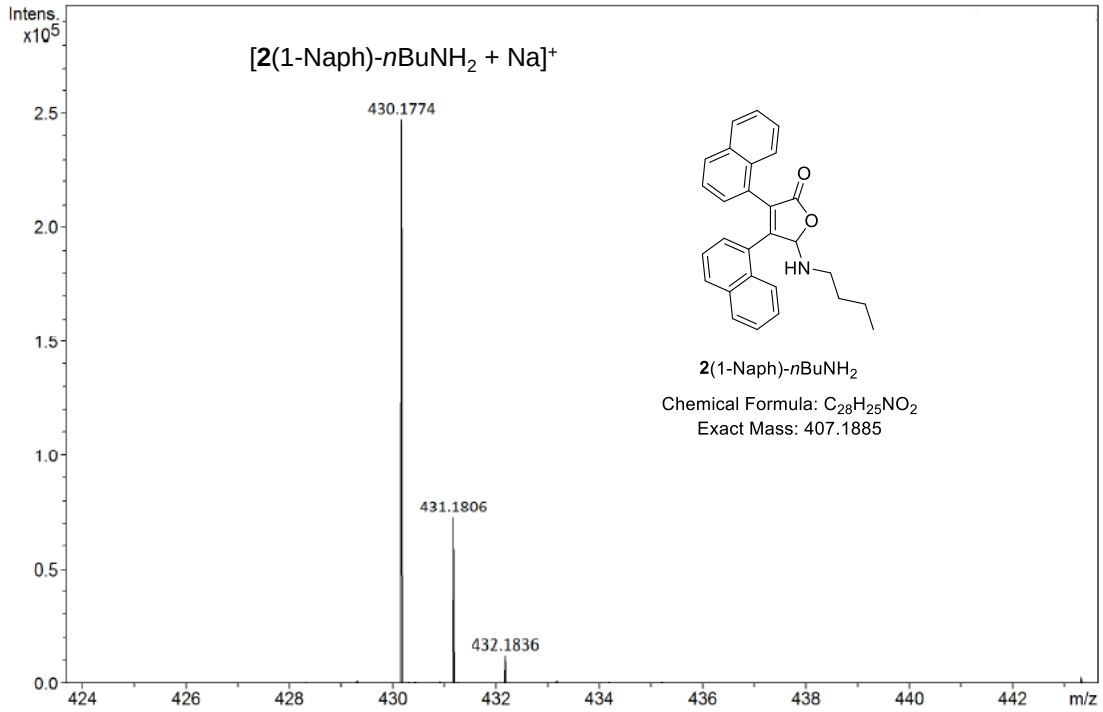

Figure S114. ESI mass spectrum of the solid-state reaction of **1**(1-Naph) and 1-butylamine.

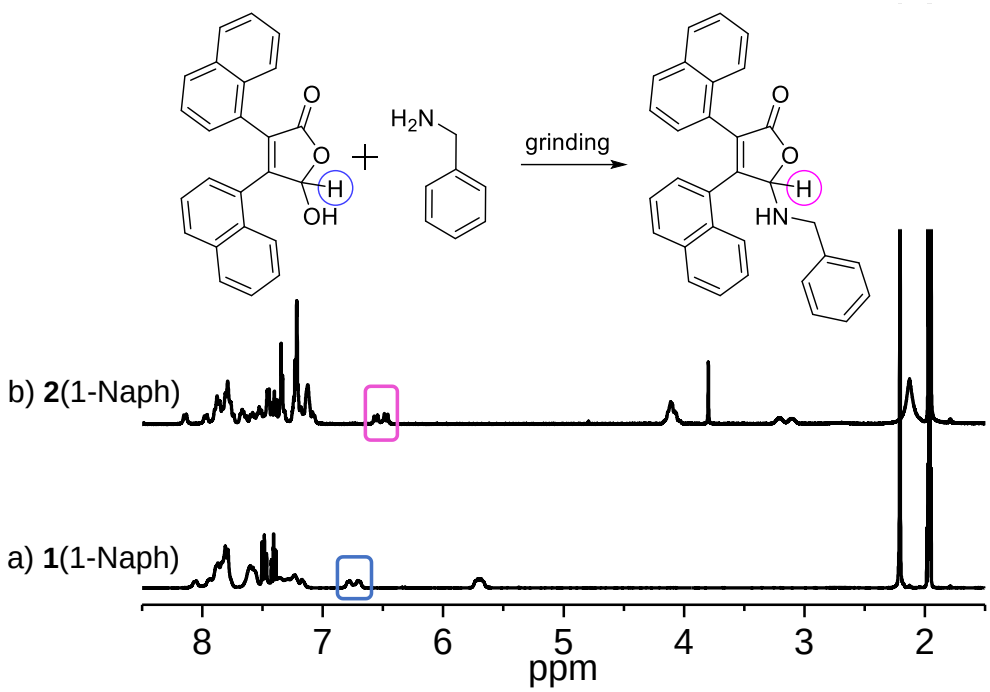

Figure S115. ^{1}H NMR spectra of **1**(1-Naph) (a) and its reaction with benzylamine (1.2 equiv., b) in the solid state, checked in CD_3CN. **2**(1-Naph) was obtained by grinding the solid mixture of **1**(1-Naph) (~10 mg, 1.0 equiv.) and benzylamine (1.2 equiv.) in a quartz mortar for 25 min.

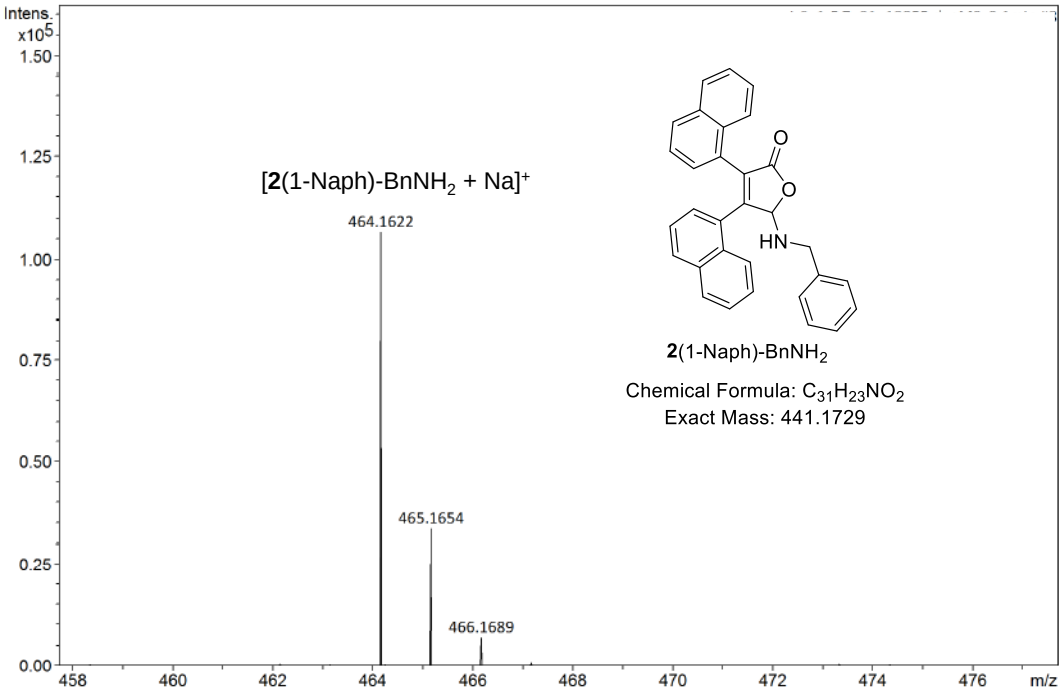

Figure S116. ESI mass spectrum of the solid-state reaction of **1**(1-Naph) and Benzylamine.

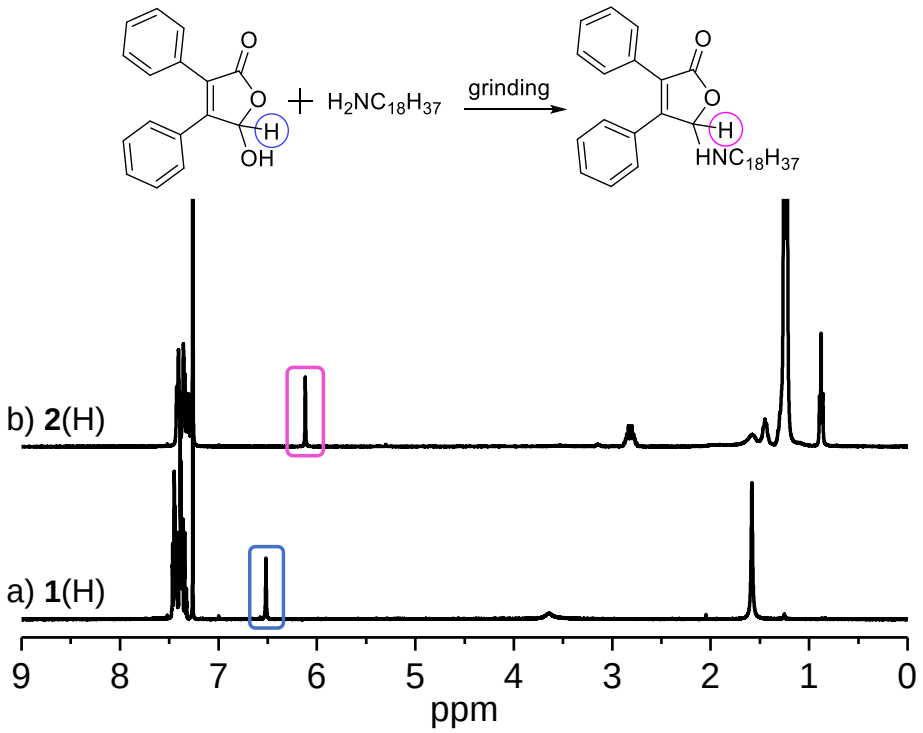

Figure S117. ^{1}H NMR spectra of **1**(H) (a) and its reaction with 1-octadecylamine (1.2 equiv., b) in the solid state, checked in $CDCl_3$. **2**(H) was obtained by grinding the solid mixture of **1**(H) (~10 mg, 1.0 equiv.) and 1-octadecylamine (1.2 equiv.) in a quartz mortar for 20 min.

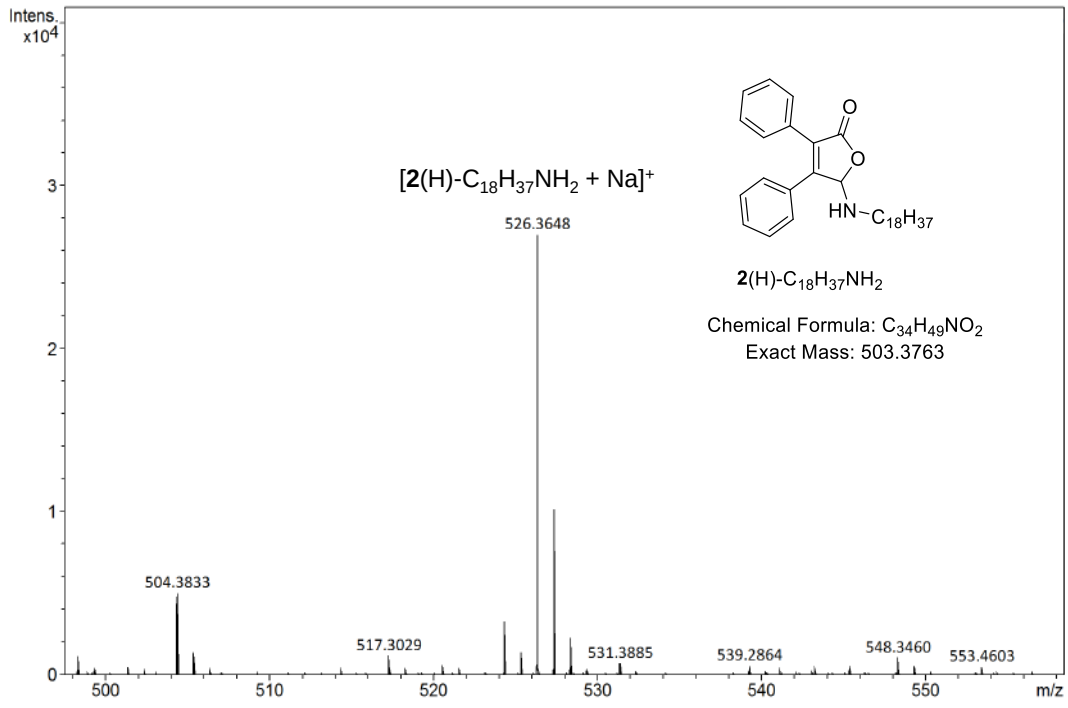

Figure S118. ESI mass spectrum of the solid-state reaction of **1**(H) and 1-octadecylamine.

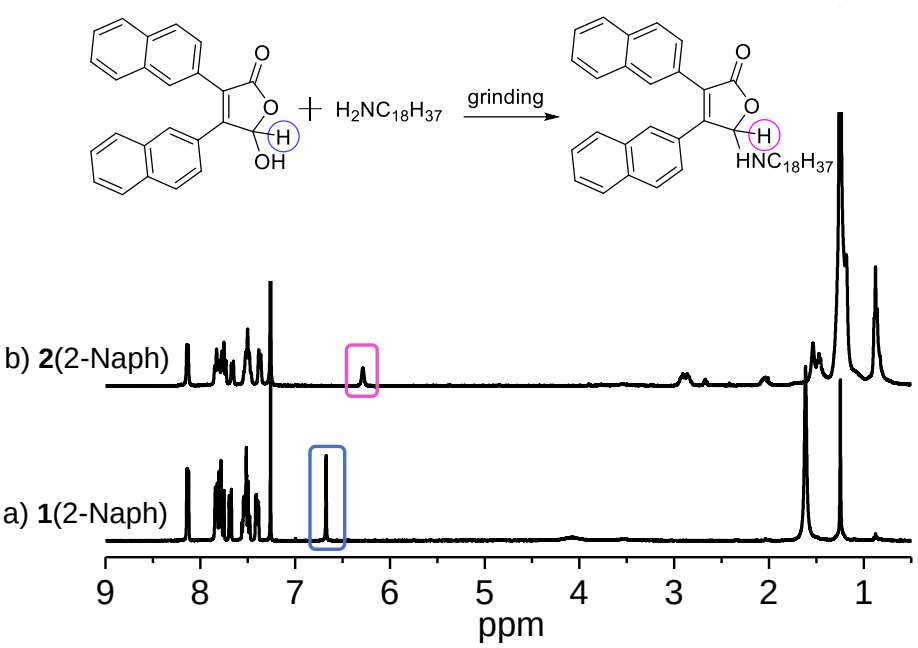

Figure S119. ^{1}H NMR spectra of **1**(2-Naph) (a) and its reaction with 1-octadecylamine (1.2 equiv., b) in the solid state, checked in $CDCl_3$. **2**(2-Naph) was obtained by grinding the solid mixture of **1**(2-Naph) (~10 mg, 1.0 equiv.) and 1-octadecylamine (1.2 equiv.) in a quartz mortar for 60 min.

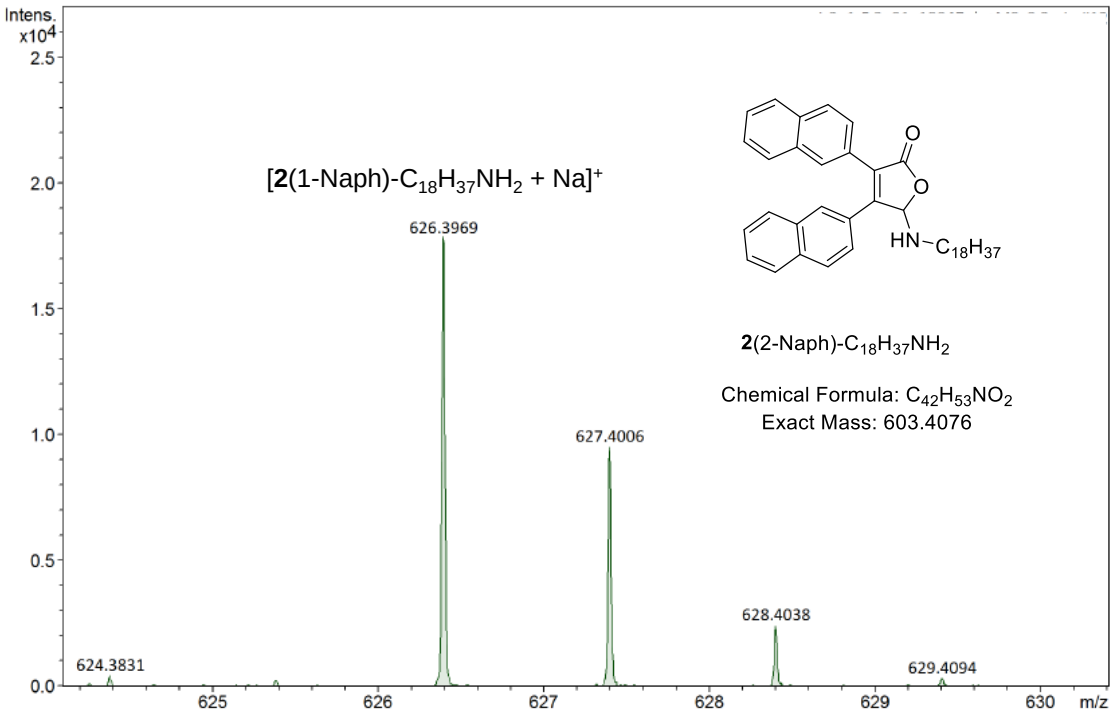

Figure S120. ESI mass spectrum of the solid-state reaction of **1**(2-Naph) and 1-octadecylamine.

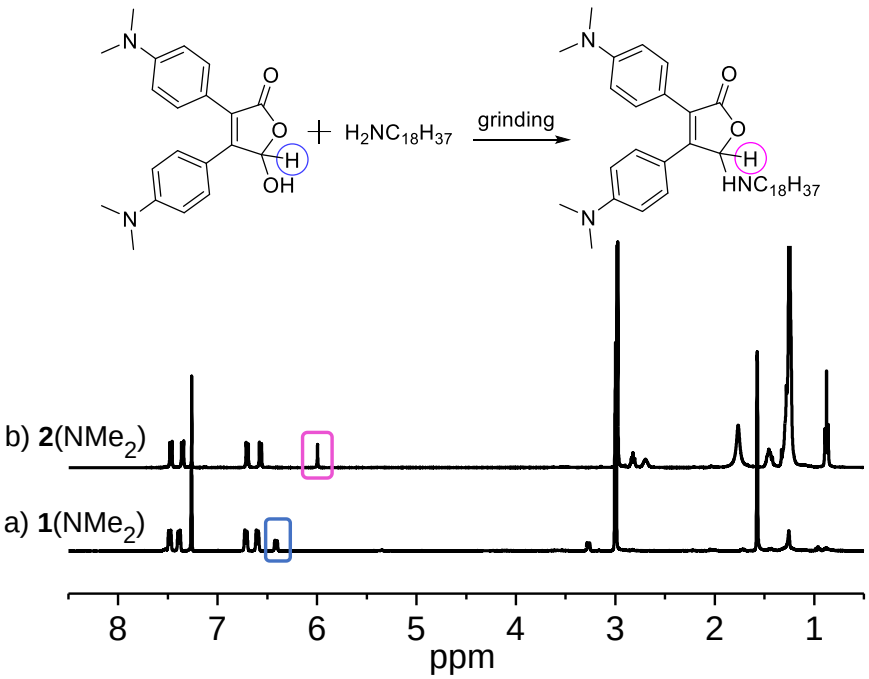

Figure S121. ^{1}H NMR spectra of **1**(NMe_2) (a) and its reaction with 1-octadecylamine (1.2 equiv., b) in the solid state, checked in $CDCl_3$. **2**(NMe_2) was obtained by grinding the solid mixture of **1**(NMe_2) (~10 mg, 1.0 equiv.) and 1-octadecylamine (1.2 equiv.) in a quartz mortar for 5 h.

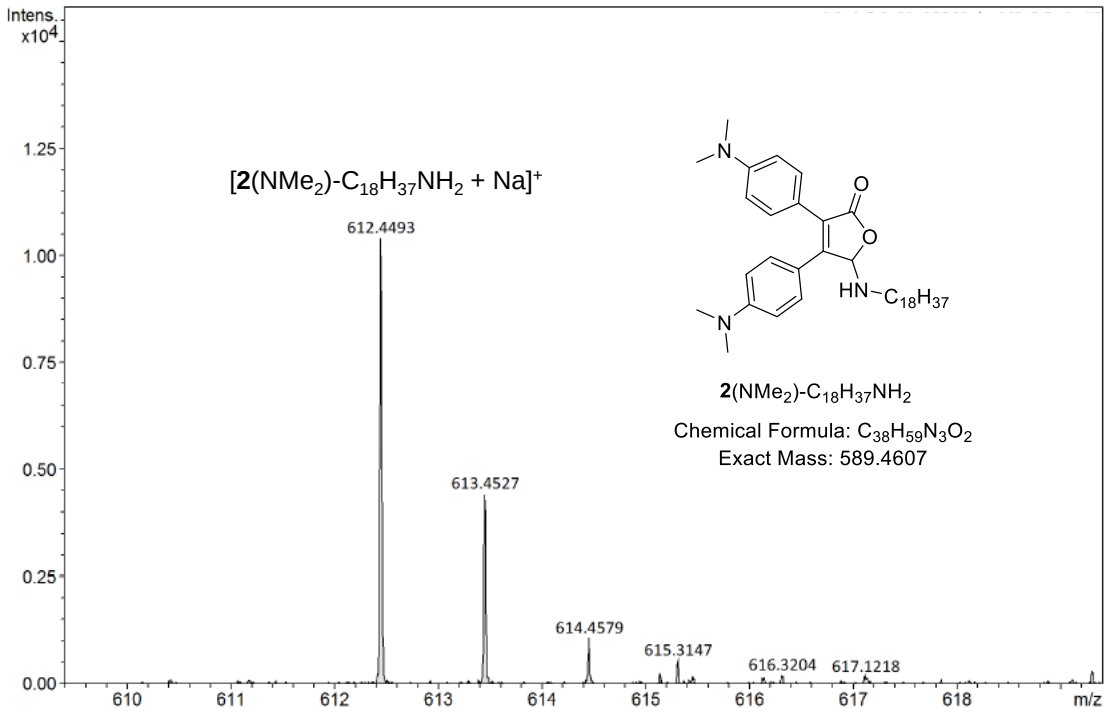

Figure S122. ESI mass spectrum of the solid-state reaction of **1**(NMe_2) and 1-octadecylamine.

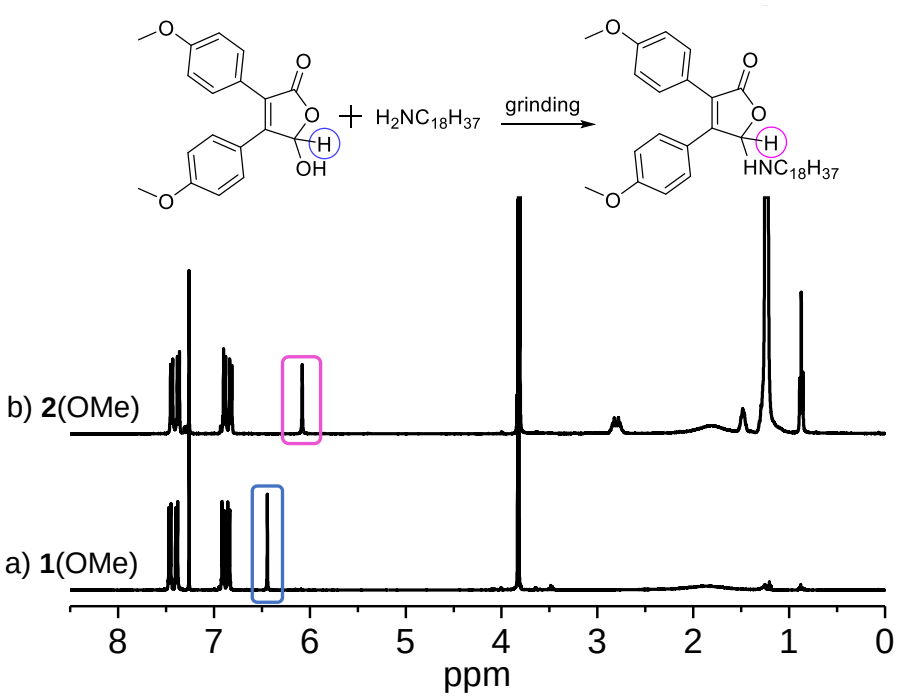

Figure S123. ^{1}H NMR spectra of **1**(OMe) (a) and its reaction with 1-octadecylamine (1.2 equiv., b) in the solid state, checked in $CDCl_3$. **2**(OMe) was obtained by grinding the solid mixture of **1**(OMe) (~10 mg, 1.0 equiv.) and 1-octadecylamine (1.2 equiv.) in a quartz mortar for 90 min.

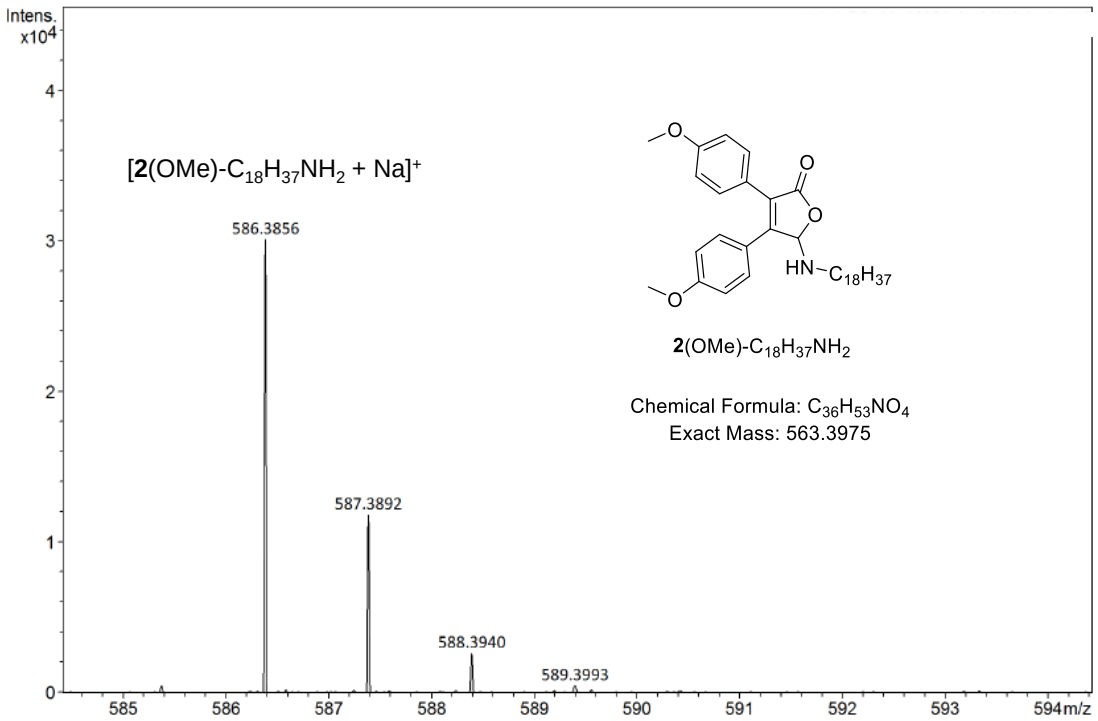

Figure S124. ESI mass spectrum of the solid-state reaction of **1**(OMe) and 1-octadecylamine.

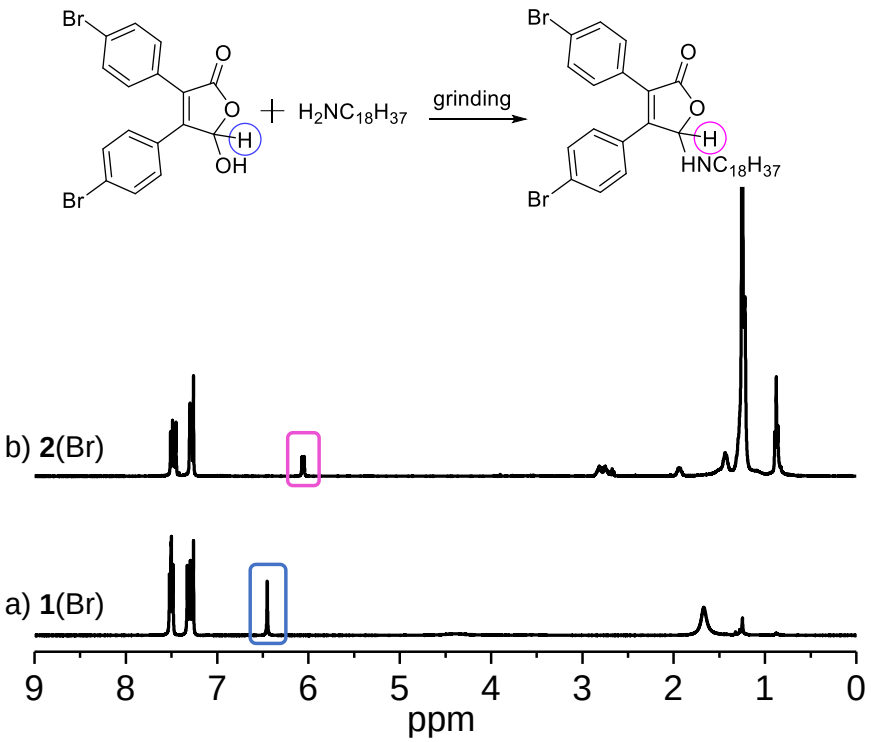

Figure S125. ^{1}H NMR spectra of **1**(Br) (a) and its reaction with 1-octadecylamine (1.2 equiv., b) in the solid state, checked in $CDCl_3$. **2**(Br) was obtained by grinding the solid mixture of **1**(Br) (~10 mg, 1.0 equiv.) and 1-octadecylamine (1.2 equiv.) in a quartz mortar for 60 min.

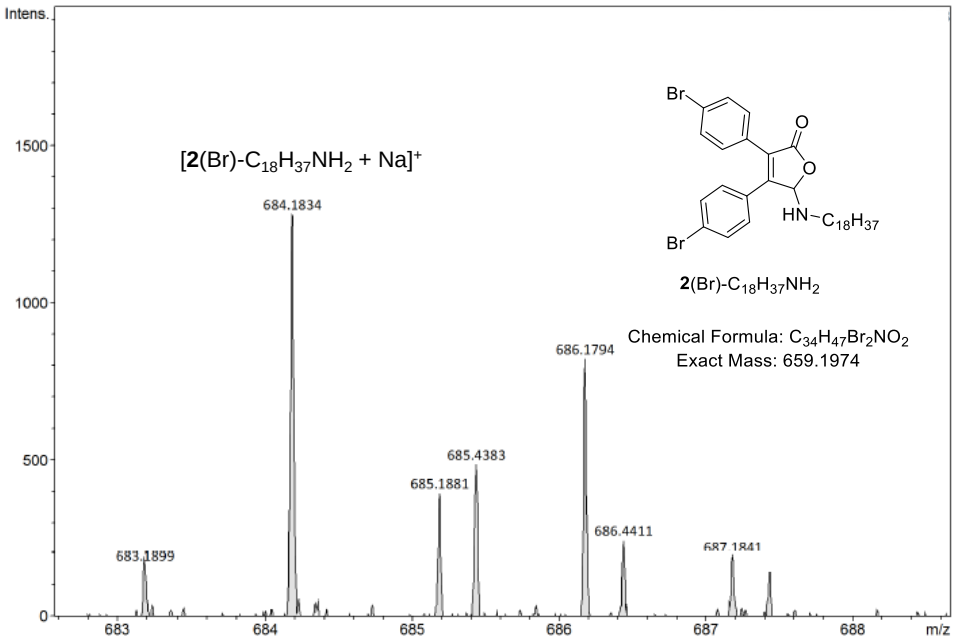

Figure S126. ESI mass spectrum of the solid-state reaction of **1**(Br) and 1-octadecylamine.

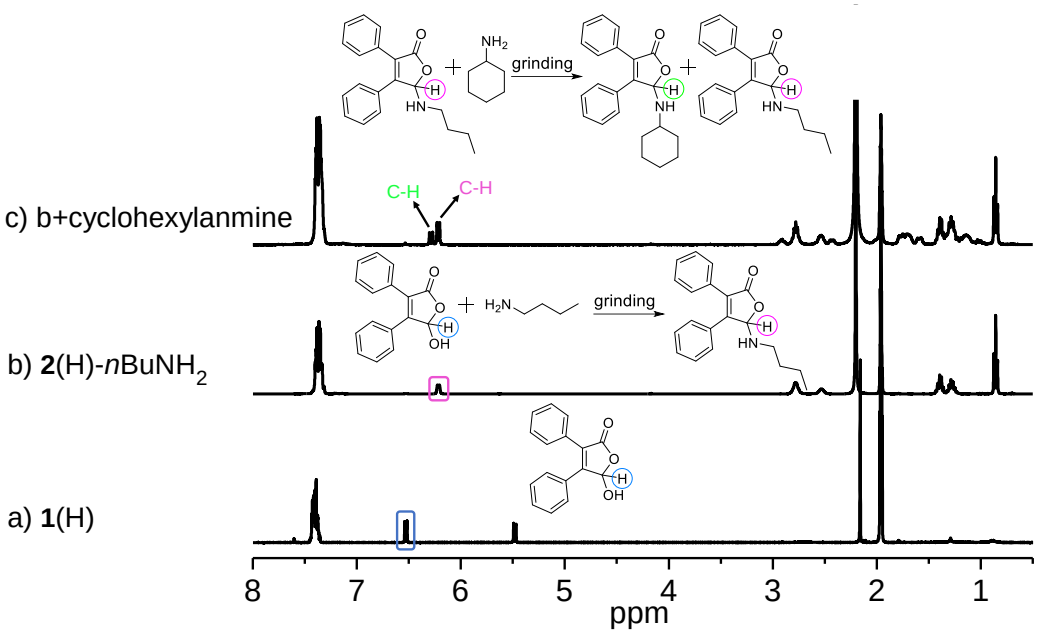

Figure S127. ^{1}H NMR spectra of **1**(H) (a), 1-butylamine (1.2 equiv.) derived **2**(H) (b), and dynamic amine exchange with cyclohexylamine (1.2 equiv., c) in solid state, checked in CD_3CN. Amine exchange was conducted by grinding the solid mixture of **2**(H)-*n*$BuNH_2$ (~10 mg, 1.0 equiv.) and cyclohexylamine (1.2 equiv.) in a quartz mortar for 30 min.

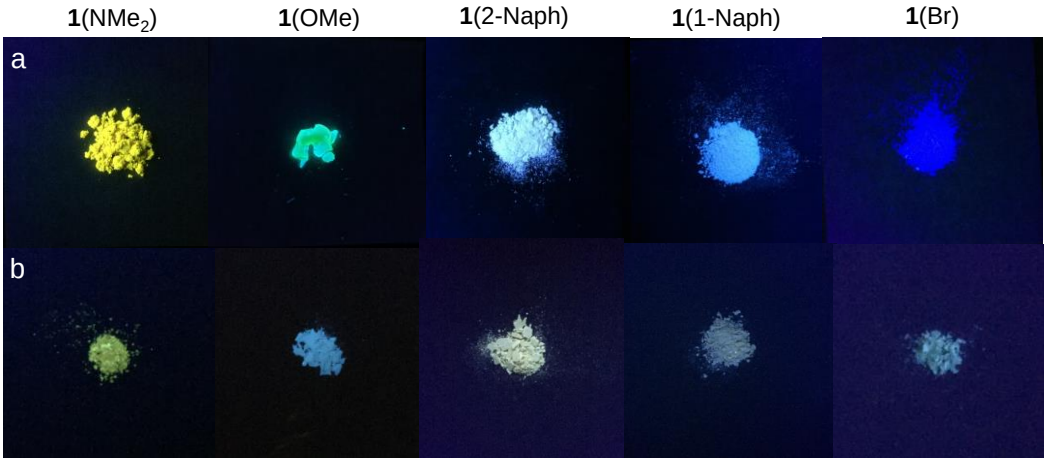

Figure S128. Photographs of **1**(NMe_2), **1**(MeO), **1**(2-Naph), **1**(1-Naph), and **1**(Br) (a) and their reaction products (b) with 1-octadecylamine (1.2 equiv.) in the solid state taken under UV light (365 nm) irradiation.

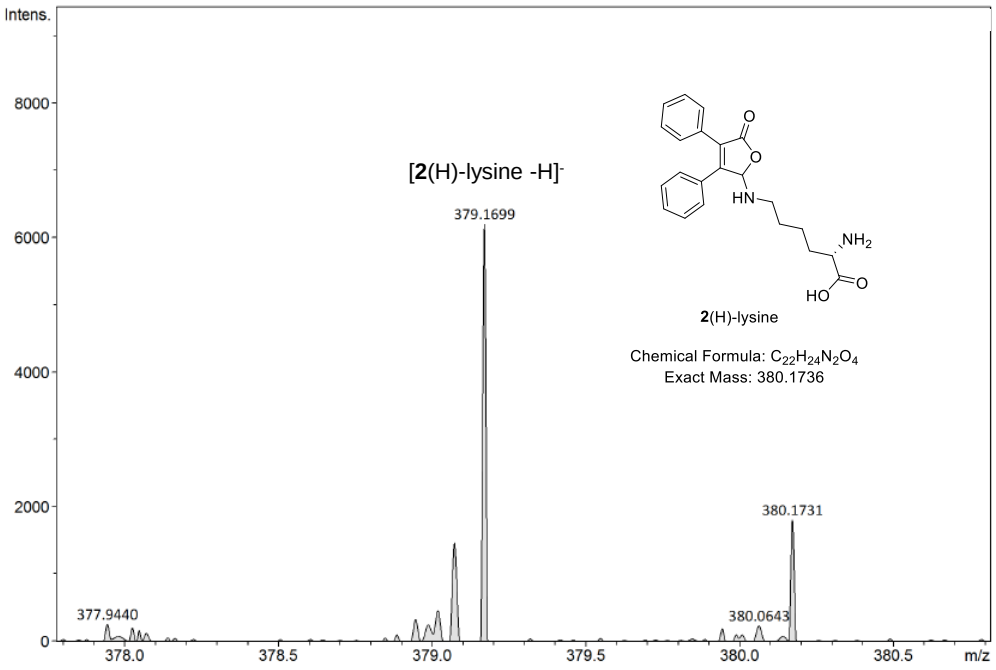

Figure S129. ESI mass spectrum of the solid-state reaction of **1**(H) and L-lysine.

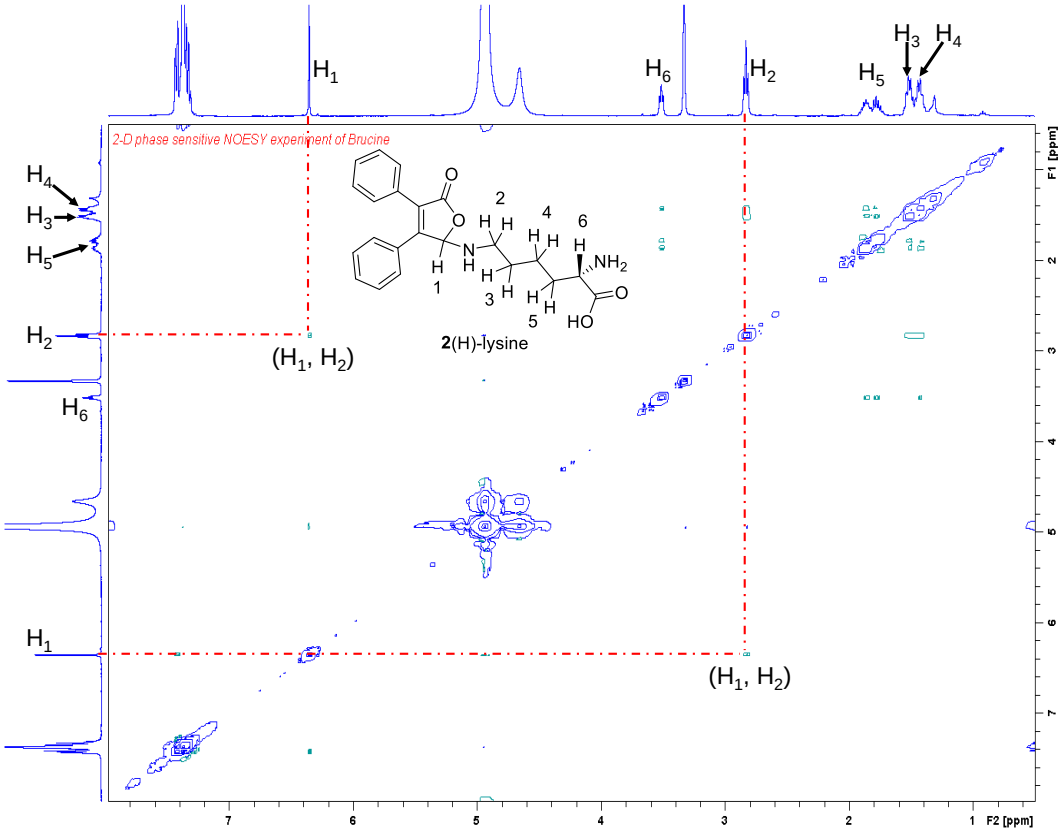

Figure S130. A section of 400 MHz ^{1}H-^{1}H 2D-NOESY spectrum of **2**(H)-lysine in CD_3OD. The structure of **2**(H)-lysine is shown.

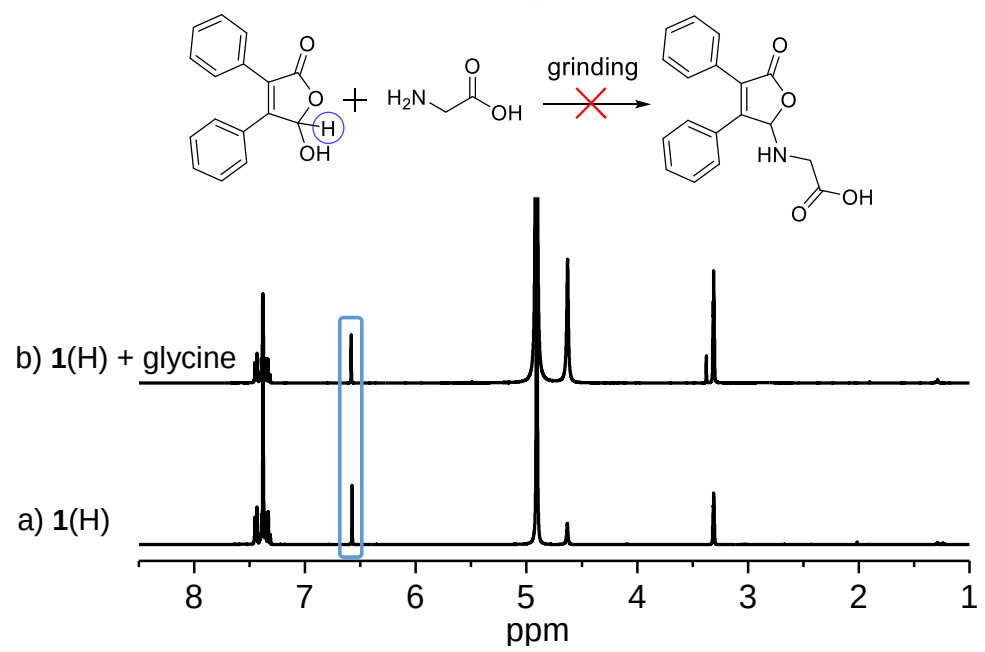

Figure S131. ^{1}H NMR spectra of **1**(H) (a) and its reaction with glycine (1.2 equiv., b) in the solid state, checked in CD_3OD. No reaction occurred under this condition.

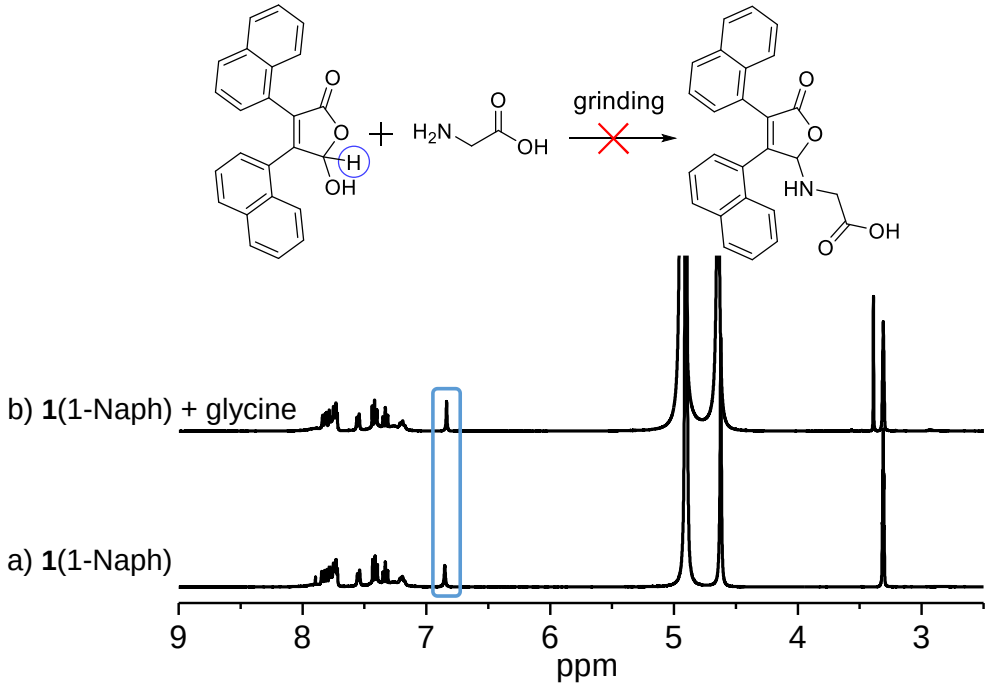

Figure S132. ^{1}H NMR spectra of **1**(1-Naph) (a) and its reaction with glycine (1.2 equiv., b) in the solid state, checked in CD_3OD. No reaction occurred under this condition.

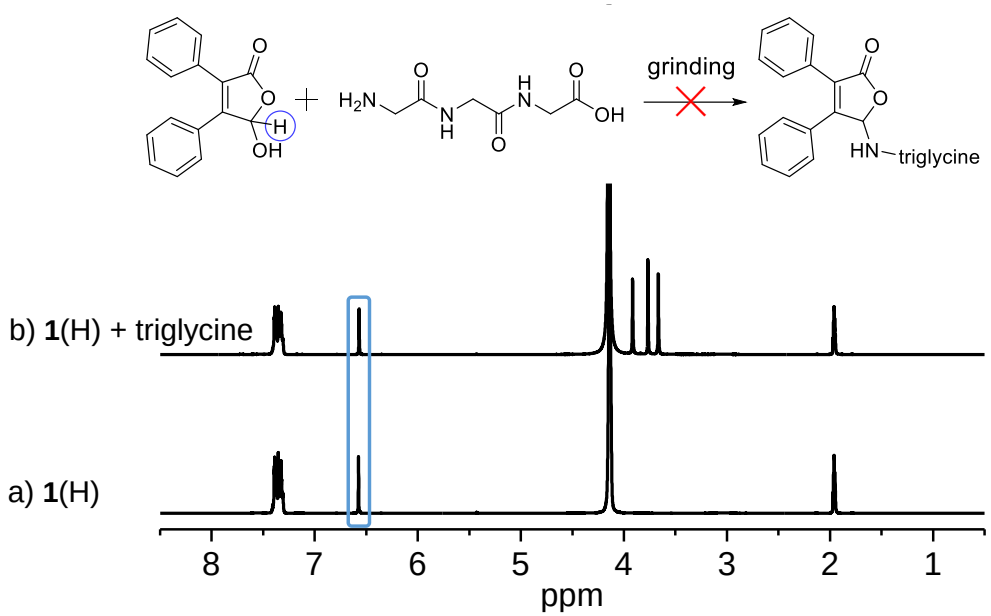

Figure S133. ^{1}H NMR spectra of **1**(H) (a) and its reaction with triglycine (1.2 equiv., b) in the solid state, checked in CD_3CN/D_2O (3:2, v/v). No reaction occurred under this condition.

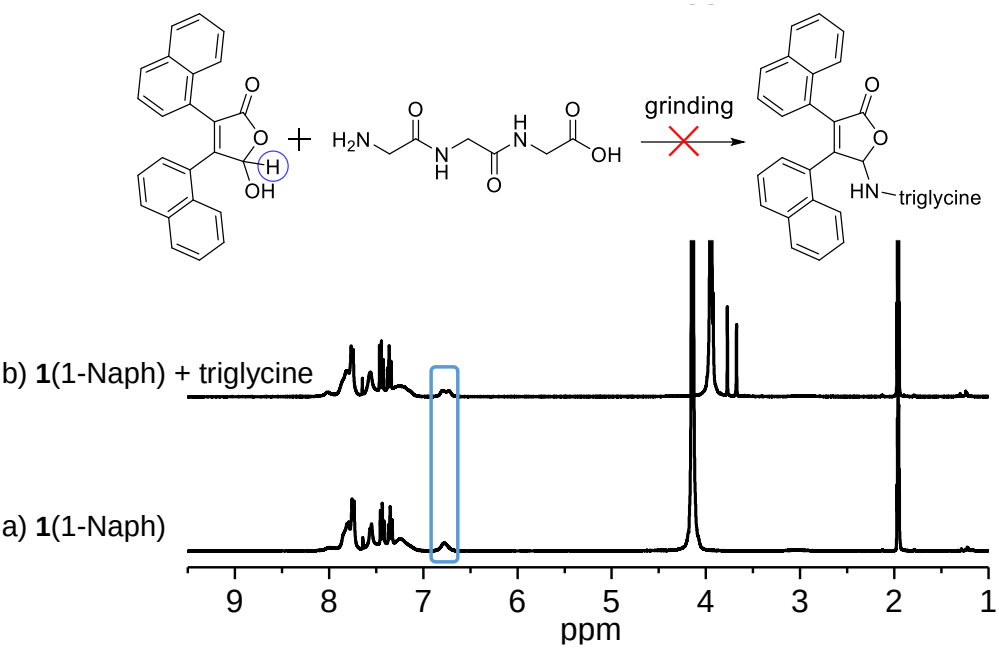

Figure S134. ^{1}H NMR spectra of **1**(1-Naph) (a) and its reaction with triglycine (1.2 equiv., b) in the solid state, checked in CD_3CN/D_2O (3:2, v/v). No reaction occurred under this condition.

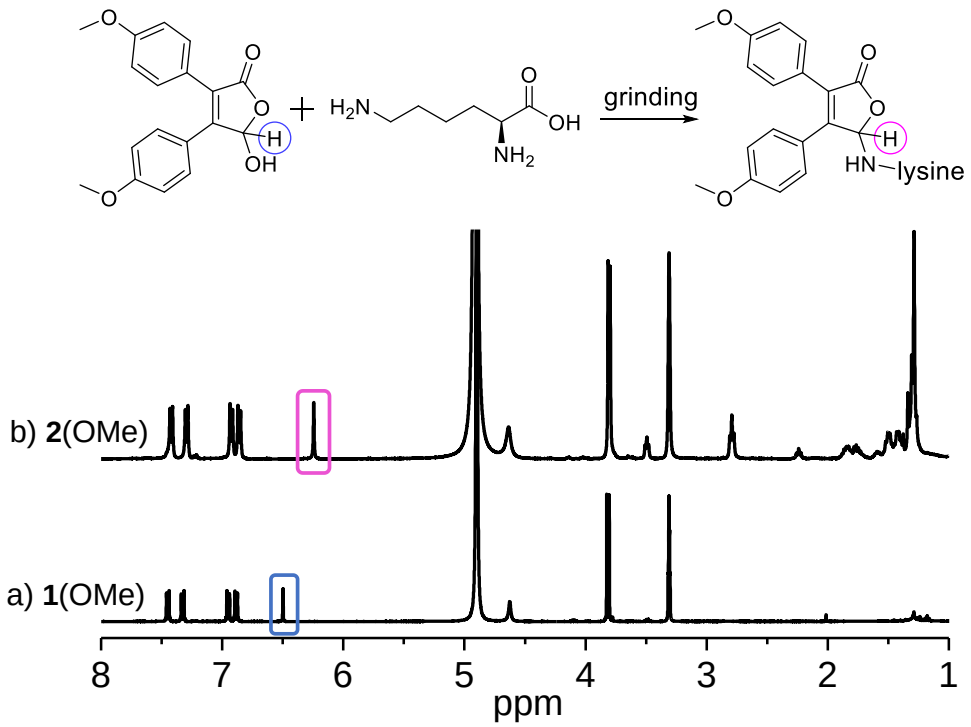

Figure S135. ^{1}H NMR spectra of **1**(OMe) (a) and its reaction with L-lysine (1.2 equiv., b) in the solid state, checked in CD_3OD.

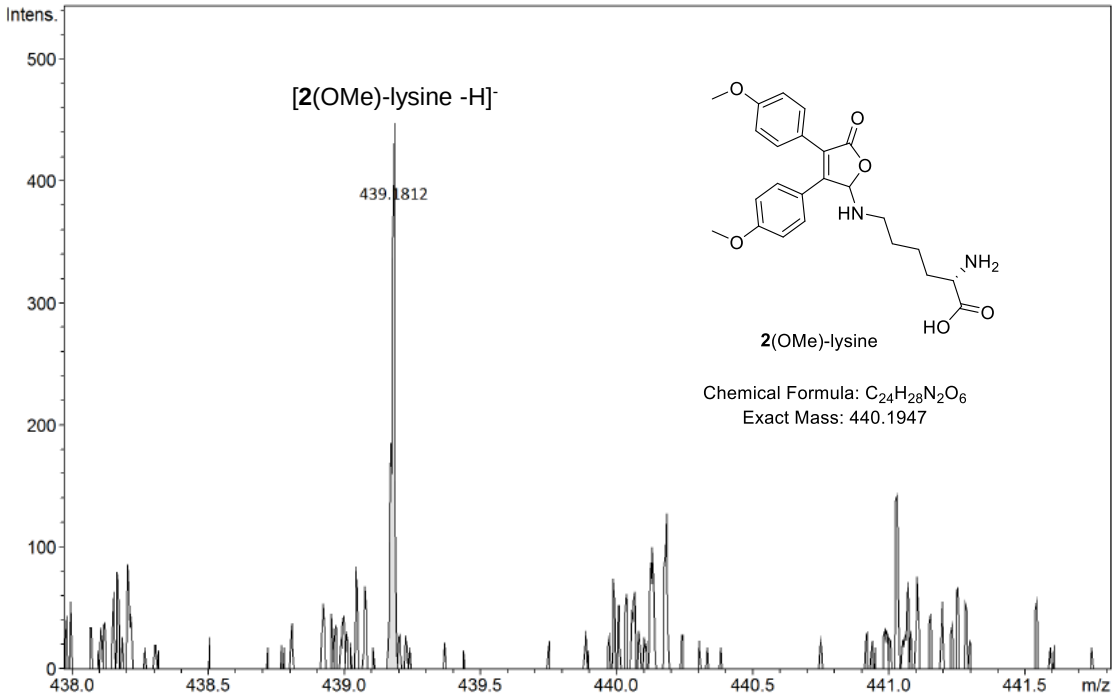

Figure S136. ESI mass spectrum of the solid-state reaction of **1**(OMe) and L-lysine.

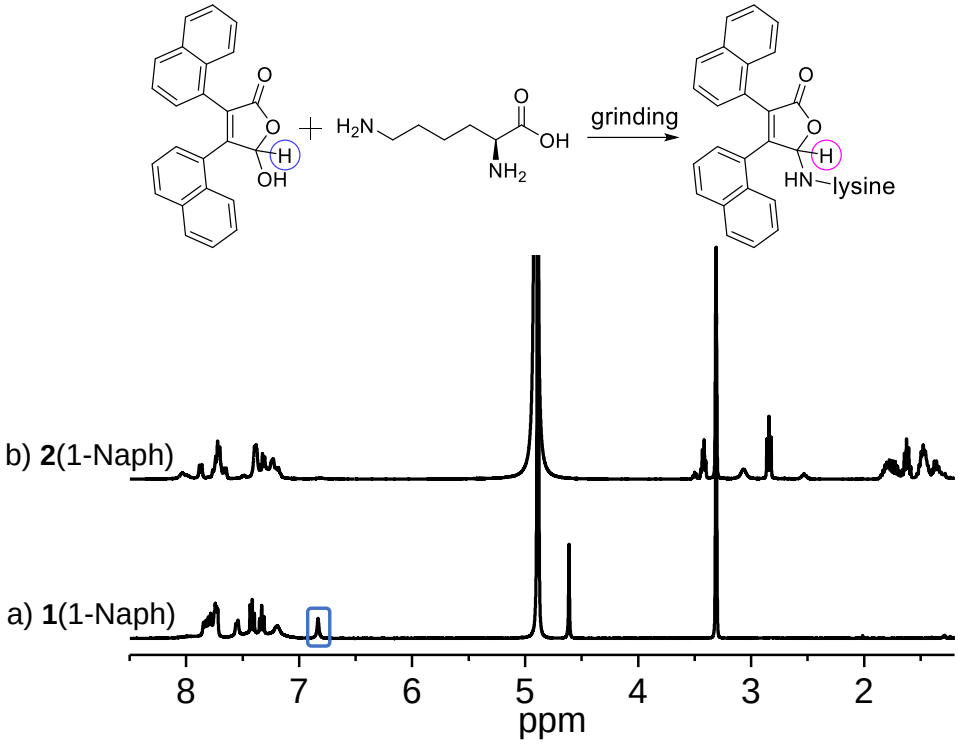

Figure S137. ^{1}H NMR spectra of **1**(1-Naph) (a) and its reaction with L-lysine (1.2 equiv., b) in the solid state, checked in CD_3OD.

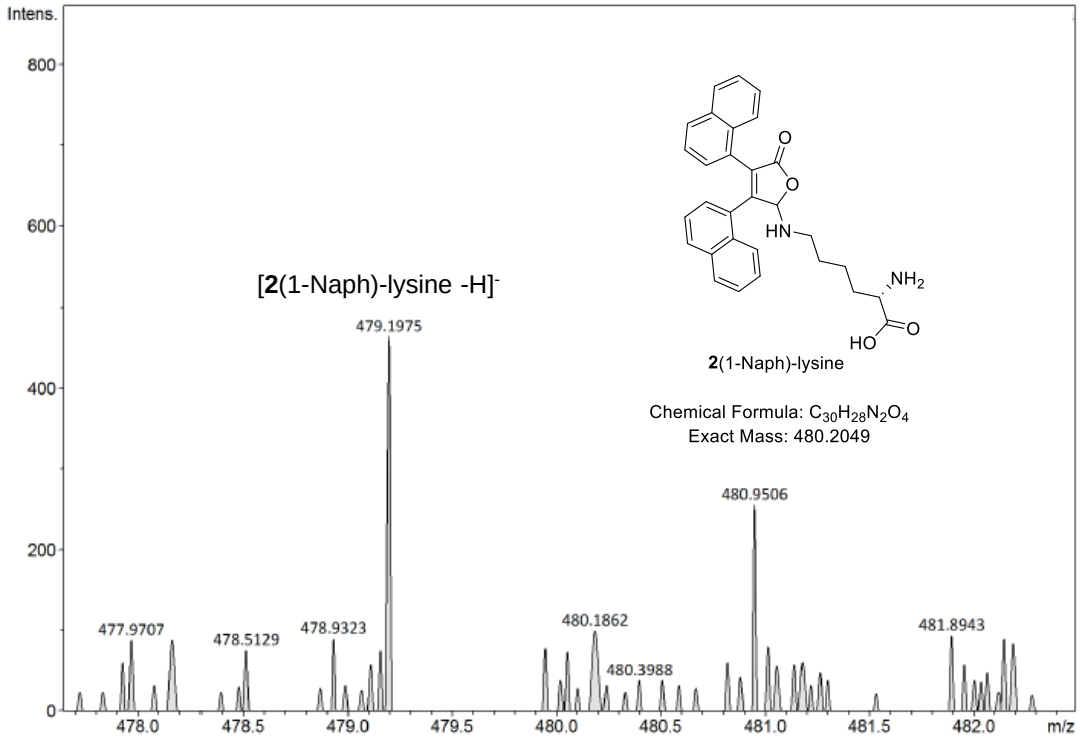

Figure S138. ESI mass spectrum of the solid-state reaction of **1**(1-Naph) and L-lysine.

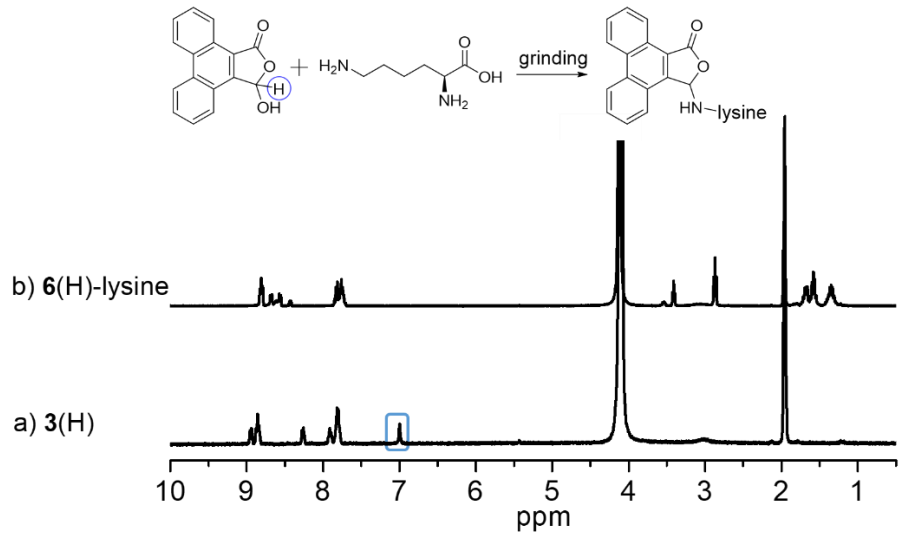

Figure S139. ^{1}H NMR spectra of **3**(H) (a) and its reaction with L-lysine (1.2 equiv., b) in the solid state, checked in CD_3CN/D_2O (3:2, v/v).

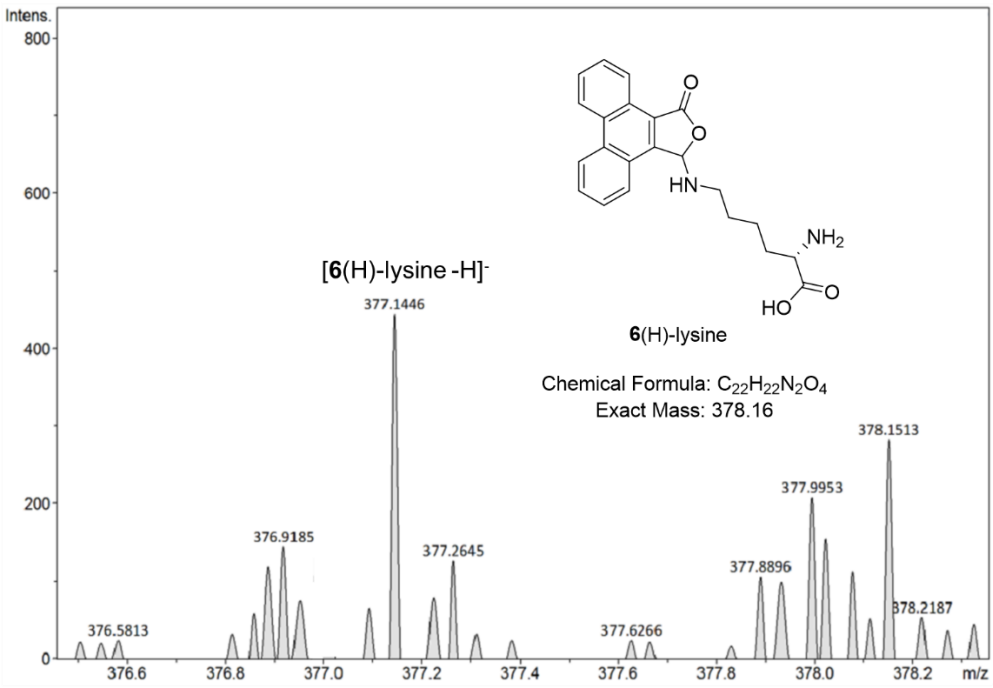

Figure S140. ESI mass spectrum of the solid-state reaction of **3**(H) and L-lysine.

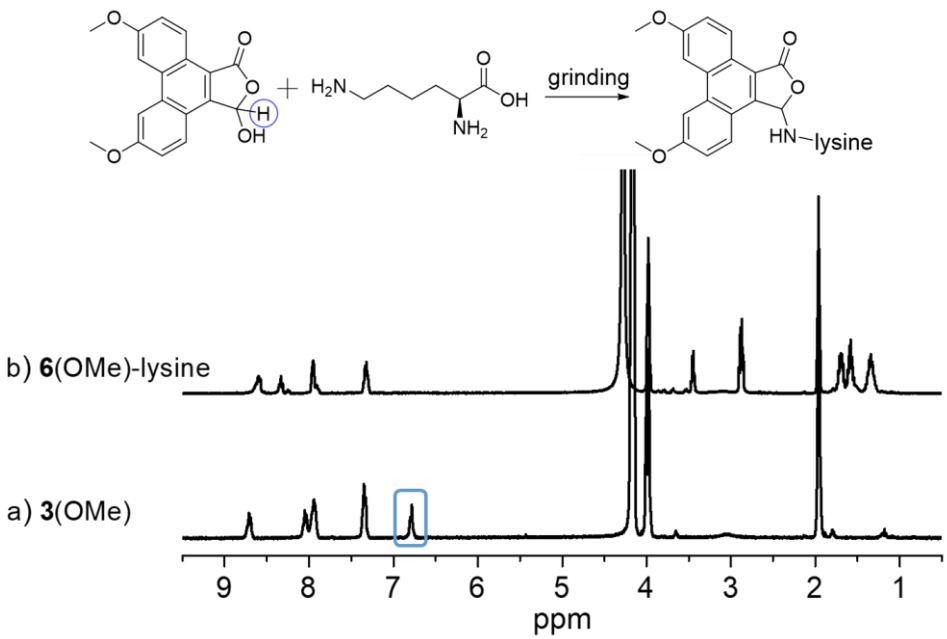

Figure S141. ^{1}H NMR spectra of **3**(OMe) (a) and its reaction with L-lysine (1.2 equiv., b) in the solid state, checked in CD_3CN/D_2O (3:2, v/v).

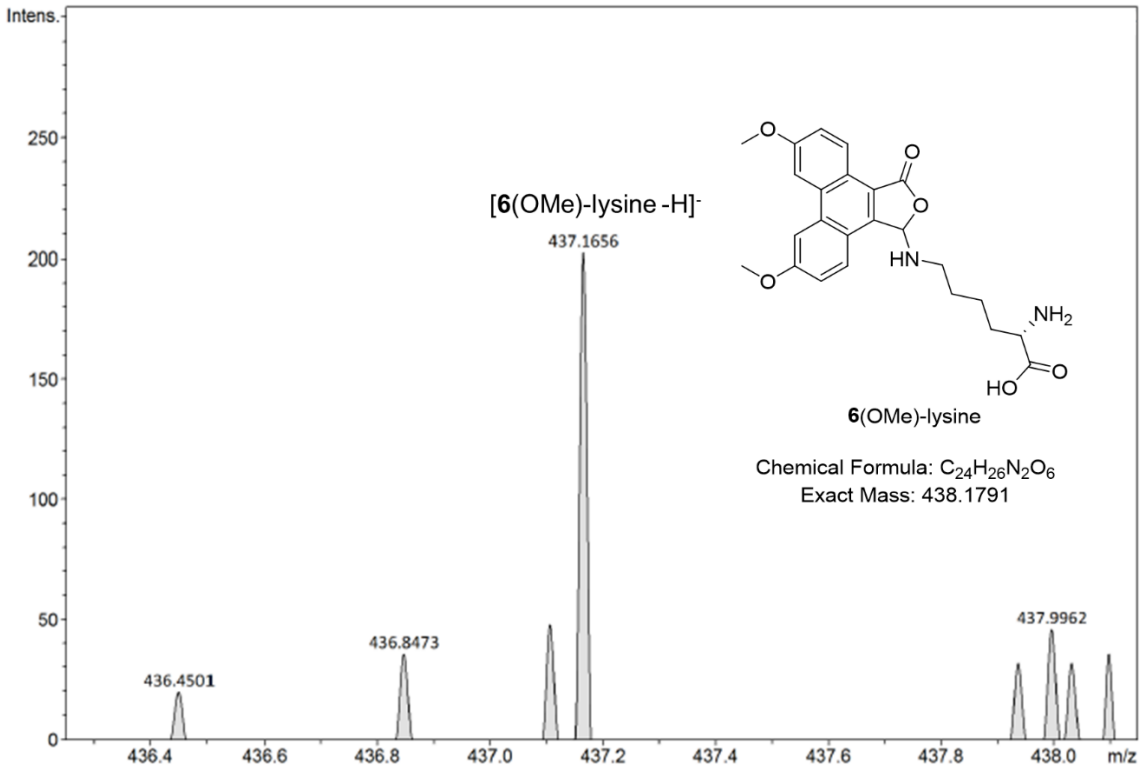

Figure S142. ESI mass spectrum of the solid-state reaction of **3**(OMe) and L-lysine.

8. References

S1. J. E. Boyer, F. C. J. M. van. Veggel, Absolute Quantum Yield Measurements of Colloidal $NaYF_4$: Er_3^+, Yb_3^+ Upconverting Nanoparticles. *Nanoscale*, 2010, **2**, 1417–1419.

S2. H. Ishida, S. Tobita, Y. Hasegawa, R. Katoh, K. Nozaki, Recent Advances in Instrumentation for Absolute Emission Quantum Yield Measurements. *Coord. Chem. Rev.*, 2010, **254**, 2449–2458.

S3. H.-C. Yeh, W.-C. Wu, Y.-S. Wen, D.-C. Dai, J.-K. Wang, C.-T. Chen, Derivative of *α, β*-Dicyanostilbene: Convenient Precursor for the Synthesis of Diphenylmaleimide Compounds, *E-Z* Isomerization, Crystal Structure, and Solid-State Fluorescence. *J. Org. Chem.*, 2004, **69**, 6455−6462.

S4. Z. Lin, Y. Ma, X. Zheng, L. Huang, E. Yang, C.-Y. Wu, T. J. Chow, and Q. Ling, Amide-based Diarylmaleimide Derivatives and Polymers: Highly Selective and Ratiometric Fluorescence Sensing for Anions. *Dyes Pigm.*, 2015, **113**, 129–137.

S5. X. Mei, J. Wang, Z. Zhou, S. Wu, L. Huang, Z. Lin, Q. Ling, Diarylmaleic Anhydrides: Unusual Organic Luminescence, Multi-Stimuli Response and Photochromism. *J. Mater. Chem. C*, 2017, **5**, 2135−2141.

S6. W. Li, Y. Pan, L. Yao, H. Liu, S. Zhang, C. Wang, F. Shen, P. Lu, B. Yang, and Y. Ma, Hybridized Local and Charge Transfer Excited State for Highly Efficient Fluorescent OLEDs: Molecular Design, Spectral Character and Full Exciton Utilization. *Adv. Opt. Mater*., 2014, **2**, 892–901.

S7. Gaussian 09, Revision D.01, M. J. Frisch, G. W. Trucks, H. B. Schlegel, G. E. Scuseria, M. A. Robb, J. R. Cheeseman, G. Scalmani, V. Barone, B. Mennucci, G. A. Petersson, H. Nakatsuji, M. Caricato, X. Li, H. P. Hratchian, A. F. Izmaylov, J. Bloino, G. Zheng, J. L. Sonnenberg, M. Hada, M. Ehara, K. Toyota, R. Fukuda, J. Hasegawa, M. Ishida, T. Nakajima, Y. Honda, O. Kitao, H. Nakai, T. Vreven, J. A. Jr. Montgomery, J. E. Peralta, F. Ogliaro, M. Bearpark, J. J. Heyd, E. Brothers, K. N. Kudin, V. N. Staroverov, R. Kobayashi, J. Normand, K. Raghavachari, A. Rendell, J. C. Burant, S. S. Iyengar, J. Tomasi, M. Cossi, N. Rega, J. M. Millam, M. Klene, J. E.

Knox, J. B. Cross, V. Bakken, C. Adamo, J. Jaramillo, R. Gomperts, R. E. Stratmann, O. Yazyev, A. J. Austin, R. Cammi, C. Pomelli, J. W. Ochterski, R. L. Martin, K. Morokuma, V. G. Zakrzewski, G. A. Voth, P. Salvador, J. J. Dannenberg, S. Dapprich, A. D. Daniels, Ö. Farkas, J. B. Foresman, J. V. Ortiz, J. Cioslowski, D. J. Fox, Gaussian, Inc., Wallingford CT, **2009**.